

โปรแกรมตรวจสอบการคำนวณปริมาณรังสีสำหรับเทคนิคการรักษาแบบปรับความเข้มลำรังสีโดย  
ใช้ข้อมูลผู้ป่วยจากภาพคอมพิวเตอร์โทโมกราฟี



นายฉันทวัฒน์ ฐิติ

## ศูนย์วิทยทรัพยากร

วิทยานิพนธ์นี้เป็นส่วนหนึ่งของการศึกษาตามหลักสูตรปริญญาวิทยาศาสตรดุษฎีบัณฑิต

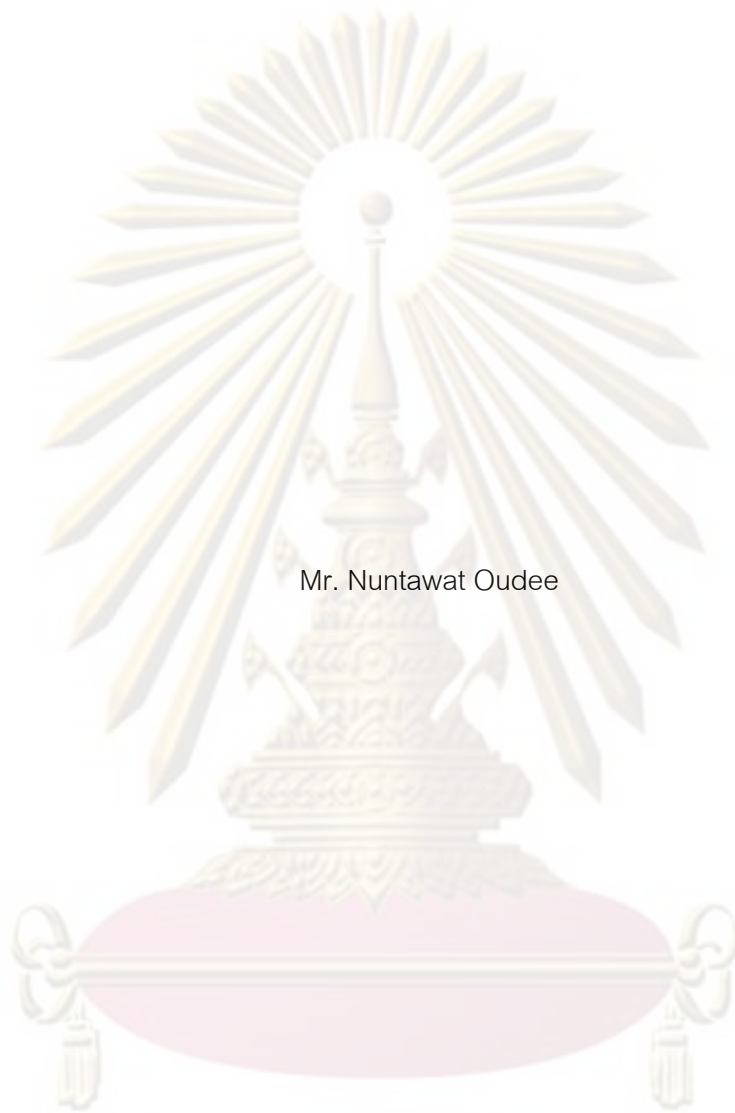
สาขาวิชาวิศวกรรมนิวเคลียร์ ภาควิชานิวเคลียร์เทคโนโลยี

คณะวิศวกรรมศาสตร์ จุฬาลงกรณ์มหาวิทยาลัย

ปีการศึกษา 2552

ลิขสิทธิ์ของจุฬาลงกรณ์มหาวิทยาลัย

AN INDEPENDENT SOFTWARE FOR IMRT DOSE VERIFICATION IN CT-BASED  
PATIENT DATA



Mr. Nuntawat Oudee

A Dissertation Submitted in Partial Fulfillment of the Requirements  
for the Degree of Doctor of Engineering Program in Nuclear Engineering

Department of Nuclear Technology

Faculty of Engineering

Chulalongkorn University


Academic Year 2009

Copyright of Chulalongkorn University

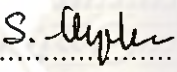
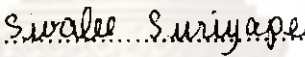
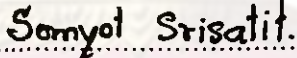
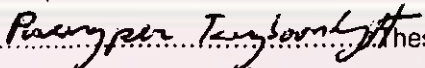

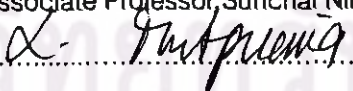

Thesis Title AN INDEPENDENT SOFTWARE FOR IMRT DOSE  
VERIFICATION IN CT-BASED PATIENT DATA  
By Mr. Nuntwat Oudee  
Field of Study Nuclear Engineering  
Thesis Advisor Associate Professor Sivalee Suriyapee  
Thesis Co-Advisor Associate Professor Somyot Srisatit  
Thesis Co-Advisor Puangpen Tangboonduangjit, Ph.D.

---

Accepted by the Faculty of Engineering, Chulalongkorn University in Partial  
Fulfillment of the Requirements for the Doctoral Degree

.....Dean of the Faculty of Engineering  
(Associate Professor Boonsom Lerthirunwong, Dr. Ing.)

THESIS COMMITTEE

.....Chairman  
(Associate Professor Supitcha Chanyotha, Ph.D.)  
.....Thesis Advisor  
(Associate Professor Sivalee Suriyapee)  
.....Thesis Co-Advisor  
(Associate Professor Somyot Srisatit)  
.....Thesis Co-Advisor  
(Puangpen Tangboonduangjit, Ph.D.)  
.....Examiner  
(Associate Professor Sunchai Nilsuwankosit, Ph.D.)  
.....External Examiner  
(Associate Professor Lalida Tuntipumiamorn)  
.....External Examiner  
(Assistant Professor Nakorn Phaisangittisakul, Ph.D.)

นันทวัฒน์ อู่ดี : โปรแกรมตรวจสอบการคำนวณปริมาณรังสีสำหรับเทคนิคการรักษาแบบปรับความเข้มลำรังสีโดยใช้ข้อมูลผู้ป่วยจากภาพคอมพิวเตอร์โทโมกราฟี. (AN INDEPENDENT SOFTWARE FOR IMRT DOSE VERIFICATION IN CT-BASED PATIENT DATA) อ.ที่ปรึกษาวิทยานิพนธ์หลัก: รศ.ศิวลี สุริยปี่, อ. ที่ปรึกษาวิทยานิพนธ์ร่วม: รศ.สมยศ ศรีสถิตย์, อ. ที่ปรึกษาวิทยานิพนธ์ร่วม: อ.ทวงเพ็ญ ตั้งบุญดวงจิตร, 120 หน้า.

การตรวจสอบการคำนวณปริมาณรังสีในผู้ป่วยมีความจำเป็นในงานรังสีรักษาโดยเฉพาะเทคนิคการฉายรังสีแบบปรับความเข้ม ในการศึกษาค้นคว้าครั้งนี้ได้พัฒนาโปรแกรมตรวจสอบการคำนวณปริมาณรังสี (ISOFT) เพื่อคำนวณปริมาณรังสีจากเทคนิคการฉายรังสีจำกัดขอบเขตแบบสามมิติ และการฉายรังสีแบบปรับความเข้มในหุ่นจำลองทรวงอก (CIRS) โดยประยุกต์วิธีการคำนวณระหว่างวิธีคลากสัน (Clarkson's method) ร่วมกับการคำนวณแบบสามมิติ (3D-BSM)

เปอร์เซ็นต์ความแตกต่างระหว่างการวัดปริมาณรังสีเป็นจุดโดยใช้หัววัดรังสีและการคำนวณโดยโปรแกรมตรวจสอบการคำนวณปริมาณรังสีและเครื่องคอมพิวเตอร์วางแผนการรักษาในพื้นที่ลำรังสีสี่เหลี่ยมจัตุรัส สี่เหลี่ยมผืนผ้าและรูปทรงต่างๆ โดยใช้เครื่องจำกัดลำรังสีแบบซีทีระดับความลึกตั้งแต่ 1.5 ซม. ถึง 15 ซม. ในหุ่นจำลองน้ำมีค่าไม่เกิน 2 เปอร์เซ็นต์ สำหรับการตรวจสอบปริมาณรังสีที่ได้จากเทคนิคการฉายรังสีจำกัดขอบเขตแบบสามมิติและการฉายรังสีแบบปรับความเข้มได้ทำการเปรียบเทียบปริมาณรังสีที่ได้จากการคำนวณโดยโปรแกรมตรวจสอบการคำนวณปริมาณรังสีและเครื่องคอมพิวเตอร์วางแผนการรักษากับหัววัดรังสีและฟิล์มวัดรังสีในหุ่นจำลองทรวงอก การวัดปริมาณรังสีในปอดมีค่าต่ำกว่าการคำนวณทุกวิธี เปอร์เซ็นต์ความแตกต่างระหว่างการวัดและการคำนวณด้วยโปรแกรมตรวจสอบการคำนวณปริมาณรังสีอยู่ภายใน 5 เปอร์เซ็นต์ซึ่งเป็นค่าขอบเขตการยอมรับได้ ดังนั้นโปรแกรมตรวจสอบการคำนวณปริมาณรังสีสามารถใช้เป็นโปรแกรมสำหรับตรวจสอบปริมาณรังสีสัมบูรณ์ทั้งเทคนิคการฉายรังสีจำกัดขอบเขตแบบสามมิติและการฉายรังสีแบบปรับความเข้มในศอกกลางที่ไม่ได้เป็นเนื้อเดียวกันโดยใช้ข้อมูลภาพคอมพิวเตอร์โทโมกราฟี นอกจากนี้โปรแกรมยังสามารถแก้ค่าความโค้งของผิวหนังได้ข้อจำกัดของโปรแกรมคือสามารถคำนวณได้สำหรับลำรังสีลำเดียวทิศทาง 90 องศา รวมทั้งไม่สามารถแก้ค่าการเพิ่มขึ้นของปริมาณรังสีใกล้ผิว (build up doses) และบริเวณรอยต่อได้อย่างถูกต้อง

ภาควิชา.....นิวเคลียร์เทคโนโลยี.....ลายมือชื่อนิสิต.....นันทวัฒน์ อู่ดี  
 สาขาวิชา.....วิศวกรรมนิวเคลียร์.....ลายมือชื่อ อ.ที่ปรึกษาวิทยานิพนธ์หลัก.....ศิวลี สุริยปี่  
 ปีการศึกษา 2552.....ลายมือชื่อ อ.ที่ปรึกษาวิทยานิพนธ์ร่วม.....นิพนธ์ วงศ์สิทธิ์  
 ลายมือชื่อ อ.ที่ปรึกษาวิทยานิพนธ์ร่วม.....ทวงเพ็ญ ตั้งบุญดวงจิตร

## 4871812821: MAJOR NUCLEAR ENGINEERING

KEYWORDS: INTENSITY MODULATED RADIATION THERAPY / CT-BASED PATIENT DATA / RADIATION TREATMENT PLANNING SYSTEM / CLARKSON INTEGRATION ALGORITHM / THREE DIMENTION BEAM SUBTRACTION METHOD

NUNTAWAT OUDEE: AN INDEPENDENT SOFTWARE FOR IMRT DOSE VERIFICATION IN CT-BASED PATIENT DATA. THESIS ADVISOR: ASSOC. PROF. SIVALEE SURIYAPEE, M. ENG., THESIS CO-ADVISOR : ASSOC. PROF. SOMYOT SRISATIT, M. ENG., THESIS CO-ADVISOR : PUANGPEN TANGBOONDUANGJIT, PH.D., 120 pp.

The patient specific dose verification is necessary process in advanced radiation therapy. In this study, the independent software (ISOFT) was developed to calculate absolute dose from 3 dimensional conformal radiation therapy (3D-CRT) and intensity modulated radiation therapy (IMRT) field in CIRS thorax phantom by combining modified Clarkson integration with 3D beam subtraction method (3D-BSM).

The overall of percent deviation of point dose between measured by ion chamber and calculated by ISOFT and Eclipse system for square, rectangular and shaped MLC field at 1.5 to 15 cm depths in homogeneous phantom was within 2%. For the verification of 3D-CRT and IMRT plans, the doses from ISOFT and Eclipse system were compared with ion chamber and EDR2 film in CIRS thorax phantom. The measured lung dose presented mostly the lower dose than calculated by ISOFT and Eclipse system. The percent deviation between measurement and ISOFT was within 5% which reached the acceptable criteria. So ISOFT can be used as an independent software to verify absolute dose of 3D-CRT and IMRT field in inhomogeneous medium for CT base patient data. The correction of external body contour was included. The limitation of ISOFT was the only one field can be applied at 90 degree gantry angle. The build up doses at the surface and interface could not be determined correctly.

Department : .....Engineering..... Student's Signature *Nuntawat Oudee*

Field of Study : .....Nuclear Engineering..... Advisor's Signature *Sivalee Suriyapee*

Academic Year : .....2009..... Co-Advisor's Signature *Somyot Srisatit*

Co-Advisor's Signature *Puangpen Tangboonduangjit*

## ACKNOWLEDGEMENTS

I would like to express gratitude and deepest appreciation to Associate Professor Sivalee Suriyapee, Head of Physicist at Division of Radiation Oncology, Department of Radiology, Faculty of Medicine, Chulalongkorn University, my major advisor for her guidance, invaluable advice, supervision, constructive comments and English language proof in this research. I am equally grateful to Assoc.Prof. Somyot Srisatit, at Department of Nuclear Technology, Faculty of Engineering, Chulalongkorn University and Dr. Puangpen Tangboonduangjit, Division of Radiation Oncology, Department of Radiology, Faculty of Medicine, Ramathibodi Hospital, my co-advisors for their help in the experiment, kind suggestion and constructive comments in the experiments.

I would like to deeply thank Associate Professor Supitcha Chanyotha; Chair of Degree of Doctor of Engineering Program in Nuclear Engineering at Department of Nuclear Technology, Faculty of Engineering, Chulalongkorn University, my teacher for advice and comments in the research.

I would like to deeply thank Associate Professor Sunchai Nilswankosit; Head of Department of Nuclear Technology, Faculty of Engineering, Chulalongkorn University, my teacher for advice and comments in the research.

I would like to thank Assistant Professor Nakorn Phaisangittisakul from Department of Physics, Faculty of Sciences and Associate Professor Lalida Tuntipumiamorn from Department of Radiology, Faculty of Medicine, Siriraj hospital, who were the external examiner of the thesis defense for their help in the experiment, kind suggestion, and constructive comments in the experiments.

I would like to thank the physicists and staffs at the Division of Radiation Oncology, Department of Radiology, Faculty of Medicine, Chulalongkorn University, for their help in my research.

Finally, I am grateful of my family for their financial support, valuable encouragement, entirely care, and understanding during the entire course of study.

## CONTENTS

	Page
ABSTRACT (THAI).....	iv
ABSTRACT (ENGLISH).....	v
ACKNOWLEDGEMENTS.....	vi
CONTENTS.....	vii
LIST OF TABLES.....	xi
LIST OF FIGURES.....	xii
LIST OF ABBREVIATIONS.....	xv
CHAPTER I INTRODUCTION.....	1
1.1 Background and rationale.....	1
1.2 Research objectives.....	3
CHAPTER II REVIEW OF RELATED LITERATURES.....	4
2.1 Theory.....	4
2.1.1 Physics of radiation.....	4
2.1.2 The radiation dose calculation methods.....	6
2.1.3 Inhomogeneity correction methods.....	8
2.1.4 Dose calculation algorithms for inhomogeneity.....	9
2.1.5 Intensity-modulated radiation therapy (IMRT).....	15
2.1.6 Contour irregularities correction.....	18
2.1.7 Modified Clarkson integration algorithm.....	18
2.1.8 Multiplanar reconstructions (MPRs).....	19
2.1.9 Quality assessment of computerized treatment planning systems.....	20
2.2 Related literatures.....	22
CHAPTER III RESEARCH METHODOLOGY.....	27
3.1 Research design.....	27

3.2	Research design model.....	28
3.3	Key word.....	28
3.4	Research questions.....	28
	3.4.1 Primary question.....	28
	3.4.2 Secondary question.....	28
3.5	Scope of dissertation.....	28
3.6	Material.....	28
	3.6.1 Computed Tomography Simulation.....	30
	3.6.2 Linear accelerator (LINAC).....	31
	3.6.3 Eclipse radiation treatment planning system....	32
	3.6.4 Electron density phantom.....	33
	3.6.5 IMRT thorax phantom.....	34
	3.6.6 Film measurement.....	35
	3.6.7 Vidar scanner.....	36
	3.6.8 Ionization chamber.....	36
	3.6.8.1 CC13 ionization chamber.....	36
	3.6.8.2 FC65-P ionization chamber.....	37
	3.6.9 Electrometer.....	38
	3.6.10 Three dimension beam analyzing system.....	39
	3.6.11 One dimension water phantom.....	40
	3.6.12 ImageJ program.....	41
	3.6.13 Personal computer (PC).....	41
3.7	Method.....	41
	3.7.1 Beam data preparing.....	
	3.7.2 Code development for modified Clarkson integration algorithm with 3D-BSM.....	42
	3.7.3 Dose verifications of MLC fields in homogeneous phantom.....	46
	3.7.4 Dose verifications of 3D-CRT and IMRT fields in	50



inhomogeneous phantom.....	55
3.8 Outcome.....	55
3.9 Measurement.....	56
3.10 Data collection.....	56
3.11 Data analysis.....	56
3.12 Benefit of the study.....	57
CHAPTER IV RESULTS.....	
4.1 Code development for modified Clarkson integration algorithm with 3D-BSM .....	57
4.1.1 Code of image and MLC field .....	57
4.1.2 Code for dose calculation .....	61
4.2 Dose verifications of MLC fields in homogeneous phantom.....	61
4.2.1 Square fields.....	63
4.2.2 Rectangular fields.....	65
4.2.3 Shaped fields.....	
4.3 Dose Verification of 3D-CRT and IMRT plans in inhomogeneous phantom.....	68
4.3.1 The measurement by ionization chamber .....	70
4.3.2 Film and scanner calibration.....	74
4.3.3 Film measurement.....	80
CHAPTER V DISCUSSION AND CONCLUSION.....	80
5.1 Dose verifications of MLC fields in homogeneous phantom.....	
5.2 Dose verification of 3D-CRT and IMRT plans in inhomogeneous phantom.....	80
5.3 Limitation of ISOFT software.....	82
5.4 Comparison with the other studies .....	84
REFERENCES.....	88
APPENDICES.....	89
APPENDIX A: The table of beam data requirement .....	

APPENDIX B: An example of .mlc file of square MLC fields for dose	107
Verification.....	108
APPENDIX C An example of .mlc file of static 3D-CRT field: .....	109
APPENDIX D The user manual of ISOFT software.....	120
VITAE.....	



# ศูนย์วิทยทรัพยากร จุฬาลงกรณ์มหาวิทยาลัย

## LIST OF TABLES

Table	Page
2.1 The criteria of acceptability for photon dose calculation algorithm by IAEA TRS. 430.....	21
3.1 The physical density ( $\text{g/cm}^3$ ) and electron density relative to water of electron density phantom GMMEX 467.....	33
3.2 Summarize the setting parameters for square fields.....	48
3.3 Summarize the setting parameters for rectangular fields.....	48
3.4 Summarize the setting parameters for shaped fields.....	49
4.1 The comparison of measured and calculated by ISOFT software and treatment planning for $10 \times 10$ and $5 \times 5$ $\text{cm}^2$ square fields at 1.5, 5, 10 and 15 cm depths for 6 MV photon beams at 100 cm SAD.....	63
4.2 The comparison of measured and calculated by ISOFT software and treatment planning for $30 \times 5$ and $5 \times 30$ $\text{cm}^2$ rectangular fields at 1.5, 5, 10 and 15 cm depths for 6 MV photon beams at 100 cm SAD.....	65
4.3 The comparison of measured and calculated by ISOFT software and treatment planning for corner block, circular field, inverted Y field and irregular field at 1.5, 5, 10 and 15 cm depths for 6 MV photon beams of 100 cm SAD.....	67
4.4 The comparison between point doses measured by ionization chamber and calculated by AAA, Modified Batho and ISOFT software of 3D-CRT at left lung, mediastinum and right lung.....	69
4.5 The comparison between point doses measured by ionization chamber and calculated by AAA, Modified Batho and ISOFT software of IMRT at left lung, mediastinum and right lung.....	70
4.6 The densitometer signal of standard step film for scanner calibration.....	71
4.7 The densitometer signal of standard step film for film calibration.....	73

## LIST OF FIGURES

Figure	Page
2.1 The primary dose and scattered dose components within irradiated volume.....	7
2.2 The primary distribution with varying magnitude of scatter in water of 5 MeV photon pencil beam.....	8
2.3 The rectangular heterogeneity material in an irregular field with dimensions 2X and 2Y.....	13
2.4 Show the regions of criteria acceptability for photon beam dose calculations...	21
3.1 Computed Tomography Simulation Light speed RT manufactured by General Electric GE.....	29
3.2 Linear accelerator Clinac 21EX manufactured by Varian Associates, Palo Alto, USA.....	30
3.3 The radiation treatment planning system Eclipse Version 6.5 manufactured by Varian Associates Palo Alto, USA.....	31
3.4 Electron density phantom GAMMEX 467 Middleton, USA.....	32
3.5 The CIRS Model 002LFC IMRT Thorax Phantom.....	34
3.6 The Kodak's Ready-Pack film EDR2 for 2D dose distribution.....	35
3.7 The film scanning system Vidar-16 Dosimetry Pro.....	36
3.8 Ionization chamber (Scanditronix/Wellhofer Dosimetries) (a) The CC13 ionization chamber (b) FC65-P ionization chamber.....	37
3.9 DOSE1 electrometer manufactured by Wellhofer Dosimetrie, Schwarzenbruck, Germany.....	38
3.10 Three dimension beam analyzing system manufactured by Scanditronix/Wellhofer Dosimetrie, Schwarzenbruck, Germany.....	39
3.11 One dimension water phantom manufactured by Scanditronix/ Wellhofer Dosimetrie, Schwarzenbruck, Germany.....	40
3.12 ImageJ program.....	41

## LIST OF FIGURES (continue)

Figure	Page
3.13 The simple setup geometry showing the radius $l$ and intersection $j$ .....	44
3.14 The sagittal view showing the pixel, radius and intersection.....	46
3.15 Schematic of 6MV MLC beam geometry of water phantom at 90 SSD and 1.5, 5, 10 and 15 cm depth.....	47
3.16 Tumor image from the Eclipse RTPS of 3D-CRT plan 1 and IMRT plan 1.....	51
3.17 Tumor image from the Eclipse RTPS of 3D-CRT plan 2 and IMRT plan 2.....	51
3.18 The calibration of ionization chamber in CIRS thorax phantom.....	52
3.19 The calibration of EDR2 film in solid water phantom.....	54
3.20 Two dimensional dose measurements for 3D-CRT or IMRT plan in CIRS thorax phantom by film.....	55
4.1 Screenshot of ISOFT homogeneous phantom and MLC window.....	59
4.2 Screenshot of ISOFT inhomogeneous phantom window.....	59
4.3 Screenshot of ISOFT MLC window that contained CT images, patient information and MLC position of treatment field. The surface contour was created by ISOFT software.....	60
4.4 The ISOFT software displays sagittal view of CIRS IMRT phantom that is divided into calculation grid.....	60
4.5 The MLC of square field verification by ISOFT software (a) A square field of $10 \times 10 \text{ cm}^2$ (b) A square field of $5 \times 5 \text{ cm}^2$ .....	62
4.6 The MLC of rectangular field verification by ISOFT software.(a) A rectangular field of $30 \times 5 \text{ cm}^2$ (b) A rectangular field of $5 \times 30 \text{ cm}^2$ .....	64
4.7 The The MLC of shaped field of corner block, circular field, inverted Y field and irregular field by ISOFT software.....	66
4.8 The correlation between optical density and ADC of dose response curve of Kodak EDR2 film.....	72

## LIST OF FIGURES (continue)

Figure	Page
4.9 The correlation between optical density and dose of dose response curve of Kodak EDR2 film.....	73
4.10 The EDR2 film image using digital camera of 3D-CRT field technique at central axis in parallel setup of 6 MV beams of patient plan 1.....	75
4.11 The EDR2 film image using digital camera of 3D-CRT field technique at central axis in parallel setup of 6 MV beams of patient plan 2.....	75
4.12 The EDR2 film image using digital camera of IMRT field technique at central axis in parallel setup of 6 MV beams of patient plan 1.....	76
4.13 The EDR2 film image using digital camera of IMRT field technique at central axis in parallel setup of 6 MV beams of patient plan 2.....	76
4.14 Subfields of planar dose maps of IMRT plan 1 from the Eclipse RTPS, 6 MV beam at 100 cm SAD.....	77
4.15 Subfields of planar dose maps of IMRT plan 2 from the Eclipse RTPS, 6 MV beam at 100 cm SAD.....	77
4.16 Central axis depth dose curve of 3D CRT plan 1 with the beam irradiated from left to right side of CIRS thorax phantom.....	78
4.17 Central axis depth dose curve of 3D-CRT plan 2 with the beam irradiated from left to right side of CIRS thorax phantom.....	78
4.18 Central axis depth dose curve of IMRT plan 1 with the beam irradiated from left to right side of CIRS thorax phantom.....	79
4.19 Central axis depth dose curve of IMRT plan 2 with the beam irradiated from left to right side of CIRS thorax phantom.....	79

## LIST OF ABBREVIATIONS

Abbreviation	Terms
2D	Two dimension
3D	Three dimension
3D-CRT	Three dimensional conformal radiation therapy
AAPM	American Association of Physicist in Medicine
ADC	Analog to digital converter
C	Coulomb
cGy	Centigray
cm	Centimeter
cm <sup>2</sup>	Square centimeter
CPE	Charge particle equilibrium
CSDA	Continuous slowing down approximation
CT	Computed tomography
$d_{max}$	Depth of dose maximum
DMLC	Dynamic multileaf collimator
DRR	Digitally reconstructed radiographys
dSAR	Differential scatter-air ratios
DVOL	Delta volume method

## LIST OF ABBREVIATIONS (Continued)

Abbreviation	Terms
E	Energy
EDR	Extended dose range
EPL	Effective path length
ETAR	Equivalent tissue air ratio
eV	electronvolt
FFT	Fast Fourier transform
g	Gram
Gy	Gray
H&D curve	Hurter and Driffield curve
ICF	Inhomogeneity correction factor
IMB	Intensity modulated beam
IMRT	Intensity modulated radiation therapy
J	Joule
KERMA	Kinetic energy released to charged particles per unit mass
Kg	Kilogram
L	Length



## LIST OF ABBREVIATIONS (Continued)

Abbreviation	Terms
LINAC	Linear accelerator
MC	Monte Carlo
MeV	Megaelectronvolt
MLC	Multileaf collimator
MPR	Multiplanar reformatting
MRI	Magnetic resonance imaging
MU	Monitor units
MV	Mass
min	Minute
mm	Millimeter
mm <sup>2</sup>	Square millimeter
NTCP	Normal tissue complications probability
nC	Nanocoulomb
OAR	Organ at risk
OD	Optical density
PC	Personal computer
PET	Positron emission tomography

## LIST OF ABBREVIATIONS (Continued)

Abbreviation	Terms
Z	Atomic number



ศูนย์วิทยทรัพยากร  
จุฬาลงกรณ์มหาวิทยาลัย

## CHAPTER I

### INTRODUCTION

#### 1.1 Background and Rationale

The accuracy of dose delivery is essential for the success of radiotherapy. The ICRU (1976) recommends the dose to be delivered with an error of less than  $\pm 5\%$ . To satisfy this recommendation, each step involved in dose delivery (dose calculation, patient positioning, machine calibration, etc.) needs to be performed with an accuracy much better than  $\pm 5\%$  [1]. For the difficult problem of dose calculations in treatment planning, the necessary accuracy may be set at 2-3% for homogeneous medium and increase up to 5% for inhomogeneity medium [2]. The dose calculation algorithm is an essential element of the treatment process and requires extensive testing before being used clinically.

A long-standing problem in precise patient dosimetry is how to account for the effect on the dose of internal non-water like inhomogeneities present in the body (e.g. lungs, bones, air cavities). While it is relatively simple to calculate the perturbation of the primary dose, scatter calculation is more complex. Most methods of clinical dose calculation are accurate for the primary dose but the scatter dose is ignored or approximated. For high energy photon beams, methods for inhomogeneity corrections were proposed in 1950's and improved by many investigators. Most inhomogeneity correction algorithms are semi-empirical and accurate for only a limited set of simplified geometries. Monte Carlo method is one of the models that can predict dose distribution in complex geometries. But the calculation time is time consumed. Normally, the radiation treatment planning system (RTPS) used CT-based patient data to perform the heterogeneous correction including the Batho, the Equivalent tissue air ratio (ETAR), simplified the Ratio of tissue-air ratio (RTAR) or 3D beam subtraction method (3D-BSM) algorithms. At present, the superposition/convolution algorithm and Monte Carlo method were including inhomogeneous correction in the calculation of patient dose.

Advanced techniques in radiotherapy, like intensity modulated radiotherapy (IMRT), increase the planning and delivery complexity. The high dose gradient is the result of varying intensity of the individual beams using a number of small beams, potentially with different monitor units, is one of the ways to get the required modulation in the field. This complex nature makes it necessary to check the consistency between calculated and delivered dose before treatment. Although the absolute point dose can be measured with good accuracy using ionization chamber. Two-dimensional dose distribution can be performed by radiographic film or radio-chromic film or detector array. But these types of measurements are time consume, labor intensive and some specific equipments needed. In the last few years, a few groups have developed independent dose calculation algorithms to verify the dose distribution of the IMRT plan including heterogeneous correction. Some authors [3, 4, 5, 6, 7, 8, 9, 10] proposed the verification point dose calculation using the Clarkson method for IMRT plan in homogeneous medium. The results showed the comparison of Clarkson method and treatment planning system which was within 2.7% [10]. For inhomogeneity medium, the best method of calculation is Monte Carlo Simulation but it is time consume and not suitable to be served as an independent dose verification tool. For the semi empirical algorithms, the scatter correction for inhomogeneity is approximated. Most methods of inhomogeneity correction in high energy x-ray beams assume an infinite lateral extent of the heterogeneous volumes (slab models) or require sophisticated time-consuming computer algorithms. The 3D beam subtraction is developed for parallelepiped inhomogeneities based on a beam subtraction concept combined with a chosen conventional slab model, it provides the agreement with measurement within 1% [11]. The method of 3D-BSM can be accounted properly for the scatter modification according to the size and position of the inhomogeneous volume. The combined Clarkson method with 3D-BSM predicts the correction factors for irregular fields included inhomogeneities [12]. The agreement between the combination of Clarkson method with 3D-BSM and Monte Carlo is within 1.5%. The method improves the basic inhomogeneities correction by taking into account anywhere in the irradiating volume

and the shape of the field. This method of calculation is a new tool to serve as an independent dosimetric verification in complex treatment plan.

In this study, the combination of the modified Clarkson integration algorithm with 3D-BSM are developed for 3D-CRT and IMRT step and shoot dosimetric verification in CT-based patient data. The MLCs pattern and CT-based patient data from RTPS are transferred to the independent software. The independent software manipulates the CT-based patient data to axial and sagittal views; furthermore, the independent software converts CT number to electron density for heterogeneous correction. The results of point doses from depth dose curves are obtained and analyzed. The dose differences of the developed independent software and RTPS results are compared.

### 1.2 Research objective

To develop an independent software for 3D-CRT and IMRT point dose verification in CT-based patient data.



ศูนย์วิทยทรัพยากร  
จุฬาลงกรณ์มหาวิทยาลัย

## CHAPTER II

### REVIEW OF RELATED LITERATURES

#### 2.1 Theory

##### 2.1.1 Physics of radiation [2, 15]

The physical process of photon interactions were the energy deposited within material and the kinetic energy imparted to charged particle. The absorption of photon energy in material was characterized to two step process.

##### 2.1.1.1 Photon interaction

The interactions of initial photon within material are characterized by the probability of photon interaction per unit distance called the linear attenuation coefficient ( $\mu$ ). This coefficient depends on the incident photon energy (E) in MeV, the tissue density ( $\rho$ ) unit ( $\text{g}/\text{cm}^2$ ), and the effective atomic number (Z) of the tissue. The amount of incident photon in material is characterized by energy fluence ( $\text{MeV cm}^{-2}$ ). The total energy released per unit mass (TERMA) is calculated by the product of the total mass attenuation coefficient ( $\mu/\rho$ ) and the energy fluence ( $\Psi$ ) at the point of interaction.

$$\text{TERMA} = \frac{\mu}{\rho} \times \Psi \quad \dots(2.1)$$

The kinetic energy released to charged particles per unit mass is the KERMA that defined by the quotient of the  $d\bar{E}_{\text{tr}}$  by  $dm$ , where  $d\bar{E}_{\text{tr}}$  is the sum of the initial kinetic energies of all the charged ionizing particles liberated by uncharged particles (photons) in a material unit mass  $dm$ .

$$\text{KERMA} = \left[ \frac{d\bar{E}_{\text{tr}}}{dm} \right] \quad \dots(2.2)$$

The unit of KERMA is Gy or J/kg. For the energy transferred to material, the kerma is proportional to the energy fluence ( $\Psi$ ) at the point of interaction and is given by

$$\text{KERMA} = \frac{\mu_{en}}{\rho} \times \Psi \quad \dots(2.3)$$

where  $\mu_{en}/\rho$  is the mass energy transfer coefficient for medium averaged over the energy fluence spectrum. The charged particles were losing energy by inelastic collisions (ionization and excitation) with electron of material. Some of electron was losing energy with the atomic nuclei by radiative loss (bremsstrahlung interactions) that does not deposit their energy in local medium. The energy absorption coefficient ( $\mu_{en}$ ) is defined by the product of energy transfer coefficient and is given by

$$\mu_{en} = \mu_{tr} (1 - g) \quad \dots(2.4)$$

where  $g$  is the fraction of the energy of secondary charged particles which lost to bremsstrahlung in the material. Then equation 2.3 is

$$\text{KERMA} = \frac{\mu_{en}}{\rho} \times \Psi \quad \dots(2.5)$$

However, the kerma can be divided into two parts

$$\text{KERMA} = K_{col} + K_{rad} \quad \dots(2.6)$$

where  $K_{col}$  and  $K_{rad}$  are the collision and the radiation process of kerma, respectively.

#### 2.1.1.2 Electron interaction

The interaction of photons within material by photoelectric, Compton or pair production processes, some of energy releases to recoil charged particles. The interactions of charged particle are mediated by Coulomb force between traveling particle and electric fields of orbital electrons and atomic nuclei of the material.

The collision process of the charged particle with the orbital electrons results in ionization and excitation of atoms. The collision process of the charged particle with the atomic nuclei results in bremsstrahlung which the energy deposited out of local volume of interest. For the local energy deposition, the stopping power ( $S$ )

defined as the rate of kinetic energy loss per unit path length of the particle ( $dE/dl$ ) and the  $S_{col}/\rho$  defined as the stopping power per density of medium ( $\text{MeV cm}^2/\text{g}$ ).

$$\frac{S_{col}}{\rho} = \left[ \frac{d\bar{E}}{\rho dl} \right] \quad \dots(2.7)$$

where  $d\bar{E}$  is an average energy that lost locally to the medium per unit density and per unit path length traversed  $dl$ . The mass collision stopping power depends on the energy and charge of the decelerating particle and the atomic number of the stopping medium and density independent. The continuous slowing down approximation (CSDA) is used to assume charged particle lose of energy in material. The range of CSDA ( $R_{CSDA}$ ) of charges particle is given by

$$R_{CSDA} = \int_0^E \left[ \frac{d\bar{E}}{\rho dl} \right]^{-1} \times dE \quad \left( \frac{g}{cm^2} \right) \quad \dots(2.8)$$

#### 2.1.2 The radiation dose calculation methods [13]

The dose is dividing into primary and secondary radiation components that are individually affected by tissue inhomogeneities and field boundaries. The primary and scattered radiation components are independently within the material irradiated. The primary radiation produced by the radiation source and other interactions within the head of treatment machine. Most of primary radiations reach in material at point of interest without any interaction in the patient. These interactions are Compton scattering process that generates secondary electrons to scattered photon. The pair production process, the incident photon energy greater than 1.02 MeV, produce the electron-positron pairs and resulting in the generation of photons with energy of 0.51 MeV from positron annihilation. The dose from primary radiation at the central axis of open field at specific depth in phantom will depend on distance from the source, head scatter that will depend upon collimator setting and beam modifiers (block, wedges) and attenuation including absorption and scattering in phantom, determined by depth and beam energy.



The scattered dose component reaches the interesting point by indirect routes through multiple pathways within the patient. The scattered dose component is the region of the dose that is imparted by photons resulting previously interacted at least once in the medium. The amount of scattered doses depends upon photon energy and the irradiated volume including field size, depth and patient thickness. The calculation dose obtained by integrating the primary with secondary dose components is shown in figure 2.1 [13].

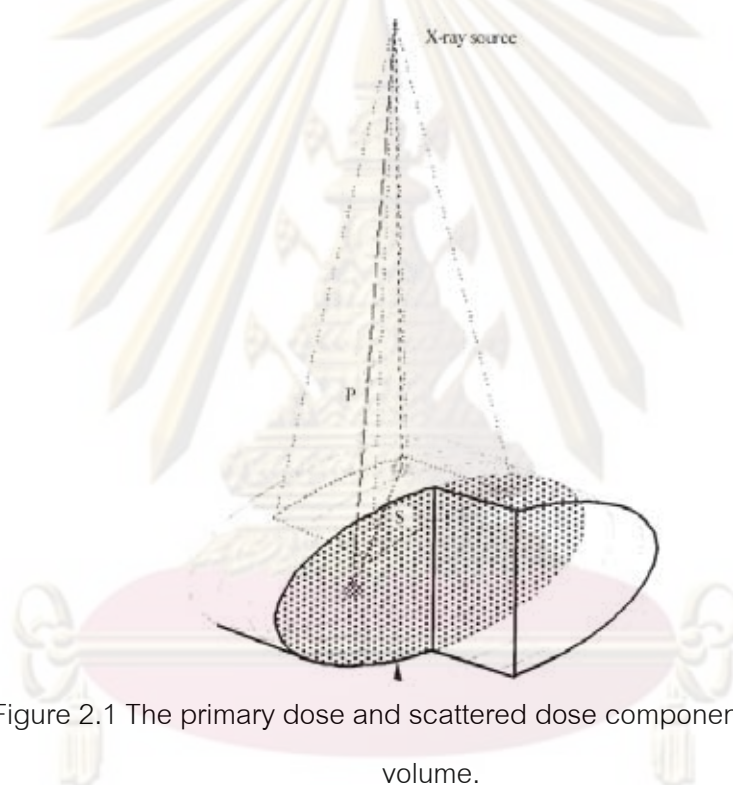


Figure 2.1 The primary dose and scattered dose components within irradiated volume.

However, the primary and scattered dose component can be separated by using direct measurement or Monte Carlo simulations. The total dose at central axis can be calculated by

$$D = D_p + D_s \quad \dots(2.9)$$

where  $D_p$  and  $D_s$  are the primary and scattered dose respectively. The primary dose component is the primary collision KERMA that is the dose deposited from charged particles generated by the primary photons only. The scattered dose is the

contribution of all secondary radiation including Compton scattered photon, annihilation photons and bremsstrahlung. The initial photons generate the scatter radiations energy and spread in material. These scattered radiations are called dose spread functions or scatter kernels. In the material, the primary radiation composes of a spectrum of different particles that originate from any points. The scatter radiations are complex as shown in figure 2.2 [13].

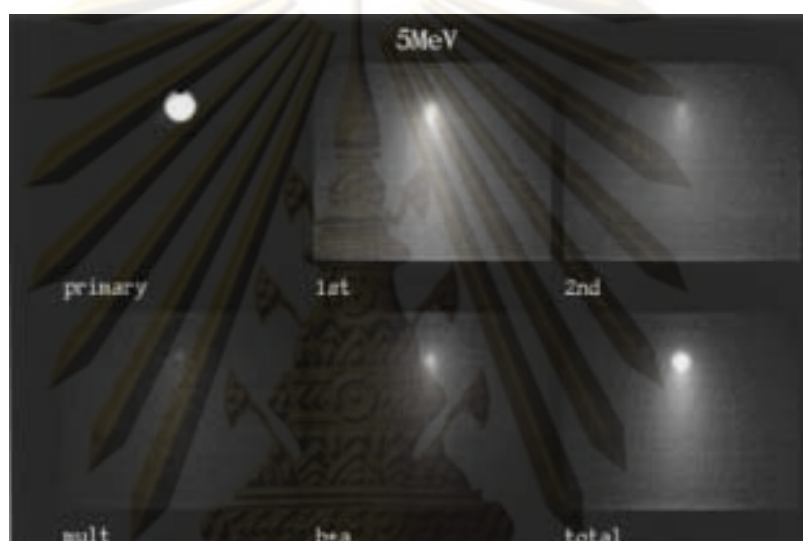


Figure 2.2 The primary distribution with varying magnitude of scatter in water of 5 MeV photon pencil beam.

### 2.1.3 Inhomogeneity correction methods [2]

Since, various inhomogeneities in the human body will affect to the calculation of dose distribution. Thus the accuracy of dose calculation with inhomogeneities should be considered. The major effect for calculation point along the inhomogeneities was the attenuation of the primary radiation. For scattered radiation, the dose distribution was altered near the inhomogeneities than beneath it. In addition, the scattered radiation affects the medium within the inhomogeneities and at the boundaries. The method of dose calculations in tissue heterogeneity can be classified into two categories. Firstly, the conventional form which a relative dose distribution is calculated using assumption of the patient consisting of homogeneous water-like density. The correction of

inhomogeneities obtains by using corrected factor to account for variations in tissue density. The inhomogeneity correction factor (ICF) is defined by

$$\text{ICF} = \frac{\text{The dose in heterogeneous media}}{\text{The dose at same point in homogeneous media}} \quad \dots(2.10)$$

Secondly, the dose at point of interest is calculated in inhomogeneities directly using a model of radiation transport to obtained absolute dose. In therapeutic radiation, Compton interaction is a major predominant of high energy photon beam, so the attenuation of beam in medium depends on electron density.

The corrections of the inhomogeneity in the radiation treatment planning were in three steps. Firstly, the doses were calculated in the water-like medium from the data measurement in water phantom that can be modeling the effect of irregularly fields, patient contour and primary beam modulators. Secondly, the information data of patient from image modalities including anatomy, tissue density and atomic number are required dose calculation. Lastly, the correction of inhomogeneities is necessary for corrected tissue density and atomic number. The modern treatment planning system requires advance image modality that capable to display 3 dimensional patient data and processing. The modern imaging modality for treatment planning process are computed tomography (CT), magnetic resonance imaging (MRI), ultrasound (US), single positron emission tomography (SPECT) or positron emission tomography (PET). However, the computed tomography is the most commonly used in imaging source which can be calculated in a matrix form. The matrix is comprised of 512x512. Each pixel presents the attenuation coefficient of tissue substitutes (CT number). The CT number is essential converted to tissue density value by using electron density phantom.

#### 2.1.4 Dose calculation algorithms for inhomogeneity

The calculation of dose distribution was performed by the computerized radiation treatment planning systems since the middle of the 1950's [15]. The RTPS are predicted dose in tissue by various calculation algorithms. The accuracy of dose calculation of RTPS depends on tissue composition and calculation times. Generally, the

more complex algorithms the fewer uncertainties however the calculation needs longer times [13].

#### 2.1.4.1 Correction based methods [2]

The correction based methods calculated the point dose using particularly primary radiation interaction. These methods suppose that the patient is consisting of semi-infinite slab geometry per calculation point and photon deposited all energies at the point of interaction. The total dose at point of calculation is obtained by integration of the primary and scattered radiation. The limitations of dose calculation depend on the data measurements in homogeneous medium, beam modifier corrections, contour correction and inhomogeneity corrections.

##### 2.1.4.1.1 Linear attenuation

The ordinary of inhomogeneity correction is to adjust the point dose by foundation of the thickness of the inhomogeneity medium by using a percentage per centimeter correction. The inhomogeneity correction is given by

$$\text{ICF} = (\% \text{ per cm}) \times \text{inhomogeneities thickness (cm)} \quad \dots(2.11)$$

where the percentage per cm is obtained by the experiment (+3.0% in lung and -2.0% in bone for 4-6 MV). In addition, this method is not corrected for patient specific densities and the irradiated beam parameters such as field size.

##### 2.1.4.1.2 Effective attenuation coefficient

The correction was developed and resemble of the effective attenuation coefficient. The inhomogeneity correction is obtained by

$$\text{ICF} = e^{\mu'(d-d')} \quad \dots(2.12)$$

where  $\mu'$  is the effective attenuation coefficient of water for a particular beam quality.  $d$  is the physical depth from the surface to the point of calculation and  $d'$  is the radiological depth that is given by

$$d' = \sum_i (\Delta d_i) \times \rho_i \quad \dots (2.13)$$

where  $\Delta d_i$  are the thicknesses of tissues with different relative electron densities ( $\rho_i$ ) lying above the point of calculation.

#### 2.1.4.1.3 Ratio of tissue air ratios (RTAR)

The older commercial treatment planning systems used this method for inhomogeneities correction. In present day, physicists often perform manual point dose calculation that called “effective SSD method” or “isodose shift method”. The correction is defined as

$$ICF = \frac{TAR(d',r)}{TAR(d,r)} \quad \dots (2.14)$$

where  $d'$  is the equivalent path length given by equation 2.13,  $d$  is the physical depth and  $r$  is the field size at the depth of interest. Therefore, the primary component generates a radiological depth that is applied for looking up a revised tissue air ratio (TAR) value. If the condition of electron equilibrium (CPE) occurs, this method accords a certain correction for the primary fluence. Notwithstanding, the tissue maximum ratio (TMR) values were used instead of the TAR values as they are formally identical. The facility of this method leads to favor manual dose calculation; anyway it's the best of one's ability to approximately account for scatter changes due to field size and effective depth. Howbeit, the drawback of this method is its compromised modeling of the lateral component of the scattered photon contribution which results in an over correction in case of low density medium and under correction when the density more than water.

#### 2.1.4.1.4 Power law (Batho) method

The Batho method was proposed by Batho in 1964 and Young and Gaylard in 1970, afterward Sontag and Cunningham's modified the correction factor at calculation point lying in a two layer slab [17, 18, 19, 20 and 21]. The inhomogeneity correction of TAR depends on density of medium as given by

$$\text{ICF} = \frac{\text{TAR}(d_1, r_d)^{\rho_1 - \rho_2}}{\text{TAR}(d_2, r_d)^{1 - \rho_2}} \quad \dots(2.15)$$

where  $\rho_1$  is relative electron density of the medium in which the point of calculation lies,  $\rho_2$  is relative electron density of the overlying material,  $d_1$  is depth within this medium, and  $d_2$  is distance to the upper surface of overlying material. However, Sontag and Cunningham (1977) proposed the assumptions for this equation by [20]: firstly, it is assumed that the material below the point is the same as it lies. Secondly, the effect of an inhomogeneities on the dose to a point is independent of the thickness of tissue ( $\rho=1$ ) above the inhomogeneity. Thirdly, the electronic equilibrium is remained. Finally, the lateral dimensions of all regions are assumed to equal at least those of the beam. The models of Batho method are distinction of exponential nature of photon attenuation with the multiplicative power law and extended to multilayer geometries.

The advent of computed tomography (CT) introduced the 1D method in which tissue densities were available. Afterward this method was modified by Webb and Fox [22] that they applied the CT data to inhomogeneity correction as given by

$$\text{ICF} = \frac{(\mu_{\text{en}}/\rho)_N}{(\mu_{\text{en}}/\rho)} \prod_{m=1}^N \text{TAR}(d_m, A)^{\frac{(\mu_m - (\mu_{m-1}))}{\mu_0}} \quad \dots(2.16)$$

where N is number of layers of different densities above the point of calculation, m is layer number,  $d_m$  is distance from point of interest to the surface of the  $m^{\text{th}}$  layer,  $\mu_m$ ,  $\mu_0$  is linear attenuation coefficient of the  $m^{\text{th}}$  layer, A is the field size,  $(\mu_{\text{en}}/\rho)$  is mass energy absorption coefficient for water and  $(\mu_{\text{en}}/\rho)_N$  is mass energy absorption coefficient of the inhomogeneity layer N. The adjustment of this equation used TMR instead of TAR that the depth of  $d_{\text{max}}$  is added to the depth  $d_m$  as defined by

$$\text{ICF} = \frac{(\mu_{\text{en}}/\rho)_N}{(\mu_{\text{en}}/\rho)} \prod_{m=1}^N \text{TMR}(d_m + d_{\text{max}}, A)^{\frac{(\mu_m - (\mu_{m-1}))}{\mu_0}} \quad \dots(2.17)$$

## 2.1.4.1.5 3-D beam subtraction method [11, 23, 24, 25, 26]

Kappas and Rosenwald proposed 3-D beam subtraction method developed for parallelepiped inhomogeneities and based on a beam subtraction method. The original method is based on Day method that point dose at any off axis in rectangular  $2X \times 2Y$  irradiated field calculated by the average dose contributions from four independent rectangular sections located around P as shown in figure 2.3.

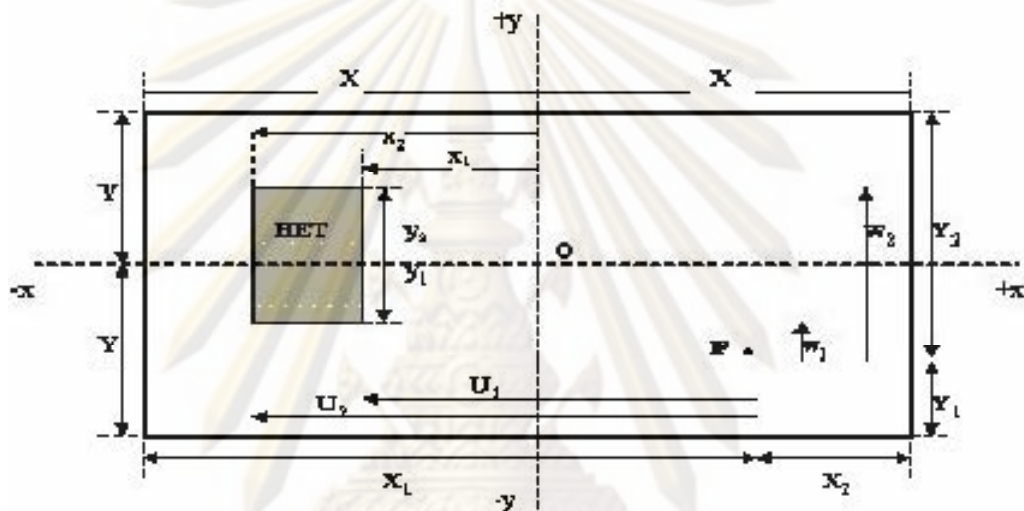


Figure 2.3 The rectangular heterogeneity material in an irregular field with dimensions  $2X$  and  $2Y$ .

The assumption of this method is the electronic equilibrium existed and using the two approximations. Firstly, the primary dose is altered by the presence of inhomogeneities that lying on the central axis. Secondly, the lateral dimensions of the inhomogeneities larger than the field dimensions. Then the inhomogeneity correction is given as [11]

$$ICF = 1 + \frac{\sum_{i=1}^2 (-1)^i \sum_{j=1}^2 (-1)^j [\epsilon'_{ij} (C_{ij} - 1) D_0^W(U_i, W_j)]}{\sum_{i=1}^2 \sum_{j=1}^2 [\epsilon'_{ij} D_0^W(X_i, Y_j)]} \quad \dots (2.18)$$

where  $\epsilon'_{ij}$  is the sign of the product  $U_i, W_j$ . The  $U_i$  and  $W_j$  is the algebraic distances from point P to the inhomogeneities limits.  $D_0^W(U_i, W_j)$  is the dose at the center of the corresponding rectangular field in the absence of the inhomogeneity.  $X_i, Y_j$  are the distances from the point of calculation to the rectangular field. The

correction factor  $C_{ij}$  is the on-axis conventional correction factor for the field  $U_i$  and  $W_j$  such as power law Batho or ETAR methods. The scatter dose from the lateral neighboring homogeneous medium assumed that it is not modified by the presence of the inhomogeneity. For this assumption, the dose within tissue densities less than unity is underestimated.

#### 2.1.4.2 Model based methods [15]

The model based principles calculated dose distribution by modeling the actual radiation transport involved in the scatter photon and electrons from the interaction site. For high energy photon beams (more than 6MV), the scatter component is less important. The assumption of electronic equilibrium existed by above are not adequate to estimate dose. The effects of electrons set in motion by photons directed to higher dose changes locally.

##### 2.1.4.2.1 Convolution methods

The model based methods have been developed based on the transport of secondary electrons imparted from primary photon interactions. The energy deposited kernels were model from the site of photon interaction in water by analytical approximation or Monte Carlo simulations. The kernel that the pattern of energy deposited in an infinite medium around the primary photon site is the point kernel. For the pattern of energy deposited in a semi-infinite medium from a point monodirectional beam is the pencil beam kernel. The dose obtained the energy fluence distribution convolved with the scatter spread kernel.

##### (a). Point kernel methods

The first scatter photons transferred energy depended on the constitution of the medium between the primary photon interaction site and the dose deposition point.

##### (b). Pencil kernel methods

The developing algorithms which entirely account for beam modulations and irregular fields but rely on broad beam scaling/correction



methods to handle heterogeneities and patient outlines (Batho Method) are pencil kernel methods. The pencil kernel is the energy deposited in a semi-infinite medium from a point monodirectional beam.

#### 2.1.4.2.2 Convolution- superposition methods

The principle of the dose calculation of convolution and superposition methods is based on circumstance of inhomogeneity correction for both the TERMA distribution and the dose spread kernel. The kernel describes the distribution of the scatter from primary interaction. This algorithm including a convolution equation which separately considers the transport of primary photons and the scatter photon and electron occur from the primary photon interaction. The analytical anisotropic algorithm (AAA) is based on the convolution method that the dose of each pencil beam is calculated through a convolution [27, 28, 29]. The pencil beam split to beamlet involved the beamlet energy fluence. The beamlet energy fluence includes the primary photons, extrafocal photons and contaminant electron component creating from the flattening filter, ion chamber, collimating jaws and air. The model of dose contribution from beamlet is convolution of the fluence and energy deposition density function with scatter kernel that defines the lateral dose scattering in the phantom. Each contributing function including fluence, energy deposition density function, and scatter kernel is defined separately for each of the energy fluence components. The analytical method is the function demonstrated the energy fluence components and the primary and scatter kernels. The convolution integral through the beamlet dimensions are solved analytically. The accuracy at the boundary of inhomogeneities depends on the photon scatter that is convolved with a density scaled kernel along the beamlet direction. The total dose deposited in irradiated area is calculated as superposition of beamlet contributions.

#### 2.1.5 Intensity-modulated radiation therapy (IMRT) [30]

The process that changed beam intensity profiles of treatment plan is called intensity modulation. Normally, conventional radiation therapy is delivered uniform

intensity though tumor volume. The 3D-CRT is defined by irradiating target volume in a three dimensional anatomic image with individual beam shaped to conform the target. This technique required computed tomography (CT) to reconstruct images for geometric and dosimetric computations and MLCs to block normal tissues surrounding tumor volume. The IMRT is developed from 3D-CRT to non-uniform dose distributions that achieved tumor dose while dose at organ at risk (OAR) is minimized.

#### 2.1.5.1 Fixed-Gantry IMRT

Fixed-gantry IMRT is based on number of fixed beam directions as likely 3D-CRT. However, the modification of the intensity profiles may be used wedges or compensators called compensator-based delivery. In modern treatment machine, the multileaf collimators (MLCs) are used to modulate the known as MLC-based delivery. For this method, the dose optimization generates intensity profile for each incident beam and creates the MLC sequence files which are used to control the MLC movement for radiation delivery. The radiation dose delivery is divided into step-and-shoot and dynamic modes. The beamlet width in which dimension is perpendicular to the leaf travel direction depends on the MLC leaf width.

#### 2.1.5.2 Treatment planning for IMRT

The manual forward planning for dose delivery that uses in simple cases is not adequate for IMRT. Generally, an inverse treatment planning obtains the optimal beam parameters by starting from a prescribed dose distribution. In this method, computer optimization algorithm determined the optimal beam parameters leads to a solution output that specified by a desired dose distribution, dose volume histograms (DVHs) or even the tumor control probability (TCP) and normal tissue complication probability (NTCP).

#### 2.1.5.3 Dose optimization algorithms

The numerous algorithms have been developed for the optimization of a multidimensional function in sciences and engineering over the years. The selection of

an optimization technique depends on the specific form of the objective function. The methods based on inverse planning are divided into two categories.

The iterative method is the most available of technique in dose optimization. The method calculates an initial approximation solution and results to optimal one. The process of iterative provides many steps. Firstly, assume an initial set of beam profiles. Secondly, compute the dose at a voxel. Thirdly, compare the calculated and prescribed doses. Fourthly, obtain correction factors to the beamlets that irradiate the voxel. Finally, apply the correction to the contributing beamlets and then repeat from step 2 for the next voxel. The process is repeated until the requirement accuracy is obtained.

Simulated annealing algorithm is originally from Monte Carlo simulation algorithm. The simulated annealing solves the behavior of metals annealing. The process involves a controlled process of slow cooling and to maintain thermal equilibrium while reaching the ground state. This algorithm was used to calculate dose optimization to minimize the overall cost function until the desired goal is achieved in which the difference between the calculated dose distribution and the prescribed dose is minimized.

#### 2.1.5.4 The dose delivery methods for fixed-gantry IMRT

The IMRT is complexed 3D conformal radiation therapy technique that employs non-uniform dose distributions to maximum dose at target volume while dose to organ at risk (OAR) is reduced. In conventional radiation therapy, the computer-controlled MLC is used to shape beam and modulate intensity beam to dose delivery IMRT.

##### 2.1.5.4.1 Step-and-shoot delivery

A step-and-shoot method creates subfields and leaf sequence to generate the intensity modulation. The total dose for all beamlets is obtained from the superposition of series of subfields that the number of subfields ranging from 20 to 100.

The accelerator is turn-off when MLCs travel from one segment to another. The intensity modulated beam was produced by dose integrated delivery to each subfield.

#### 2.1.5.4.2 Dynamic delivery

Unlike step-and-shoot mode, the leaves of dynamic delivery move simultaneously during beam on. When the radiation is on, each leaf has different velocity as a function of time depended on treatment planning system.

#### 2.1.6 Contour irregularities correction [15, 31]

The incident beam was perpendicular to a surface contour which may be curved or irregular in shape. The dose distributions were corrected by Tissue-Maximum Ratio method. The principle of tissue-maximum ratio method depended on the tissue-maximum ratio at the specific depth and field size. If the tissue deficit above calculation point is  $h$  cm and depth below surface contour is  $d$  cm. The correction factor obtained by the ratio of tissue-maximum ratio for depths  $d$  and  $d + h$  is given by

$$CCF = \frac{TMR(d,r)}{TMR(d+h,r)} \quad \dots(2.19)$$

where **CCF** is contour correction factor, **TMR** is the tissue-maximum ratio and **r** is the field size projected at calculation point.

#### 2.1.7 Modified Clarkson integration algorithm [8, 15, 31]

The Clarkson's method has been used to calculate the point dose for irregular fields. The principal of Clarkson's method is based on the irregular field split to scatter dose from primary dose at specific depth and radii. The modification of Clarkson integration is developed to calculate any point dose inside MLC treatment field based on circular field data. This method needs some special quantities from measured data, those are: the tissue maximum ratio  $TMR_{(d,r)}$ , the tissue maximum ratio at zero field size  $TMR_{(d,0)}$ , the scatter maximum ratio  $SMR_{(d,r)}$ , the phantom scatter factor ( $Sp$ ) and the phantom scatter factor at zero field size  $Sp(0)$ . The average scattered dose is added to the primary beam, and then the dose is calculated.

A set of MLC for irregular field is divided into various angular segments for calculating dose. The scatter dose of each angular segment is calculated by the radius of circular field in irregular MLC shape. The average of scatter dose for irregular MLC shape was obtained by

$$\overline{\text{SMR}}_{(d,r)} = \frac{1}{N} \sum_{k=1}^N \text{SMR}_{(d,k)} \quad \dots(2.20)$$

where  $\text{SMR}_{(d,k)}$  is the scatter dose of a circular field with radius  $k$  at depth  $d$  and  $k$  is the radius of the  $k^{\text{th}}$  sector. The TMR of the irregular field at any point is calculated by

$$\text{TMR}_{(d,r)} = [\text{TMR}_{(d,0)} + \overline{\text{SMR}}_{(d,r)}] \times \frac{\text{Sp}(0)}{\overline{\text{Sp}}(r)} \quad \dots(2.21)$$

where  $\overline{\text{Sp}}(r)$  is the average phantom scatter factor for irregular field,  $\text{Sp}(0)$  is the phantom scatter factor for the zero field size,  $\text{TMR}_{(d,r)}$  is the tissue maximum ratio of a circular field with a radius of  $r$  at depth  $d$  and  $\overline{\text{SMR}}_{(d,r)}$  is the average scatter maximum ratio of a circular field with a radius of  $r$  at depth  $d$ . The total dose in water is obtained by

$$D(w, R)_{\text{Total}} = \text{MU} \times \text{TMR}_{(d,r)} \quad \dots(2.22)$$

where  $D(w, R)_{\text{Total}}$  is the total dose in water of irregular MLCs field, MU is the monitor unit.

#### 2.1.8 Multiplanar reconstructions (MPRs) [34]

Multiplanar reconstructions (MPRs) are images formed from reformatted CT data. They are effectively CT images through arbitrary planes of the patient. Although typically sagittal or coronal MPR cuts are used for planning and simulation, MPR images through any arbitrary plane may be obtained. Field shaping is determined with respect to both the anatomy visible on the MPR and the outlined structures projected by the Beam's eye views (BEVs). BEVs are projections of the treatment beam axes, field limits and outlined structures through the patient on to the corresponding virtual film plane, and are frequently superimposed on to the corresponding MPR, resulting in a synthetic representation of a simulation radiograph.

### 2.1.9 Quality assessment of computerized treatment planning systems [32, 33, 34, 35]

The quality control (QC) is defined as a process of comparing measurements and standard data. The quality assessment is essential to provide within confidence. Normally, the quality assessment of computerized treatment planning systems is referred to qualitative and quantitative analysis. The accuracy of calculation dose distribution depends on the parameterization by user and the dose calculation algorithm. Anywise, the percentage of deviations between the calculations and measurements is given by

$$\delta = 100 \times \frac{(D_{\text{cal}} - D_{\text{meas}})}{D_{\text{meas}}} \quad \dots(2.23)$$

where  $\delta$  is the percentage of deviation.  $D_{\text{cal}}$  is the calculated dose at a particular point in the phantom and  $D_{\text{meas}}$  is the measured dose at the same point in the phantom. The criteria of acceptability of the percentage of deviation defined the dose calculation algorithms provide better accuracy in some regions of the beam than other as shown in figure 2.4.



ศูนย์วิทยทรัพยากร  
จุฬาลงกรณ์มหาวิทยาลัย

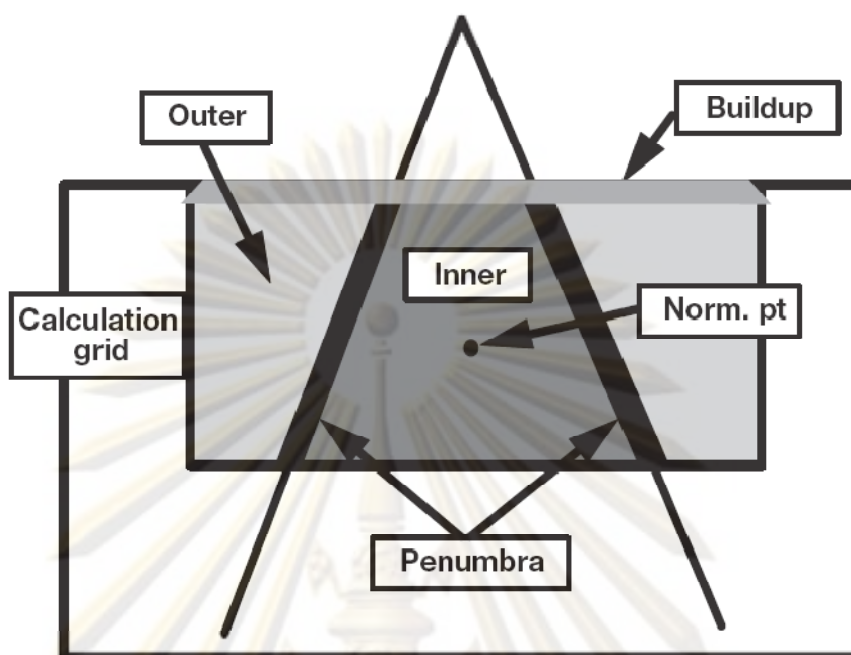


Figure 2.4 The regions of criteria acceptability for photon beam dose calculations.

The consideration of tolerances depends on the dose calculation algorithm which can be used in table 2.1.

Table 2.1 The criteria of acceptability for photon dose calculation algorithm by IAEA TRS. 430

Situation	Dose at normalization point (%) <sup>a</sup>	Central ray (%)	Inner beam (%)	Penumbra (mm)	Outer beam (%)	Buildup region (%)
Homogeneous phantoms						
Square fields	0.5	1	1.5	2	2	20
Rectangular fields	0.5	1.5	2	2	2	20
Asymmetric fields	1	2	3	2	3	20
Blocked fields	1	2	3	2	5	50
MLC shaped fields	1	2	3	3	5	20
Wedged fields	2	2	5	3	5	50
External surface variations	0.5	1	3	2	5	20
SSD variations	1	1	1.5	2	2	40
Inhomogeneous phantoms <sup>b</sup>						
Slab inhomogeneities	3	3	5	7	5	-
3-D inhomogeneities	5	5	7	7	7	-

Note: Percentages are quoted as per cent of the central ray normalization dose.

<sup>a</sup>Absolute dose values at the normalization point are relative to a standard beam calibration point.

<sup>b</sup>Excluding regions of electronic disequilibrium.

## 2.2 Related literatures

Prior studies have reported the evaluation of dose calculation algorithms of RTPS with independent monitor unit calculation softwares in homogeneous medium, some work considered the inhomogeneity effect.

George et al [5] implemented the calculation of monitor units as part of the process of commissioning a photon beam model in a treatment planning system. The monitor units were calculated using the treatment planning systems (COPPERPlan and Pinnacle) and they were compared with monitor units calculated from point dose calculations (TMR tables). A set of beam configurations, with varying rectangular field sizes, secondary blocking, wedges and SSDs was used to calculate monitor units. The COPPERPlan and Pinnacle used the fast-Fourier transform (FFT) convolution and convolution/superposition algorithms at central axis depth dose data. The discrepancy in monitor unit calculations was up to 5%. They recommended incorporating a comprehensive validation of monitor unit calculations as part of any beam commissioning process.

Haslam et al [7] reported the isocenter dose calculated by an independent monitor unit verification calculation (MUVC) software using a modified Clarkson integration technique called 'RadCalc". RadCalc was compared with a commercial radiation treatment planning system (CORVUS treatment planning system). The CORVUS planning system and RadCalc were compared with ion chamber measurements. Prior to measurement, the ion chamber was calibrated to a standard dose resulting in a measurement uncertainty of approximately 1%. The totals of 303 patients with 507 treatment plans were calculated for point dose. The site specific for head and neck, prostate, female pelvis, rectum and abdomen for dose calculations were included. The average calculation dose by RadCalc was 1.4% higher than the treatment planning dose, with a 1.2% standard deviation. They concluded that the overestimate in tissue will result in an increase of the scatter contribution to the isocenter dose. In this analysis, however, heterogeneity corrections were not performed and the contour patient's skin was performed manually by operator.



Lombardi et al [4] studied the accuracy of monitor unit (MU) calculation in clinical shaped beams by applying different methods which normally used in clinical practice. The method included empirical area weighted method, Area-to-perimeter ratio or Wrede method, Clarkson's scatter summation method and a pencil-beam based algorithm of Cadplan treatment planning. The 40 clinical irregular fields in 6MV photon beams were considered. The dose measurements were performed with an ionization chamber in an acrylic phantom. The mean deviations between measured and expected dose values were around 0 for all the methods. The difference between calculated and measured dose were within 1% for all the methods. Maximum deviations range from 1.6% of pencil beam to 3% of Wrede method.

Jingeng et al [8] verified a routine point dose calculation for IMRT/IMRS plan which was developed using the original Clarkson's method. The segmented MLC sequences created by the IMRT/IMRS inverse planning were converted into irregular subfields for Clarkson's calculation. The result of each subfield is weighted by its weighting factor and summed to provide the total dose. The point dose of an inverse plan is obtained by summing the doses of all IMRT fields. Point dose calculations were done for the 29 IMRS cases and the results were compared with that calculated by the BrainLab treatment planning software that used a pencil beam dose calculation algorithm. Comparing the doses calculated by this routine to that reported by the treatment planning system, the minimum difference was 0.064%, the maximum difference was 2.7%, and the mean difference was 1.4% with standard deviation of 0.78. The results showed that it was reliable, intuitive and accurate but did not correct for the heterogeneity of the media.

Kung et al [9] reported the accuracy of the independent monitor unit verification calculation (MUVC) in IMRT by modified Clarkson integration (MCI). They calculated the dose along a central axis (CAX). They assumed a flat tissue contour and a homogeneity tissue but did not include any second-order effects such as tongue and groove. The only MLC head scatter effects used was the radiation field offset. The computer code was written in MATHEMATICA 3.0 to implement the MCI technique. The

code used measured beam data for  $Sc$ ,  $Sp$ ,  $TPR$ ,  $(D/MU)_{ref}$  and included effects from Multileaf collimator transmission. The doses calculated with the MCI algorithm agreed within 3% of these calculated by CORVAS, which used a 1cm x 1cm pencil beam in the dose calculation. The agreement between MCI and measurement was not performed. The skin contour variations and inhomogeneities were not used.

Sotirios et al [12] proposed the principle of Clarkson's method on sector integration to take into account the position and lateral extent of the inhomogeneities with respect to the point dose calculations. This principle combined the 3D-BSM and Clarkson's method of sector integration. They predicted the correction factors for Co-60 and 6MV photon beams for irregular fields that included inhomogeneities of lower or higher densities relative to water. The results were compared against Monte Carlo calculations, with results obtained from the PLATO RTPS (Nucletron B.V., Veenendaal in the Netherlands) using ETAR and with results of the Batho. The results did not take into account the field shape. The difference among ETAR, Batho, and the 3D-BSM IRREG was about 2.5%. The agreement between the predicted correction factors and the Monte Carlo calculations was within 1.5%. They found that the BSM IRREG results were in very good agreement with the Monte Carlo results. They concluded that method improves the basic inhomogeneities correction method by taking into account that the point of calculation could be anywhere in the irradiating volume and the shape of the field could be altered by the presence of shielding blocks.

Chen et al [6] stated the Clarkson summation algorithm to calculate the dose to the isocenter of IMRT treatments. The independent dose calculation was performed using the leaf sequences generated by CORVUS treatment planning system and the patient geometry obtained from CT-simulations. The patient geometry was generated from a virtual simulation in a set of digital reconstructed radiographs (DRRs) in the beam's eye view (BEV) for each field. The results showed an agreement between the calculated isocentre doses and the CORVUS calculation to within 3%. They concluded that result was taken to be sufficient grounds to omit the ion chamber measurement for dose verification in the IMRT QA process.

Xing et al [10] informed the monitor unit calculation in IMRT as a summation of the contributions from all the beamlets. The dose from each individual beamlet was calculated using Clarkson's method and compared with CORVUS treatment planning system. Some specific issues related to the clinical implementation of the formalism, such as the effect of skin contour variation, off-axis dose calculation, effect of tissue density inhomogeneities, and the verification in the low dose region were discussed. The results showed that the calculated dose agreed with the CORVUS calculation within 4% except for the 6MV liver case where the deviation was larger than 7%.

Plessis et al [36] compared the Batho, ETAR and Monte Carlo calculation methods in CT-based patient models. Dose distributions were calculated with the Batho and ETAR inhomogeneities correction algorithms in head/sinus, lung, and prostate patient models. The dose comparisons were expressed in terms of 2D isodose distributions, percentage depth dose data, and dose difference volume histograms (DDVH's). The results showed that the Batho and ETAR methods contained inaccuracies of 20%-70% in the maxillary sinus region in the head model. Large lung inhomogeneities absorbed dose deviations of 10%-20%. The important point in this study showed that materials with densities that deviated substantially from water presented difficulties for these inhomogeneities correction algorithms due to their inability to model longitudinal and lateral electron transport. They concluded that the inhomogeneities correction methods were inaccurate for dose calculation.

Shahine et al [14] investigated the dose at air/polystyrene interface and as a function of depth. The results of this experiment were compared to the calculations using three computerized radiation treatment planning systems including Batho, modified Batho, and ETAR methods for inhomogeneities corrections. The measured results were 10% lower than three treatment planning systems. This is because the calculation algorithms employed do not incorporate electron transport. The under dose observed may be significant at depths of several centimeters from the interface for smaller field sizes and air gaps approaching the field size in their lateral dimensions.

The Batho method did not show any sensitivity to the position of air gap sidewalls. These point needed proper inclusion of disequilibrium effects and shape of inhomogeneity.



ศูนย์วิทยทรัพยากร  
จุฬาลงกรณ์มหาวิทยาลัย

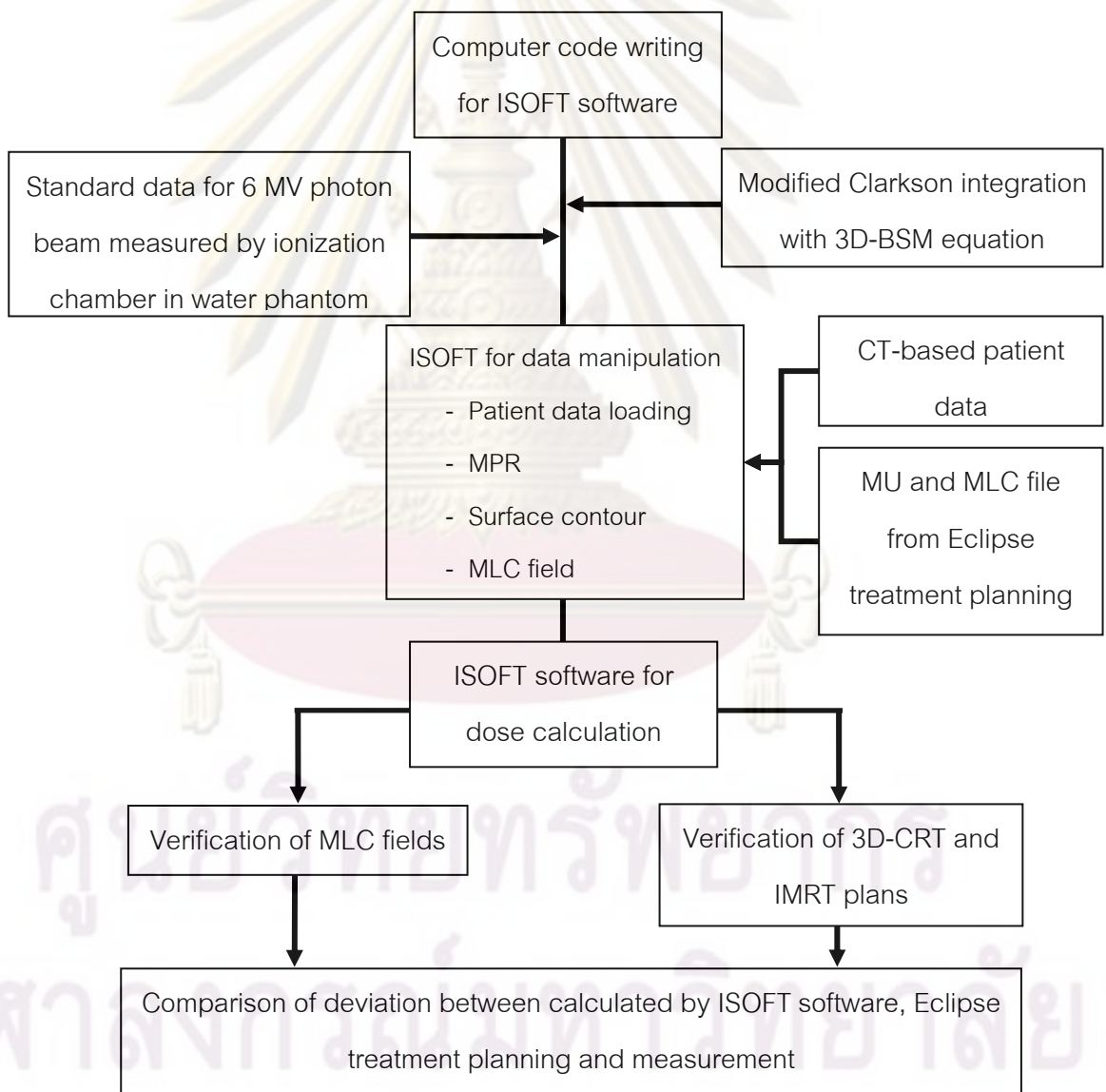
## CHAPTER III

### RESEARCH METHODOLOGY

#### 3.1 Research design

The study is the experimental study.

#### 3.2 Research design model



### 3.3 Key words

- Intensity modulated radiation therapy (IMRT)
- CT-based patient data
- Radiation treatment planning system (RTPS)
- Clarkson integration algorithm
- Three dimension beam subtraction method (3D-BSM)

### 3.4 Research questions

#### 3.4.1 Primary question

Can the developed independent software be used for dose calculation in inhomogeneities of lung phantom from CT-based patient data of intensity modulated radiation therapy (IMRT)?

#### 3.4.2 Secondary question

What is the dose difference between calculated by independent software and computerized radiation treatment planning system compared with the measurement?

### 3.5 Scope of Dissertation

The independent software is used to verify dose in homogeneous phantom and inhomogeneous lung phantoms for single field of 3D-CRT and IMRT plans. The algorithm for dose calculation of independent software is the Clarkson integration algorithm with 3D-BSM. The step and shoot IMRT is considered.

### 3.6 Materials

#### 3.6.1 Computed Tomography Simulation

The Computed Tomography Simulation (CT simulation) employed in the experiment is Light speed RT manufactured by General Electric (GE) as shown in figure 3.1. This is a standard diagnostic CT scanner with an additional laser alignment system

and software that provides beam edge display, 3D image reconstruction and high-quality digitally reconstructed radiographs (DRRs).

The major complements of a state-of-the-art CT simulator include:

1. A CT scanner and couch.
2. A CT computer console.
3. The networked 3D image and virtual simulation workstations. Virtual simulation is an software to set up the treatment field for advanced 3D geometric treatment planning. It combines powerful image processing capabilities with a full range of volume segmentation tools for creating 3D structures necessary for the design and simulation of treatment fields.
4. A moving laser marking system with 4 laser lines.
5. A laser hardcopy device.



Figure 3.1 Computed Tomography Simulation Light speed RT manufactured by General Electric GE.

### 3.6.2 Linear accelerator (LINAC)

The linear accelerator used for the experiment is Clinac 21EX manufactured by Varian Associates, Palo Alto, USA with dual x-ray energies, 6 MV and 10 MV which field sizes range from  $0.5 \times 0.5 \text{ cm}^2$  to  $40 \times 40 \text{ cm}^2$  at 100 cm source-axis distance in symmetric mode and five electron energies of 6, 9, 12, 16 and 20 MeV which field size ranged from  $4 \times 4 \text{ cm}^2$  to  $25 \times 25 \text{ cm}^2$  as shown in figure 3.2. Its independent collimator system provides motion of the upper and lower set of field defining collimators both symmetric and asymmetric mode of operation. The MLCs with 80 leaves of 1 cm width are mounted below the conventional collimator in the same direction of X-jaws. Only 6 MV and 300MU/min photon beam was chosen for the experiment.



Figure 3.2 Clinac 21EX Linear accelerator manufactured by Varian Associates, Palo Alto, USA.



### 3.6.3 Eclipse radiation treatment planning system

The treatment planning system for this experiment is Eclipse Version 6.5 manufactured by Varian Associates Palo Alto, USA as shown in figure 3.3. The system consists of multiple components both in terms of hardware as well as software that allow the user to produce and display calculated dose distributions from which a physician will prescribe a patient's radiation treatment. The Eclipse can be calculated dose distribution for all modalities such as 3D-CRT, IMRT, electron and brachytherapy. The calculation algorithms were separated to Pencil beam convolution algorithm including inhomogeneity correction of Batho method, modified Batho method and ETAR method and Analytical an Isotropic algorithm (AAA). The step and shoot technique of IMRT is selected for this study.

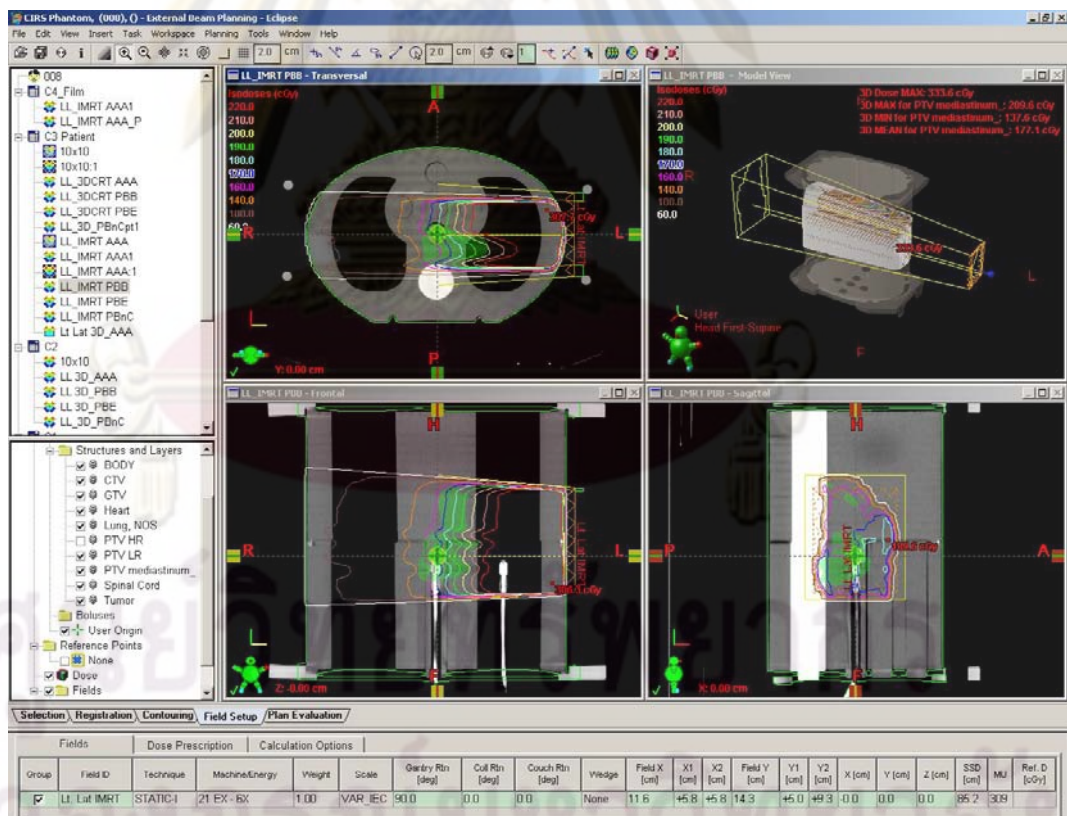


Figure 3.3 The radiation treatment planning system Eclipse Version 6.5 manufactured by

Varian Associates Palo Alto, USA.

### 3.6.4 Electron density phantom

The accuracy of dose calculation in heterogeneous materials depends on calculation algorithm of computerized treatment planning systems. The RTPS used CT data for inhomogeneity correction. Thus correlation of CT data (CT number) and electron density of various tissues are obtained by scanning the electron density phantom. In this study, the Gammex 467(Middleton, USA) tissue characterization electron density phantom which consists of sixteen different tissue references including any fluid or solid materials is selected. The positions of tissue equivalent plugs hold the position at different locations within the phantom as shown in figure 3.4. The physical density ( $\text{g/cm}^3$ ) and electron density relative to water of rod materials are shown in table 3.1.



Figure 3.4 Electron density phantom GAMMEX 467 Middleton, USA.

Table 3.1 The physical density ( $\text{g/cm}^3$ ) and electron density relative to water of electron density phantom GAMMEX 467.

Rod Material	Electron Density Relative to Water	Physical Density $\text{g/cm}^3$
Lung (LN-300)	0.28	0.30
Lung (LN-450)	0.40	0.45
Adipose (AP6)	0.90	0.92
Breast	0.96	0.99
CT Solid Water	0.99	1.02
Brain	1.05	1.05
Liver (LV1)	1.07	1.08
Inner Bone	1.09	1.12
Bone (B200)	1.11	1.15
Bone (CB2-30% Mineral)	1.28	1.34
Bone (CB2-50% Mineral)	1.47	1.56
Cortical Bone (SB3)	1.69	1.82
True Water	1.00	1.00
Optional Titanium Insert	3.79	4.59

### 3.6.5 IMRT thorax phantom

The CIRS Model 002LFC IMRT Thorax Phantom is used to measure and calculate dose as shown in figure 3.5. The 002LFC is elliptical in shape and properly represents an average human torso in proportion, density and two-dimensional structure. The dimension is  $30 \times 30 \times 20 \text{ cm}^3$  [36]. The phantom is constructed of proprietary tissue equivalent epoxy materials. Linear attenuations of the simulated tissues are within 1% of actual attenuation for water and bone, and within 3% for lung from 50 keV to 25 MeV.

Tissue equivalent inter changeable rod inserted the ionization chambers allowing for point dose measurements in multiple planes within the phantom. The

ionization chamber can be inserted for point dose verification of individual plans and delivery. A half of the phantom is divided into 12 sections, each 1 cm thickness, to support radiographic or GafChromic film.



Figure 3.5 The CIRS Model 002LFC IMRT Thorax Phantom.3.6.6 Film measurement

The Kodak's EDR2 ready-pack film is shown in figure 3.6. The EDR2 film is a very slow speed, fine grain film pressed grain cubic microcrystals. In addition, the advantages of EDR2 film are extended dose range capability and improve exposure linearity. The film emulsion is coated double layers on a 0.18 mm Estar base, which allows processing in a conventional rapid-process film processor. The responsive is ranging from 25 to 400 cGy with saturation dose approximated of 700 cGy [37, 38, 39]. For minimize batch variation, all films are selected for the same box. A Vidar film scanner (Vidar-16) is used to scan to obtain the TIFF image files with 16 bit grey scale. The scanner is performed as an optical density (OD) output and the dose distribution can be calculated if the sensitometric curve is undertaken.



Figure 3.6 The Kodak's Ready-Pack film EDR2 for 2D dose distribution.

#### 3.6.7 Vidar scanner

The digitizing scanner in this study is the Vidar VXR-16 DosimetryPRO™, the 16 bits output represented grayscale data with a resolution of 142 dots per inch (0.179 mm/pixel) as shown in figure 3.7. The film scanner is capable to meet the DICOM community for exacting application of radiation dosimetry. The film scanner represents 65,536 shades of gray with optical density (OD) ranging from 0.00 to 3.65. The accuracy of geometric is more than 1% or 2 pixels.

ศูนย์วิทยทรัพยากร  
จุฬาลงกรณ์มหาวิทยาลัย



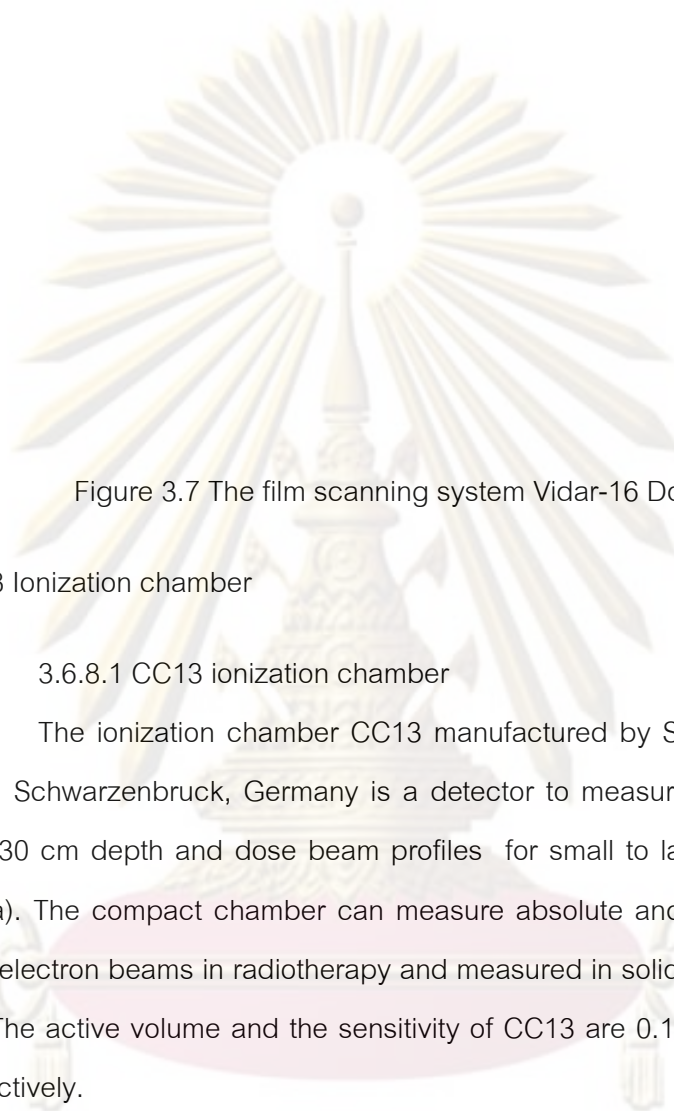


Figure 3.7 The film scanning system Vidar-16 Dosimetry Pro

### 3.6.8 Ionization chamber

#### 3.6.8.1 CC13 ionization chamber

The ionization chamber CC13 manufactured by Scanditronix/ Wellhofer Dosimetries, Schwarzenbruck, Germany is a detector to measure % depth dose data from 1.5 to 30 cm depth and dose beam profiles for small to large field as shown in figure 3.8 (a). The compact chamber can measure absolute and relative dosimetry of photon and electron beams in radiotherapy and measured in solid phantoms or in water phantoms. The active volume and the sensitivity of CC13 are  $0.13 \text{ cm}^3$  and  $2.647 \times 10^8 \text{ Gy/C}$ , respectively.

#### 3.6.8.2 FC65-P ionization chamber

The ionization chamber FC65-P manufactured by Scanditronix/ Wellhofer Dosimetries, Schwarzenbruck, Germany as shown in figure 3.8 (b) is used for point dose measurement. The absolute dose of photon beam is measured in water phantom (WP1D, Scanditronix/ Wellhofer Dosimetries, Schwarzenbruck, Germany). The active volume and the sensitivity of FC65-P are  $0.65 \text{ cm}^3$  and  $4.8344 \times 10^7 \text{ Gy/C}$ , respectively.



(a) CC13 ionization chamber

(b) FC65-P ionization chamber

Figure 3.8 Ionization chamber (Scanditronix/ Wellhofer Dosimetries).

(a) The CC13 ionization chamber (b) FC65-P ionization chamber

### 3.6.9 Electrometer

The electrometer DOSE1 manufactured by Scanditronix/ Wellhofer Dosimetrie, Schwarzenbruck, Germany is connected to ionization chambers, semiconductors and diamond detectors for the reading of charge or current. The standard DOSE1 connects to either TNC or BNC connector types. The voltage supply is set at 300 V. Maximum charge per pulse is approximate  $\pm 40$  nC/pulse. The DOSE1 dosimeter is shown in figure 3.9.



ศูนย์วิทยทรัพยากร  
จุฬาลงกรณ์มหาวิทยาลัย



Figure 3.9 DOSE1 electrometer manufactured by Scanditronix/ Wellhofer Dosimetrie, Schwarzenbruck, Germany

#### 3.6.10 Three dimension beam analyzing system

The 3D beam analyzing system (Blue phantom) manufactured by Scanditronix/ Wellhofer Dosimetries, Schwarzenbruck, Germany is the phantom for beam data measurements as shown in figure 3.10. The water phantom is made from acrylic plastic (perspex), having the scanning volume of  $48 \times 48 \times 41 \text{ cm}^3$ . The percentage depth dose and dose beam profile are measured with CC13 ionization chamber. These data are put into the treatment planning system and the algorithm calculated the isodose distribution. The phantom is controlled by OmniPro Accept software version 6.4a manufactured by IBA Advanced Radiotherapy, Scanditronix/ Wellhofer, Uppsala, Sweden.

The 3D beam analyzing system comprises of a three-dimensional high precision servo mechanism and perspex water tank. On the horizontal x-rail there is a sliding show on which detector holders are in all three dimensions or measuring both horizontal and vertical beams.



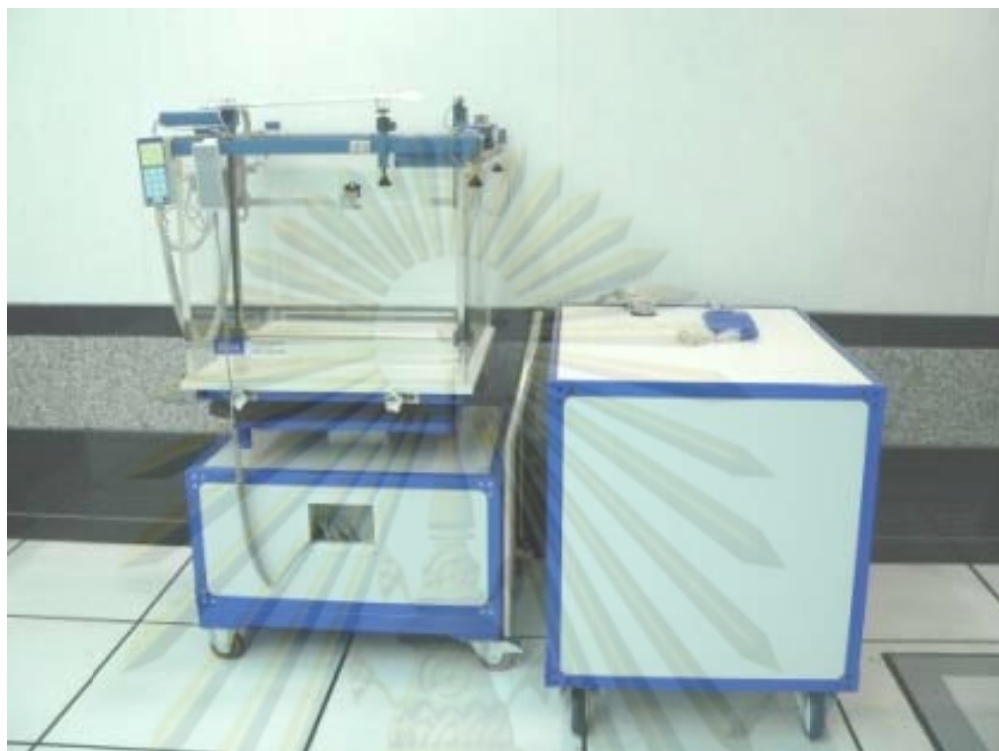


Figure 3.10 Three dimension beam analyzing system manufactured by Scanditronix/ Wellhofer Dosimetrie, Schwarzenbruck, Germany

#### 3.6.11 One dimensional water phantom

The one dimensional water phantom (WP1D) manufactured by Scanditronix/ Wellhofer Dosimetries, Schwarzenbruck, Germany is a phantom for point dose measurements, it is shown in figure 3.11. Both CC13 and FC65-P ionization chamber can be connected to the phantom. The absolute dose is measured according to TG-51 and IAEA TRS-398 dosimetry protocols [40]. The measurement depths are adjusted by motor and read out with electrometer.

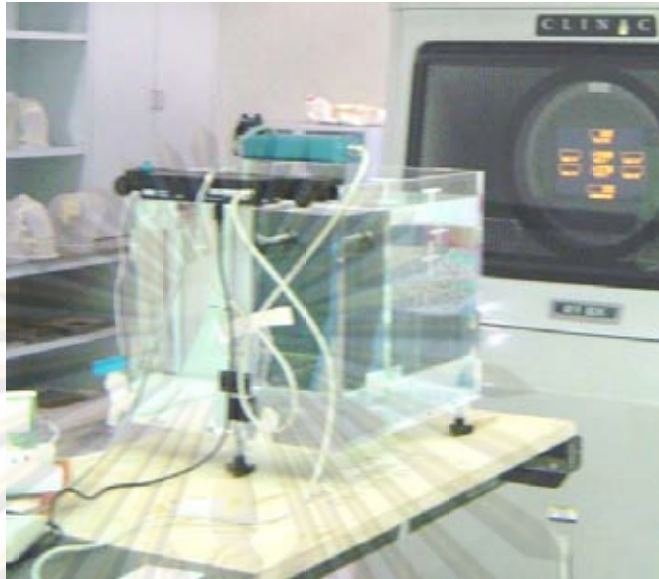


Figure 3.11 One dimensional water phantom manufactured by Scanditronix/ Wellhofer Dosimetrie, Schwarzenbruck, Germany

### 3.6.12 ImageJ program

ImageJ program converts Digital Imaging and Communications in Medicine (DICOM) image files from Eclipse treatment planning to stacks, a series of images, for calculation dose by independent software. The ImageJ is a public domain and it's free available source code, Java-based image processing program was developed at the National Institutes of Health as shown in figure 3.12. ImageJ can display, edit, analyze, process, save, and print as 8-bit, 16-bit and 32-bit images. It can read many image formats including TIFF, PNG, GIF, JPEG, BMP, DICOM, FITS, as well as raw formats.

ImageJ can calculate area and pixel value statistics of user-defined selections as well as intensity threshold objects. It can measure distances and angles. It can create density histograms and line profile plots. It supports standard image processing functions such as logical and arithmetical operations between images, contrast manipulation, convolution, Fourier analysis, sharpening, smoothing, edge detection and median filtering. It does geometric transformations such as scaling, rotation and flips. The program supports any number of images simultaneously, limited only by available memory.

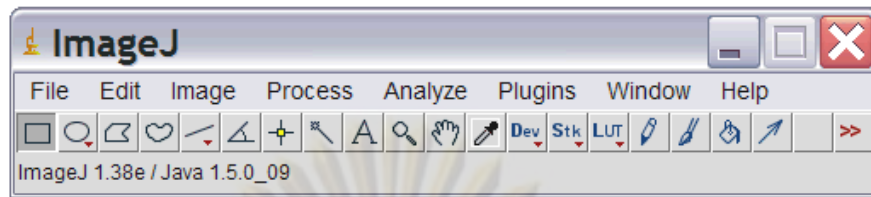


Figure 3.12 ImageJ program  
(<http://rsbweb.nih.gov/ij/index.html>)

### 3.6.13 Personal computer (PC)

The CPU for the independent software is a Pentium IV with 1.86 GHz processors, DDR RAM 1028 MB. The operating system is Microsoft Window XP Version 2002.

## 3.7 Method

The procedures were divided into four major parts including beam data preparing for independent software calculation, code development for modified Clarkson integration algorithm with 3D-BSM, dose verifications of MLC field in homogeneous phantom and dose verifications of 3D-CRT and IMRT techniques in inhomogeneous thorax phantom. The study was performed at the department of radiology at King Chulalongkorn Memorial Hospital.

### 3.7.1 Beam data preparing

The Clinac 21EX linear accelerator (Varian Medical Systems, Palo Alto, USA) 6 MV photon beam with 300 MU/min dose rate and 80 leaves, each 1 cm width were employed in this study. The tissue maximum ratio  $TMR_{(d,r)}$  data from 1.5 to 30 cm depth for collimator ranging from  $2 \times 2 \text{ cm}^2$  to  $40 \times 40 \text{ cm}^2$  were extracted from standard measurement [40] with CC13 ionization chamber in 3D beam analyzing water phantom (Scanditronix Wellhofer Dosimetric, Schwarzenbruck), then the scatter maximum ratio  $SMR_{(d,r)}$ , the tissue maximum ratio at zero field size  $TMR_{(d,0)}$  were calculated. The total scatter factor  $S_{c,p}$ , and the collimator scatter factor  $S_c$  data were also obtained from measurements with CC13 ion chamber in WP1D water phantom at any field size. The phantom scatter factor at zero field size  $S_p(0)$  and the phantom scatter factor  $S_p(r)$  could

be calculated. Appendix A shows the table of beam data that were put into the independent software.

### 3.7.2 Code development for modified Clarkson integration algorithm with 3D-BSM

The calculation program was developed on Visual Basic version 6.0 with an Intel Celeron of 1.86 GHz CPU. The developing independent software in this study is called ISOFT.

#### 3.7.2.1 Code of image and MLC field

The data transfer between Eclipse treatment planning system and ISOFT software was performed by importing the data by handy drive. The data transfers included DICOM CT images and MLC position files. The ImageJ program was used to change DICOM CT images to BMP and Text images format. The slice thickness of imported CT images from Eclipse system is 2.5 mm. The maximum number of image capable transfer to ISOFT software is 300 images. The program presented the CT number at the location at selected points in each pixel of 512x512 matrix size. The information for inhomogeneity correction due to the differing composition of human tissues were calculated by reading the CT number and converted to electron density.

$$\rho^{\omega} = 1.0 + 0.001x N_{CT} \quad \text{when} \quad -1,000 \leq N_{CT} \leq 1,000 \quad \dots(3.1)$$

and

$$\rho^{\omega} = 1.0 + 0.001x N_{CT} \quad \text{when} \quad N_{CT} \geq 100 \quad \dots(3.2)$$

where  $\rho^{\omega}$  is the electron density relative to the electron density of water and  $N_{CT}$  is the CT number. The patient's body outlines need to be defined for modified Batho inhomogeneities correction algorithm and to correct for contour irregularities. For commercial treatment planning systems, the users can automatically contour using the segmentation algorithms such as Region-based approaches or Edge detection algorithm. The Edge detection algorithm was used in ISOFT software for body

contouring because this algorithm is more easily to calculate. The ISOFT software was developed to search body outline automatically to the area that defined by the volume of interest (VOI). So only the external body contour not including the couch was drawn. The automatic contouring will enable defining body contours slice by slice.

Then multi-planar reconstructions in any planes of sagittal view were created by writing the program to draw the CT number in each row of all axial images, the same position of each row were selected, then the image in coronal plane was reconstructed. The MLC file was read for each MLC position, then the program constructed the MLC shaped field. The field shaping and the anatomy were visible on the MPR view. The code of ISOFT will display two windows of 2D images of transversal and sagittal views. The CT slice thickness affected to image resolution of MPR so the minimum slice thickness of 2.5 mm was selected.

### 3.7.2.2 Code for dose calculation

The modifications of Clarkson integration algorithm with 3D-BSM methods were employed for irregular MLC fields, step-and-shoot IMRT field and any shape of inhomogeneous structures. The measurement data included  $TMR_{(d, r)}$ ,  $TMR_{(d, 0)}$ ,  $SMR_{(d, r)}$ ,  $S_p(r)$  and  $S_p(0)$ . A set of MLC for IMRT field was divided into various angular segments. The radius of angular segments was used to calculate the scattered dose. The general correction factor (GCF) for the irregular and inhomogeneities could be calculated by 3D-BSM correction method by [11, 12]

$$GCF = 1 + \frac{1}{\text{No. Radius}} \frac{\sum_{i=1}^n \left[ \sum_{j=1}^{m-1} D_i(w, R_j) [C_i(\rho_j, R_j) - C_i(\rho_{j+1}, R_j)] + D_i(w, R_{\max}) [C_i(\rho_{\max}, R_{\max}) - 1] \right]}{D(w, R)_{\text{Total}}} \dots (3.3)$$

where No. Radius is number of radius of circular field,  $D(w, R)_{\text{Total}}$  is the total dose from all sectors in water,  $D_i(w, R_j)$  is the dose at any sector,  $R_j$  is the radius of circular field,  $n$  is the number of intersecting sectors with inhomogeneity grids,  $m$  is the number of intersections between the calculation point and boundary of the irregular field,  $i$  is the sector,  $j$  is the number of intersections from the calculation point to the field

boundary as shown in figure 3.13,  $R_{max}$  is used for the largest radius,  $C_i$  is the internal correction factor of standard method as the Batho method, ETAR or RTAR.

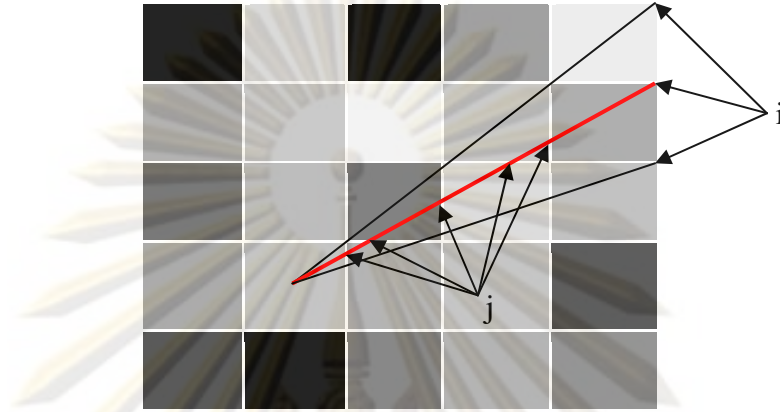


Figure 3.13 The simple setup geometry showing the radius  $i$  and intersection  $j$ .

The internal correction factor of modified Batho algorithm was selected to correct the dose distribution in each sector [14].

$$C_i = (\rho_e^\omega)_N \prod_{m=1}^N \text{TMR}(d_m + d_{max}, \text{FS})^{(\rho_e^\omega)_m - (\rho_e^\omega)_{m-1}} \quad \dots(3.4)$$

where  $N$  is index of the last layer, TMR is the tissue maximum ratio,  $m$  is index for inhomogeneity boundaries,  $d_m$  is distance between the grid point and the  $m^{\text{th}}$  inhomogeneity boundary,  $d_{max}$  is the distance which adds to the depth  $d_m$ , FS and  $(\rho_e^\omega)_m$  are field size and  $m^{\text{th}}$  material electron density relative to water, respectively.  $(\rho_e^\omega)_N$  is the ratio of the mass energy absorption coefficient for  $N^{\text{th}}$  layer to water. For CIRS IMRT phantom dose calculation, the axial images are reconstructed to sagittal view and divided into various grids.

The GCF was calculated though irregular MLCs field by ISOFT software. However, the step-and-shoot IMRT technique is consisted of many subfields. These techniques need weighting factor for weighted each subfield and integrated total dose to modulated field by equation 3.5 [41, 42]

$$\text{MU}_i = \text{MU}_{\text{Total}} \times w_i \quad \dots(3.5)$$

where  $MU_i$  is the monitor units for each subfield  $i$ ,  $MU_{Total}$  and  $w_i$  are the total amount of monitor unit and weighting factor for each subfield  $i$  calculated by Eclipse treatment planning system, respectively. The contour correction factor (CCF) is calculated by ISOFT software with tissue-maximum ratio (TMR) method from equation 2.21. The total dose  $D_{Total}$  of IMRT field is calculated by integrated all  $MU_i$  and multiplied GCF by

$$D_{Total} = GCF \times \sum_{i=1}^N MU_i \times TMR_{(d,r)} \times CCF \quad \dots(3.6)$$

The method of modified Clarkson integration algorithm with 3D-BSM inhomogeneity correction in ISOFT was started with the construction of the image in the BEV. To calculate using Modifier Clarkson Integration, the radiation field was superimposed to the calculation pixel as shown in figure 3.14. The dimension of each pixel equals to  $2.5 \times 2.5 \text{ mm}^2$ , each contained average electron density for the dose calculation. We assume that each pixel is an inhomogeneous media. The average electron density in each grid was read and used for the calculation.

From the point of interest, the radius (i) was drawn to the edge of the beam that cut to the edge of outer grid, the segment was formed by each radius separated by 2.5 mm. The points that the radius cut to the edge of each grid were specified (j) and used to determine the radius of each circle, the example was point a, b, c, d, e and f as shown in figure 3.14. The scattered doses were calculated in each circle and then the subtraction for the actual irregular field and inhomogeneity correction was undertaken by equation 3.3 and 3.4. Then the dose at any point was calculated by equation 2.20, 2.21, 2.22, 3.3 and 3.4. The data of point doses calculation were imported to the Excel sheet to plotted profile or depth dose in any interested plane in term of absolute dose.

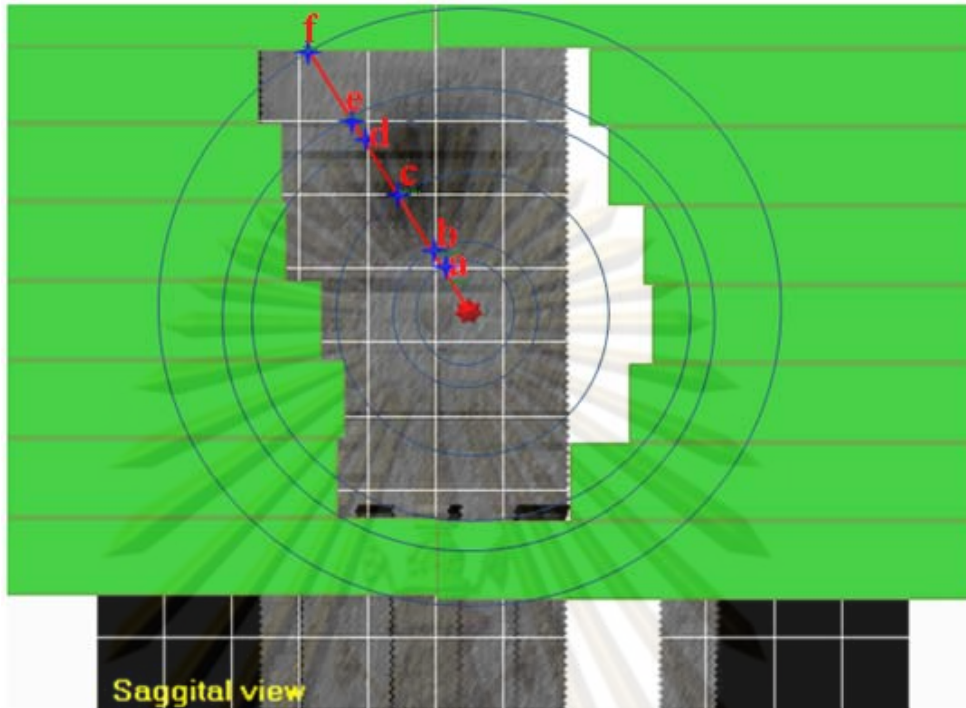


Figure 3.14 The sagittal view showing the pixel, radius and intersection

### 3.7.3 Dose verifications of MLC fields in homogeneous phantom

The ISOFT software was tested for the accuracy of the dose calculation in central axis by employing MLC shaped fields, and the dose measurement with 0.6 cc FC 65-P ion chamber and DOSE1 dosimeter in water phantom at 1.5, 5, 10 and 15 cm depth as shown in figure 3.15. All fields were given 100 cGy prescribed dose at central axis at zero degree gantry angle. The MLC test patterns consisted of square fields, rectangular fields, corner block, circular field, inverted Y field and irregular field. Table 3.2 to 3.4 summarizes the setting parameters for dose measurement in this study. The same monitor unit calculated by Eclipse treatment planning was used for the measurement. The results between dose calculations by ISOFT software, by Eclipse system and measurement with ionization chamber were compared with the criteria of acceptability for photon dose calculation by IAEA TRS no.430 [32].



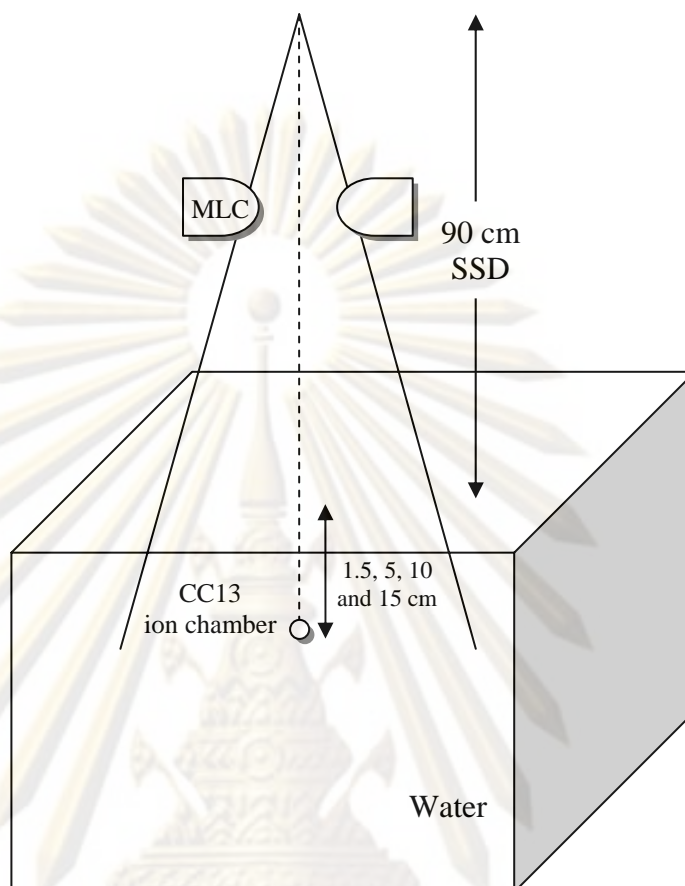


Figure 3.15 Schematic of 6MV MLC beam geometry of water phantom at 90 SSD and 1.5, 5, 10 and 15 cm depth.

ศูนย์วิทยทรัพยากร  
จุฬาลงกรณ์มหาวิทยาลัย

Table 3.2 Summarize the setting parameters for square fields.

Beam	Field type	Dose (cGy)	Field size (Collimator)	Depth (cm)
Square field	Square MLC 10x10 cm <sup>2</sup>	100	11.6x10.4 cm <sup>2</sup>	1.5
				5
				10
				15
	Square MLC 5x5 cm <sup>2</sup>	100	6.6x5.4 cm <sup>2</sup>	1.5
				5
				10
				15

Table 3.3 Summarize the setting parameters for rectangular fields.

Beam	Field type	Dose (cGy)	Field size (Collimator)	Depth (cm)
Rectangular field	Rectangular MLC 5x30 cm <sup>2</sup>	100	6.6x30.4 cm <sup>2</sup>	1.5
				5
				10
				15
	Rectangular MLC 30x5 cm <sup>2</sup>	100	31.6x6.4 cm <sup>2</sup>	1.5
				5
				10
				15

Table 3.4 Summarize the setting parameters for shaped fields.

Beam	Field type	Dose (cGy)	Field size (Collimator)	Depth (cm)
Corner block	Corner block MLC	100	22x22 cm <sup>2</sup>	1.5
				5
				10
				15
Circular field	Circular MLC Diameter 5.6 cm	100	7.2x6.4 cm <sup>2</sup>	1.5
				5
				10
				15
Inverted Y field	Inverted Y MLC	100	13.6x15.4 cm <sup>2</sup>	1.5
				5
				10
				15
Irregular field	Irregular MLC	100	13.6x8.4 cm <sup>2</sup>	1.5
				5
				10
				15

ศูนย์วิทยุรักษากร  
จุฬาลงกรณ์มหาวิทยาลัย

#### 3.7.4 Dose verifications of 3D-CRT and IMRT fields in inhomogeneous phantom

The Eclipse treatment planning system is a tool to generate 3D-CRT and IMRT plans. In this study, the doses for IMRT fields were calculated by Eclipse system with two modes of calculation: Pencil beam convolution algorithm including modified Batho inhomogeneity correction and convolution/superposition algorithm (AAA). The treatment planning process of Eclipse system was performed in CIRS thorax phantom that is elliptical in shape and properly represents an average human torso in proportion, density and 2D structure. The phantom was manufactured from unique proprietary materials that faithfully mimic water, bone and lung. The IMRT treatment planning was divided into three steps. The first step is the treatment objectives that include selected energy, beam angle, beam numbers, dose prescription and dose objectives in target and critical volume. The next step is the optimization with iterative method. The isodose distribution and dose volume histogram are optimized to meet criteria. The last step is the conversion of intensity levels to MLC positions sequence file.

Two lung tumors from clinical were loading to CIRS thorax phantom for dose calculation of a 3D-CRT and IMRT single field techniques as shown in figure 3.16 and figure 3.17. The single field for 3D-CRT and IMRT were planned and optimized so that the uniform dose in tumor was obtained. The 6 MV photon beams were delivered from Clinac21EX of 80 MLC with 300 MU/min dose rate. All plans were given 200 cGy prescribed dose at isocenter where tumor located. The grid size of  $2.5 \times 2.5 \text{ mm}^2$  was selected in this calculation. The leaf sequencing algorithm employed the number of levels equal to 20. For dose verification, the same file of patient data including CT based and MLC position with the monitor unit recorded were loaded to ISOFT software to calculate the doses with modified Clarkson integration algorithm with 3D-BSM using data.

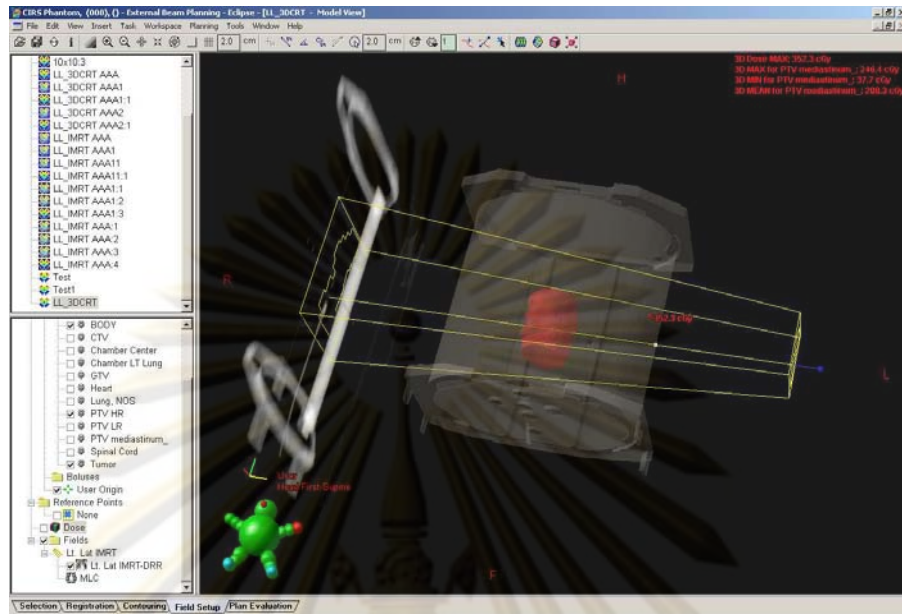


Figure 3.16 Tumor image from the Eclipse RTPS of 3D-CRT plan1 and IMRT plan1.

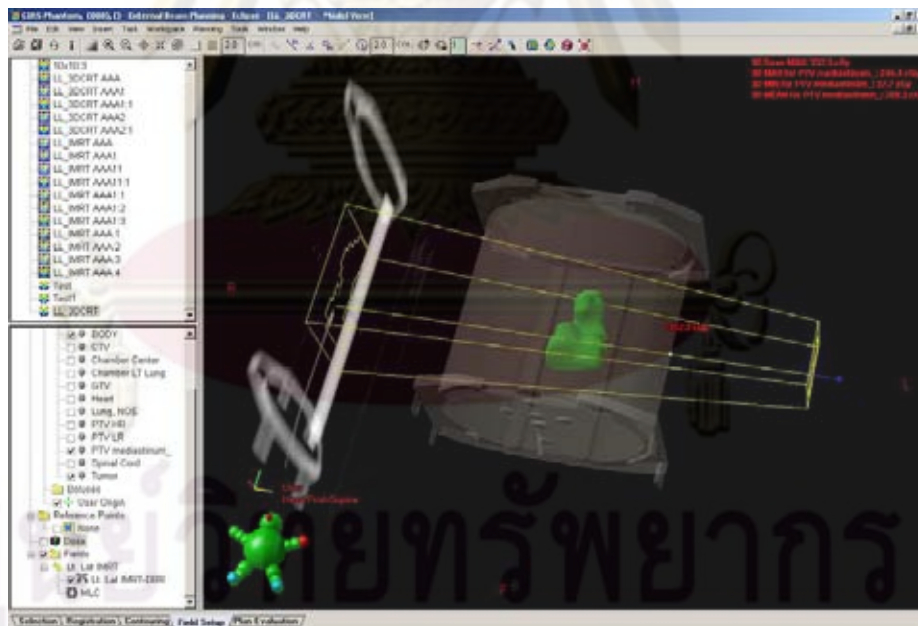


Figure 3.17 Tumor image from the Eclipse RTPS of 3D-CRT plan2 and IMRT plan2.

The experiment was performed by using the 0.13 cc ionization chamber and EDR2 film with the following steps:

#### 3.7.4.1 The measurement by ionization chamber

The point measurements were undertaken with CC13 ion chamber and DOSE1 dosimeter in a CIRS thorax phantom at the left lung, mediastinum and right lung as shown in figure 3.18. The beam entrance was from the left lateral lung to right lateral lung for both 3D-CRT and IMRT field because the inhomogeneities are predominance in lateral direction. The results of point dose measurement were compared with the calculations from ISOFT software and Eclipse system including modified Batho inhomogeneity correction and convolution/superposition algorithm (AAA) with the criteria of acceptability for photon dose calculation in inhomogeneous phantom by IAEA TRS no.430 [32].



Figure 3.18 The calibration of ionization chamber in CIRS thorax phantom

#### 3.7.4.2 Film and scanner calibration

The calibrated films were inserted in  $30 \times 30 \text{ cm}^2$  solid water phantom and irradiated by 6MV linear accelerator at 100 cm source to surface distance (SSD) technique. The EDR2 film was placed at 5 cm depth in solid water phantom and supported with 10 cm solid water phantom backscatter layers as shown in figure 3.19. All eight uniform dose levels are 20 cGy, 50 cGy, 150 cGy, 200 cGy, 250 cGy, 300 cGy, 350 cGy and 400 cGy and  $3 \times 3 \text{ cm}^2$  MLC field were irradiated on the same film. The period of time between irradiation and processing film was 2 hours for EDR2 film to reach to the stable OD values [38, 39]. Then the films were scanned by Vidar-16 Dosimetry Pro scanner with the OmniPro IMRT software. Sensitometric curves were plotted as a function of net optical density versus doses.





Figure 3.19 The calibration of EDR2 film in solid water phantom.

#### 3.7.4.3 Film measurement

The EDR2 film was inserted in CIRS phantom in parallel direction with the beam at the isocenter slice. The set up of MU for CIRS thorax phantom was shown in figure 3.20. The beam entrance was from the left lateral lung to right lateral lung for both 3D-CRT and IMRT plans because the inhomogeneities were predominance in lateral direction. The results of 2D dose measurement were compared with the calculations from ISOFT software and Eclipse system including modified Batho inhomogeneity correction and convolution/superposition algorithm (AAA) with the criteria of acceptability for photon dose calculation in inhomogeneous phantom by IAEA TRS no.430 [32].





Figure 3.20 Two dimensional dose measurements for 3D-CRT or IMRT plan in CIRS thorax phantom by film.

### 3.8 Outcome

1. Dose determination in CT-based patient data for 3D-CRT and IMRT step and shoot plans
2. Deviation of the dose between calculated by ISOFT software, RTPS and measurement

### 3.9 Measurement

Variable : Independent Variable = CT-based patient data, IMRT plan, Prescription dose, Monitor unit

: Dependent Variable = Dose measurement in a single field of 3D-CRT and IMRT plans

### 3.10 Data Collection

The doses calculated by ISOFT software, Eclipse treatment planning system and measurements are collected.

### 3.11 Data Analysis

#### 3.11.1 Summarization of Data

The doses in CT-based patient data for 3D-CRT and IMRT techniques by ISOFT software using modified Clarkson integration algorithm with 3D-BSM are calculated for the dose distribution. The percentage of dose difference between calculated by ISOFT software, RTPS and measurements are analyzed, and evaluated for the accuracy of ISOFT software.

#### 3.11.2 Data presentation

The graphs of dose difference between calculated by ISOFT software, RTPS and film measurement are presented.

### 3.12 Benefit of the study

This study is designed to develop the software for 3D-CRT and IMRT plans verification. This software is easy to use, fast and accurate dose.

ศูนย์วิทยุรักษากร  
จุฬาลงกรณ์มหาวิทยาลัย

## CHAPTER IV

### RESULTS

#### 4.1 Code development for modified Clarkson integration algorithm with 3D-BSM

The code development can be displayed in three screens including homogeneous phantom and MLC window, inhomogeneous phantom window and inhomogeneous phantom with external contour window and MLC window as shown in figure 4.1 to 4.3, respectively.

##### 4.1.1 Code of image and MLC field

The homogeneous phantom and MLC window was constructed by ISOFT to calculate point dose in water phantom as shown in figure 4.1. The CT-based patient data of CIRS inhomogeneous phantom window was imported from CT scanner as shown in figure 4.2. The inhomogeneous phantom window represented the CT number at the location of selected points. The ISOFT software can display density of a particular material in CT number for CT images. CT numbers fall in the range of -1000 to +2000 (air = -1000, water = 0). The correction of display of CT numbers was verified with RTP. The spot check show mostly agreement. The electron density values for inhomogeneity correction were calculated by ISOFT software by reading the CT number and converted to electron density by equation 3.1 and 3.2. The surface contours of all slices and the MLC field were created by ISOFT software as shown in figure 4.3.

##### 4.1.2 Code for dose calculation

The homogeneous phantom and MLC window in figure 4.1 were employed to calculate dose using modified Clarkson integration algorithm. Appendix B shows the MLC square field file. Input parameters such as tumor depth, SSD in centimeter and monitor units were specified by the user. The calculation result from ISOFT software in cGy was undertaken at the selected point dose. Then the results were compared with

the calculation from the treatment plan in percentage of deviation as shown also in figure 4.1.

The MLC window was used to calculate the inhomogeneity correction by combining the modified Clarkson integration algorithm with 3D-BSM using modified Batho correction as shown in figure 4.3. The Eclipse plans were exported to ISOFT software with MU and MLC position files. The .mlc file was transferred from Eclipse system to ISOFT software as a static MLC control file for 3D-CRT. Appendix C showed the static MLC position file. The MPR of CT images in sagittal planes is displayed by ISOFT as shown in figure 4.4. The order of the views depends on the patient's position where the original CT images were produced. The MU of Eclipse treatment planning was kept the same as the ISOFT software for point dose calculation. The effect of surface curvature was corrected by tissue-maximum ratio method from equation 3.4. The user manual of ISOFT software was shown in appendix D.

The program can support the modified Clarkson integration by reading of a large number of angular radiuses, for example the equivalent area of  $100 \text{ cm}^2$ , the number of angular radius for scattered calculation was 400. For larger field size, the numbers of angular radius were increased so that the resolution was the same as small field. The number of maximum angular radius can be increased up to 6,400. The transmission factor of MLC was corrected but the effect of tongue and groove was not considered.

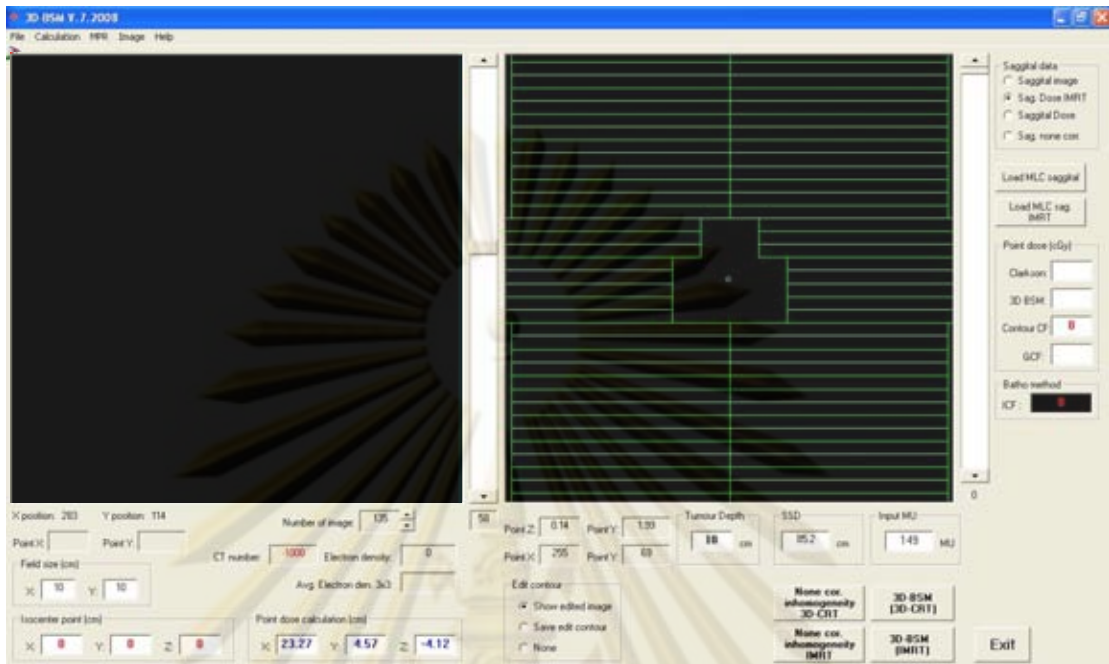


Figure 4.1 Screenshot of ISOFT homogeneous phantom and MLC window.

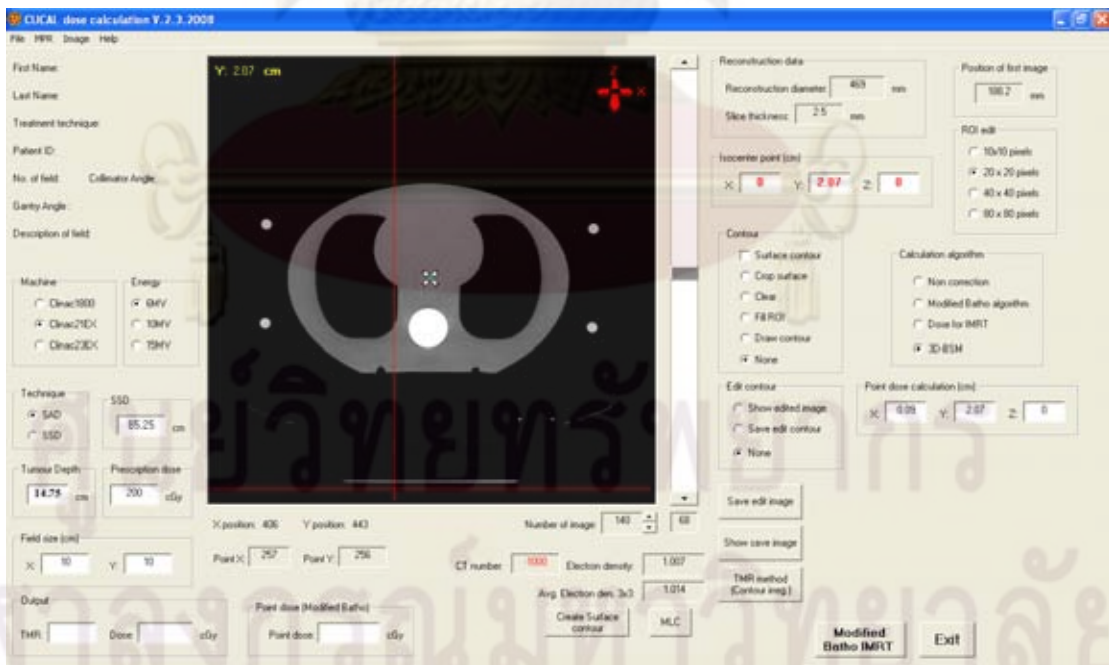


Figure 4.2 Screenshot of ISOFT inhomogeneous phantom window.

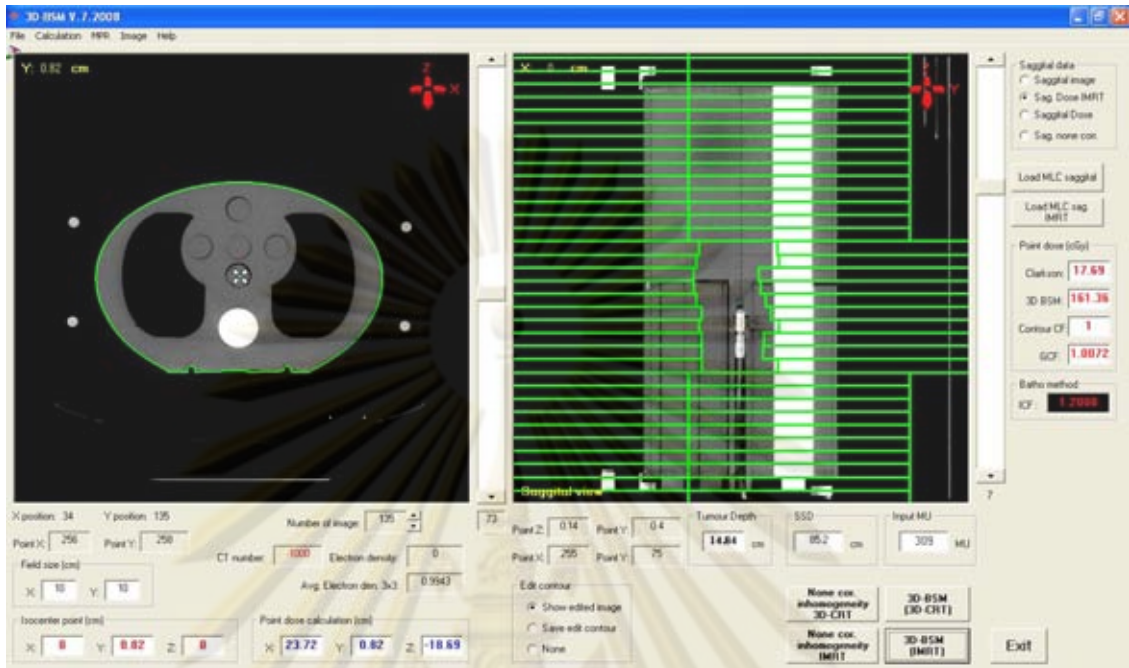


Figure 4.3 Screenshot of ISOFT MLC window that contained CT images, patient information and MLC position of treatment field. The surface contour was created by ISOFT software.

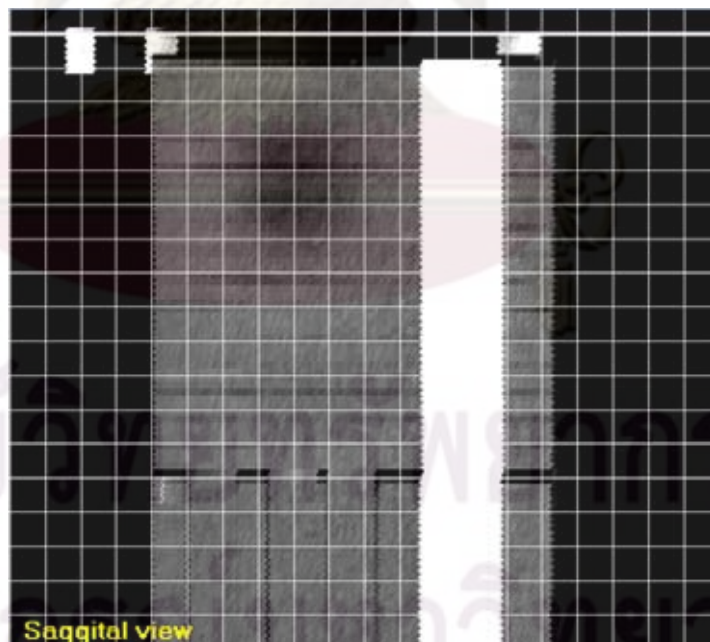


Figure 4.4 The ISOFT software displays sagittal view of CIRS IMRT phantom that is divided into calculation grid.

## 4.2 Dose verifications of MLC fields in homogeneous phantom

The tests were performed at various depths of MLC square fields ( $5 \times 5 \text{ cm}^2$ ,  $10 \times 10 \text{ cm}^2$ ), rectangular fields ( $30 \times 5 \text{ cm}^2$ ,  $5 \times 30 \text{ cm}^2$ ), corner block, circular field MLC, inverted Y field MLC and irregular field MLC. The accuracy of calculation point doses from Eclipse treatment planning system and ISOFT software were compared with measurements.

### 4.2.1 Square fields

The square MLC fields constructed by ISOFT are shown in figure 4.5(a-b) for  $10 \times 10$ ,  $5 \times 5 \text{ cm}^2$  respectively. The percent deviation between the measured and calculated point doses by ISOFT software was ranged from -0.42 to 0.56 % for all studied which are within 1 % criteria of IAEA TRS no. 430 [32] as shown in table 4.1. The maximum deviation found on Eclipse system was 0.81% and ISOFT software was 0.56%. The maximum dose deviation of ISOFT software was observed for depth 10 cm of  $10 \times 10 \text{ cm}^2$ .

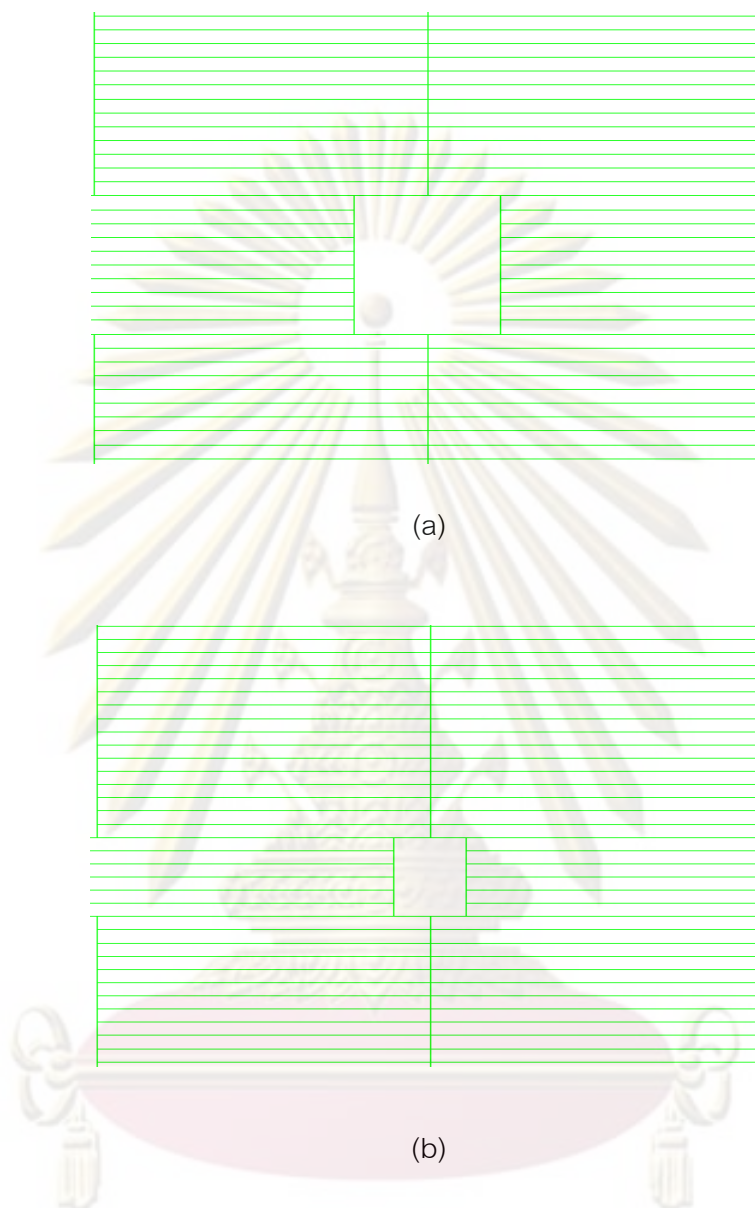


Figure 4.5 The MLC of square field verification by ISOFT software. (a) A square field of  $10 \times 10 \text{ cm}^2$  (b) A square field of  $5 \times 5 \text{ cm}^2$

ศูนย์วิทยุโทรศัทพ์  
จุฬาลงกรณ์มหาวิทยาลัย



Table 4.1 The comparison of measured and calculated by ISOFT software and treatment planning for 10x10 and 5x5 cm<sup>2</sup> square fields at 1.5, 5, 10 and 15 cm depths for 6 MV photon beams at 100 cm SAD.

Beam	MU	Depth (cm)	Measured Dose (cGy)	TPS Dose (cGy)	ISOFT Dose (cGy)	%Deviation	
						TPS&Mea.	ISOFT&Mea.
10x10 cm <sup>2</sup>	124	1.5	152.01	151.5	150.82	-0.34	-0.38
		5	130.6	130.9	129.44	0.23	-0.34
	138	10	99.31	100	100.26	0.69	0.56
		15	74.4	75	74.342	0.81	-0.08
5x5 cm <sup>2</sup>	138	1.5	160.05	159.7	159.4	-0.23	-0.31
		5	135.34	135.6	134.85	0.19	-0.26
	138	10	99.44	100	98.727	0.56	-0.42
		15	72.82	73.1	73.343	0.38	0.36

#### 4.2.2 Rectangular fields

The rectangular MLC fields constructed by ISOFT are shown in figure 4.6(a-b) for 30x5, 5x30 cm<sup>2</sup> respectively. The percent deviation between the measured and calculated point doses by ISOFT software was from -0.25 to 0.42 % for all studies which are within 1.5 % criteria of IAEA TRS no. 430 [32] as shown in table 4.2. The maximum deviation found on Eclipse system was 1.36% and ISOFT software was 0.32%. The maximum dose deviation of ISOFT software was observed for depth 15 cm of 30x5 cm<sup>2</sup>.

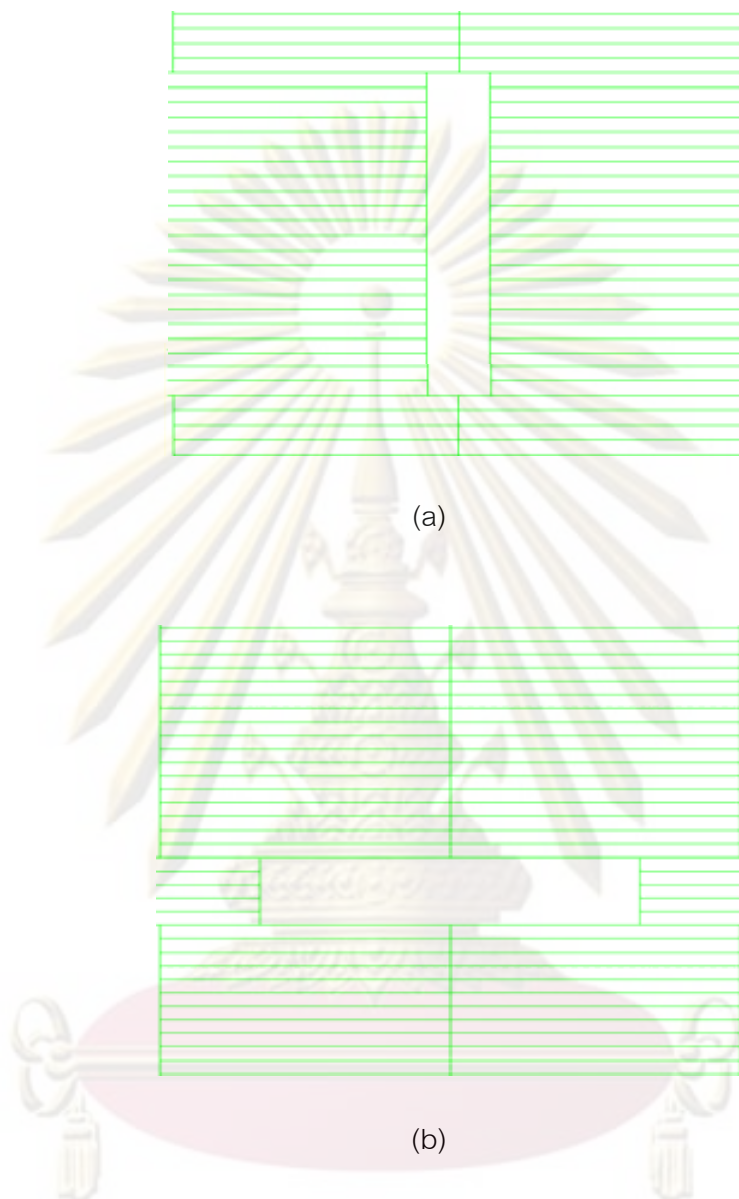


Figure 4.6 The MLC of rectangular field verification by ISOFT software. (a) A rectangular field of  $30 \times 5 \text{ cm}^2$  (b) A rectangular field of  $5 \times 30 \text{ cm}^2$

ศูนย์วิทยุวิทยาการ  
จุฬาลงกรณ์มหาวิทยาลัย

**Table 4.2** The comparison of measured and calculated by ISOFT software and treatment planning for 30x5 and 5x30 cm<sup>2</sup> rectangular fields at 1.5, 5, 10 and 15 cm depths for 6 MV photon beams at 100 cm SAD.

Beam	MU	Depth (cm)	Measured Dose (cGy)	TPS Dose (cGy)	ISOFT Dose (cGy)	%Deviation	
						TPS&Mea.	ISOFT&Mea.
Rectangular 30x5 cm <sup>2</sup>	129	1.5	154.66	154.8	154.47	0.09	-0.12
		5	131.76	132.8	131.79	0.79	0.02
		10	99.02	100	100.28	0.99	0.27
		15	73.8	74.8	74.332	1.36	0.42
Rectangular 5x30 cm <sup>2</sup>	126	1.5	155.78	154.3	154.17	-0.95	-0.23
		5	132.88	132.6	131.8	-0.21	-0.25
		10	99.99	100	100.81	0.01	0.32
		15	74.88	74.8	75.127	-0.11	0.13

#### 4.2.3 Shaped fields

The rectangular MLC fields constructed by ISOFT are shown in figure 4.7(a-b) for 30x5, 5x30 cm<sup>2</sup> respectively. The percent deviation between the measured and calculated point doses by ISOFT software was from -1.53 to 0.78 % for all field studies which are within 2% criteria of IAEA TRS no. 430 [32] as shown in table 4.3. The maximum deviation found on Eclipse system was 1.76% and ISOFT software was -1.53%. The maximum dose deviation of ISOFT software was observed for depth 10 cm of inverted Y MLC field.

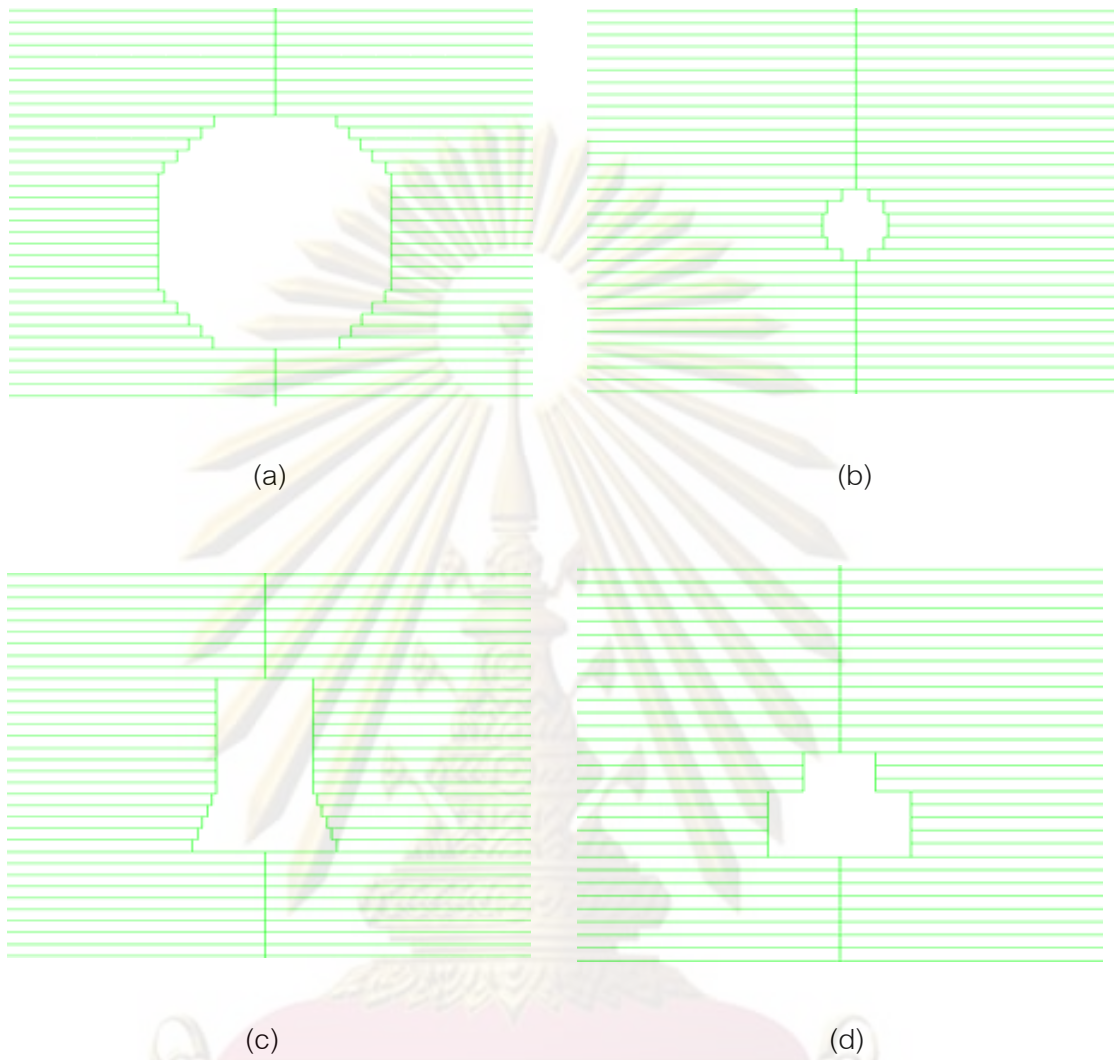


Figure 4.7 The MLC of shaped fields for corner block (a), circular field (b), inverted Y field (c) and irregular field (d) by ISOFT software.

ศูนย์วิทยทรัพยากร  
จุฬาลงกรณ์มหาวิทยาลัย

**Table 4.3** The comparison of measured and calculated by ISOFT software and treatment planning for corner block, circular field, inverted Y field and irregular field at 1.5, 5, 10 and 15 cm depth for 6 MV photon beams of 100 cm SAD.

Beam	MU	Depth (cm)	Measured Dose (cGy)	TPS Dose (cGy)	ISOFT Dose (cGy)	%Deviation	
						TPS&Mea.	ISOFT&Mea.
Corner block	113	1.5	146.61	146.6	144.66	-0.01	-0.15
MLC field		5	127.05	127.3	126.63	0.20	-0.33
		10	99.49	100	98.176	0.51	-1.32
		15	76.84	77.3	76.481	0.60	-0.47
"Circular"	137	1.5	160.15	160.1	160.28	-0.03	0.08
MLC field		5	135.09	135.8	134.79	0.53	-0.22
		10	99.05	100	98.523	0.96	-0.53
		15	72.42	72.9	73.622	0.66	0.78
"Inverted Y"	121	1.5	150.44	150.7	150.6	0.17	0.11
MLC field		5	129.31	130.6	128.9	1.00	-0.32
		10	98.56	100	96.758	1.46	-1.53
		15	74.04	75.2	73.938	1.57	-0.14
"Irregular"	127	1.5	153.33	154.1	153.55	0.50	0.14
MLC field		5	131.17	132.5	130.62	1.01	-0.42
		10	98.51	100	96.694	1.51	-1.34
		15	73.31	74.6	72.986	1.76	-0.44

### 4.3 Dose Verification of 3D-CRT and IMRT plans in inhomogeneous phantom

The verifications of two plans of 3D-CRT field and two plans of IMRT field were performed in CIRS thorax phantom. A single beam of each technique was set to  $90^{\circ}$  gantry angle. For this study, the calculation algorithms of Eclipse treatment planning system considered were the Pencil beam convolution algorithm with modified Batho inhomogeneity correction and Convolution/ superposition algorithm (AAA).

#### 4.3.1 The measurement by ionization chamber

The results of point dose verification among measured by ion chamber calculated by Eclipse system and ISOFT software at the left lung, mediastinum and right lung are shown in table 4.4 to 4.5 for 3D-CRT and IMRT fields, respectively.

For 3D-CRT fields, the measured values showed lower dose than the calculations by ISOFT software and both of dose algorithms of Eclipse system except both lungs which AAA algorithm showed lower dose than measurement. The modified Batho algorithm and ISOFT software were overpredicted doses in the lung regions. The tumor in plan 2 is more irregular shape than plan 1, so the deviations in lung dose between measured and all calculated methods were larger in plan 2 than plan 1. At right lung which showed more deviation than left lung, the percent dose deviation between measurement and AAA algorithm in plan 2 was up to 4.33%. The maximum percent dose deviation of 8.03% was found in modified Batho algorithm. The percent dose deviation between measurement and ISOFT software calculation was 4.87. The mediastinum which represented soft tissue showed less percent point dose deviation than lungs dose, the overall point dose agreement between measured and calculated by AAA and modified Batho algorithms and ISOFT software was within 2.77%.

For IMRT fields, the results of measured and calculated by Eclipse system and ISOFT software at the left lung, mediastinum and right lung are shown in table 4.7. The result was in the same trend as the 3D-CRT technique. The measured point doses illustrated mostly lower dose than AAA, modified Batho and ISOFT calculation, except right lung of AAA and mediastinum of ISOFT which showed slightly higher doses. Plan 1

gave closer of calculated and measured lung dose, while plan 2 presented more deviation dose. The point dose at left lung from ISOFT software showed higher dose than measured and AAA algorithm but mostly lower dose than modified Batho, while the point dose at mediastinum showed lower dose than measured. However, the deviation of left lung dose from the measured was within 4.58% for the two plans studied which was slightly better than modified Batho. The deviation of point dose from modified Batho was 7.19%. The AAA deviates from the measured only 2.09%. The measured point dose at right lung showed slightly higher than AAA algorithm but lower than modified Batho and ISOFT software. The deviation was less in ISOFT software compared with modified Batho, the deviation of ISOFT dose from the measured was 3.68% while deviation of modified Batho was 5.09%.

**Table 4.4** The comparison between point doses measured by ionization chamber and calculated by AAA, Modified Batho and ISOFT software of 3D-CRT at left lung, mediastinum and right lung.

Plan	MU	Region	Measured Dose (cGy)	AAA Dose (cGy)	Modified Batho Dose (cGy)	ISOFT Dose (cGy)	%Deviation		
							AAA&Mea.	Batho&Mea.	ISOFT&Mea.
1	246	Left lung	262.13	261.4	276.32	273.35	-0.28	5.41	4.28
		Mediastinum	191.79	196.1	197.1	192.98	2.25	2.77	0.62
		Right lung	125.88	121.5	131.23	129.76	-3.48	4.25	3.08
2	258	Left lung	257.44	249.2	270.76	268.81	-3.20	5.17	4.42
		Mediastinum	195.06	195.2	197.8	197.81	0.07	1.40	1.41
		Right lung	122.4	117.1	132.23	128.36	-4.33	8.03	4.87

**Table 4.5** The comparison between point doses measured by ionization chamber and calculated by AAA, Modified Batho and ISOFT software of IMRT at left lung, mediastinum and right lung.

Plan	MU	Region	Measured Dose (cGy)	AAA Dose (cGy)	Modified Batho Dose (cGy)	ISOFT Dose (cGy)	%Deviation		
							AAA&Mea.	Batho&Mea.	ISOFT&Mea.
1	333	Left lung	242.96	245.4	249.34	251.25	1.00	2.63	3.41
		Mediastinum	176.97	183.4	181.4	173.73	3.63	2.50	-1.83
		Right lung	117.9	115.2	123.93	122.26	-2.29	5.11	3.70
2	309	Left lung	229.9	234.7	246.43	240.42	2.09	7.19	4.58
		Mediastinum	167.13	174.6	170.6	163.39	4.47	2.08	-2.24
		Right lung	112.5	109.4	118.23	116.64	-2.76	5.09	3.68

### 4.3.2 Film and scanner calibration

#### 4.3.2.1 Film scanner calibration

The correlation of signal of analog to digital converter (ADC) and optical density (OD) from step film is shown in table 4.6 and figure 4.8. The densitometer curve between ADC and optical density showed the linear regression with the optical density ranging from 0.2 to 3.6 and ADC ranging from 4,000 to 57,000. This experiment performed with the optical density of the film less than 3.0.



Table 4.6 The densitometer signal of standard step film for scanner calibration.

Step	ADC	OD
1	3968	0.04
2	3995	0.17
3	5861	0.33
4	8449	0.47
5	10736	0.61
6	13061	0.78
7	15634	0.95
8	18507	1.1
9	21007	1.25
10	23619	1.41
11	26142	1.55
12	28458	1.69
13	30951	1.85
14	33476	1.99
15	35565	2.14
16	37532	2.29
17	39979	2.43
18	42192	2.62
19	45327	2.75
20	47024	2.9
21	49969	3.05
22	51720	3.2
23	53065	3.37
24	55804	3.51
25	57669	3.65

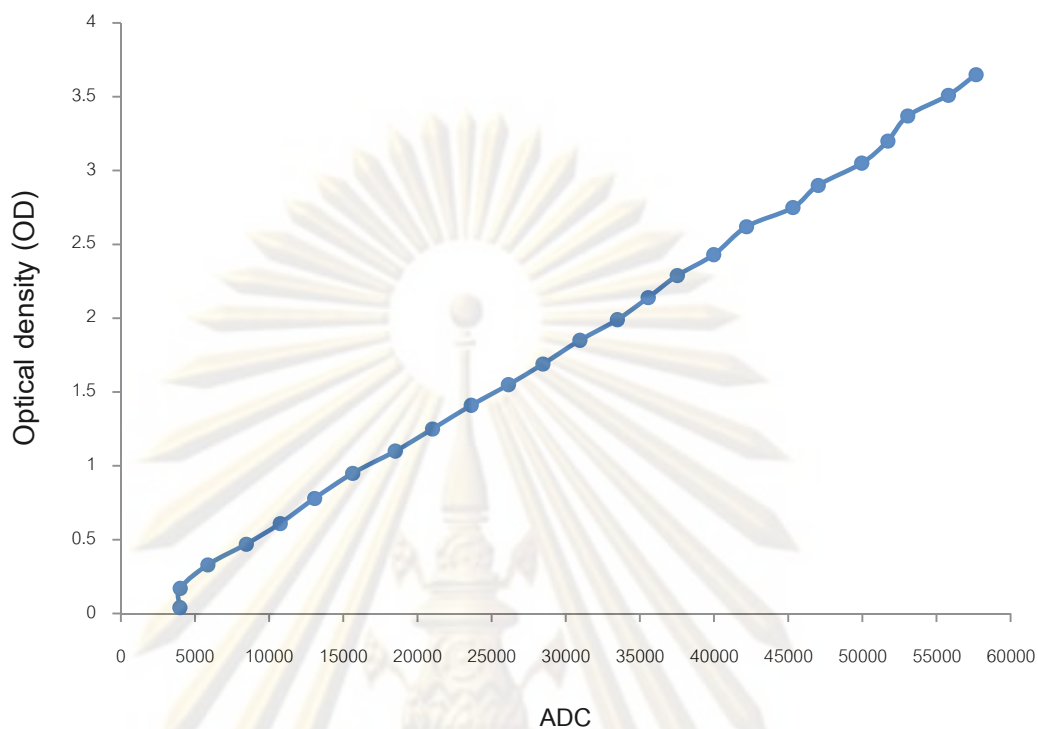


Figure 4.8 The correlation between optical density and ADC of dose response curve of Kodak EDR2 film.

#### 4.3.2.2 Film calibration

The correlation of optical density (OD) and dose unit Gray (Gy) from step film is shown in table 4.7 and figure 4.9. The sensitometer curve between OD and dose showed the linear regression with the dose ranging from 0.16 to 4 cGy and OD ranging from 0.3 to 2.5.

ศูนย์วิทยทรัพยากร  
จุฬาลงกรณ์มหาวิทยาลัย

Table 4.7 The densitometer signal of standard step film for film calibration.

Step	OD	Dose (Gy)
1	0.265	0.000
2	0.357	0.162
3	0.486	0.406
4	0.940	1.217
5	1.415	2.028
6	1.650	2.433
7	1.870	2.839
8	2.315	3.650
9	2.521	4.056

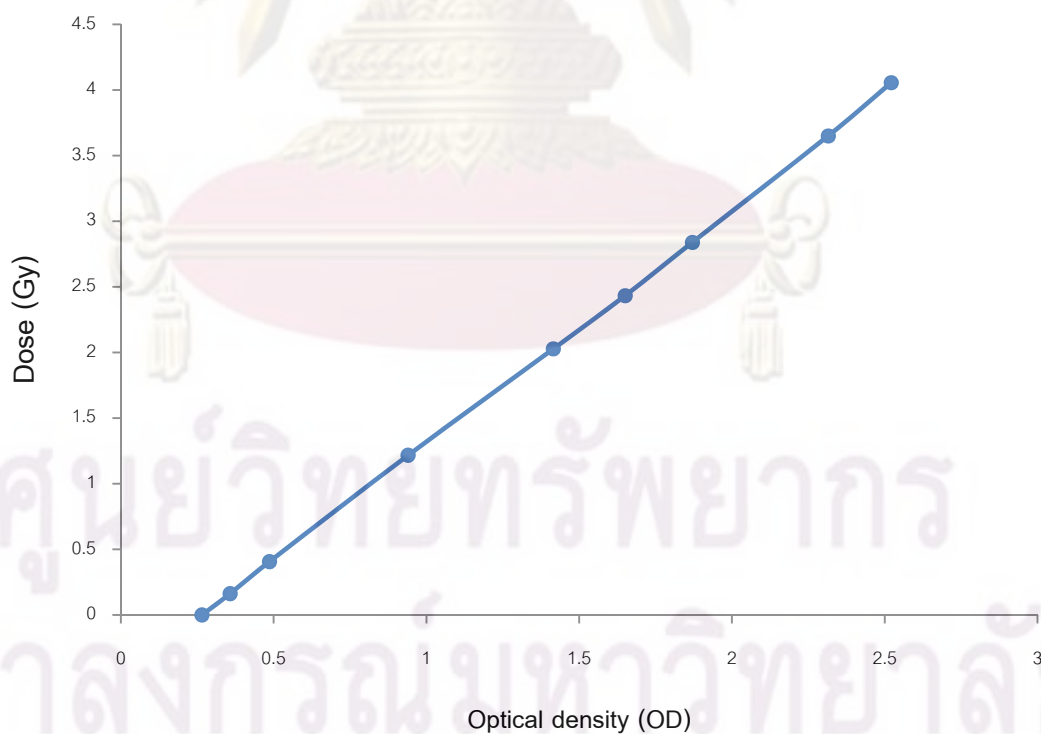


Figure 4.9 The correlation between optical density and dose of dose response curve of Kodak EDR2 film.

### 4.3.3 Film measurement

Figure 4.10 to 4.13 illustrate the EDR2 film images obtained by digital camera for 3D-CRT and IMRT fields with 6 MV photon beams of 2 patient plans, respectively. The planar dose maps from the Eclipse system of plan1 and plan2 IMRT fields are shown in figure 4.14 to 4.15, respectively. The comparisons of depth dose curves in central axis between measured dose by EDR2 film and calculated dose by Eclipse system and ISOFT software in 2 clinical plans of both 3D-CRT and IMRT fields are shown in figure 4.16 to 4.19, respectively.

The EDR2 film depth dose curves in term of absolute dose for both 3D CRT fields and IMRT fields of plan 1 and plan 2 showed the likely result as the point dose measurement. The AAA dose was closer to the measured than the other calculation methods, except at the interface region. The calculated point dose in ISOFT software was close to modified Batho and higher than the measurement for both 3D-CRT and IMRT fields of both plans. There was no consideration of the effect from secondary electron at the interface for both modified Batho and ISOFT software. The measured point dose in the left lung demonstrated the lowest dose than the three methods of calculation. The result illustrated that the less scatter due to low density in left lung is less considered in modified Batho, taken only some for AAA and a few for ISOFT software. After the interface between left lung and mediastinum, the measured point doses tended to agree with 3 different calculation methods. The doses become deviate when passed through the right lung. The systematic overprediction of point dose by modified Batho method and ISOFT software of IMRT were presented in the lung regions the same as the 3D-CRT. The average of percent deviation between ISOFT software and measured by film was within 5% which met the criteria of acceptability according to IAEA no.430 [32].

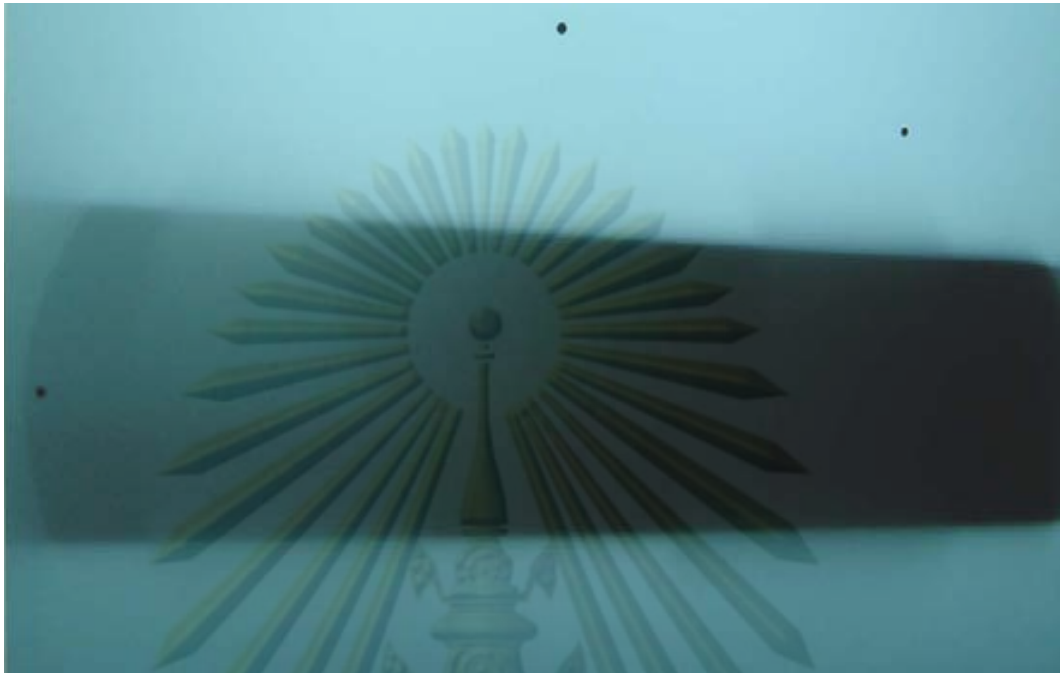


Figure 4.10 The EDR2 film image using digital camera of 3D-CRT field technique at central axis in parallel setup of 6 MV beams of patient plan 1.



Figure 4.11 The EDR2 film image using digital camera of 3D-CRT field technique at central axis in parallel setup of 6 MV beams of patient plan 2.



Figure 4.12 The EDR2 film image using digital camera of IMRT field technique at central axis in parallel setup of 6 MV beams of patient plan 1.



Figure 4.13 The EDR2 film image using digital camera of IMRT field technique at central axis in parallel setup of 6 MV beams of patient plan 2.

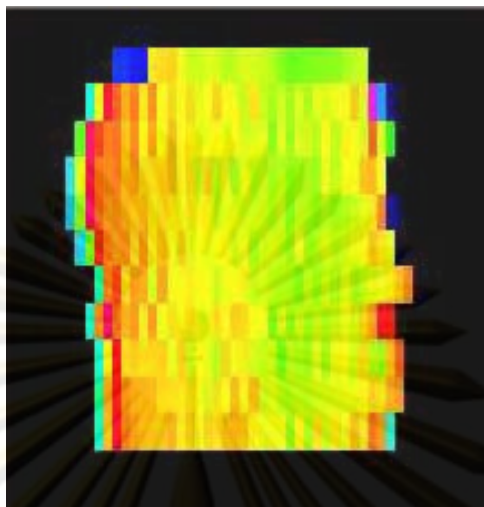


Figure 4.14 Subfields of planar dose maps of IMRT plan 1 from the Eclipse RTPS, 6 MV beam at 100 cm SAD.



Figure 4.15 Subfields of planar dose maps of IMRT plan 2 from the Eclipse RTPS, 6 MV beam at 100 cm SAD.

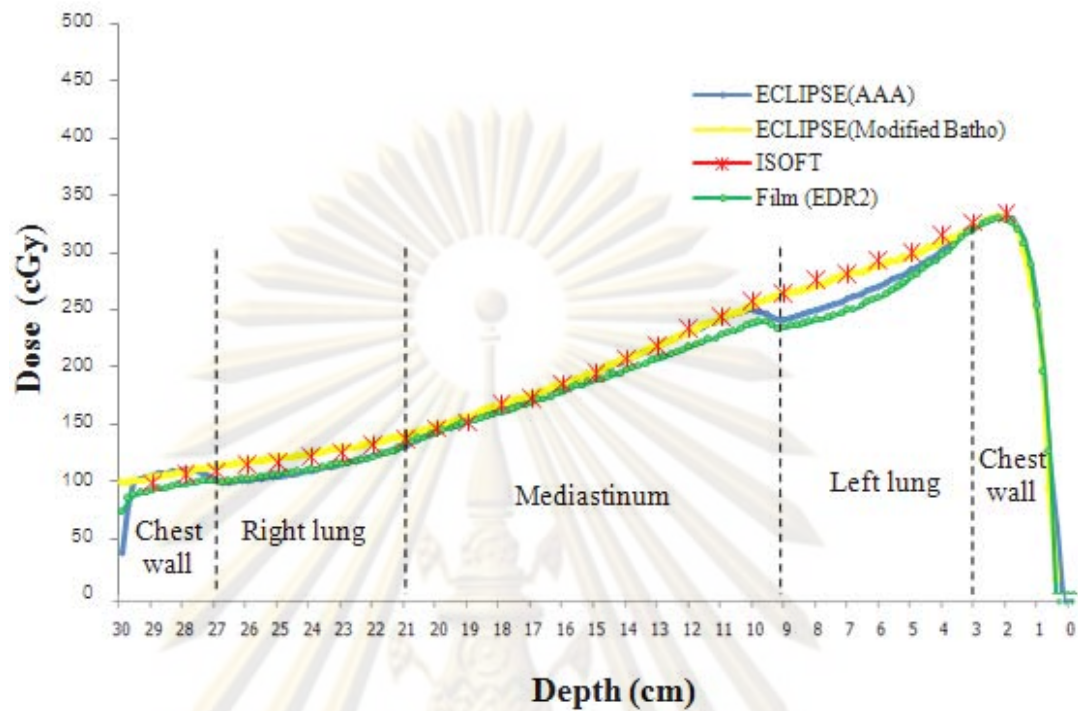


Figure 4.16 Central axis depth dose curve of 3D CRT plan 1 with the beam irradiated from left to right side of CIRS thorax phantom.

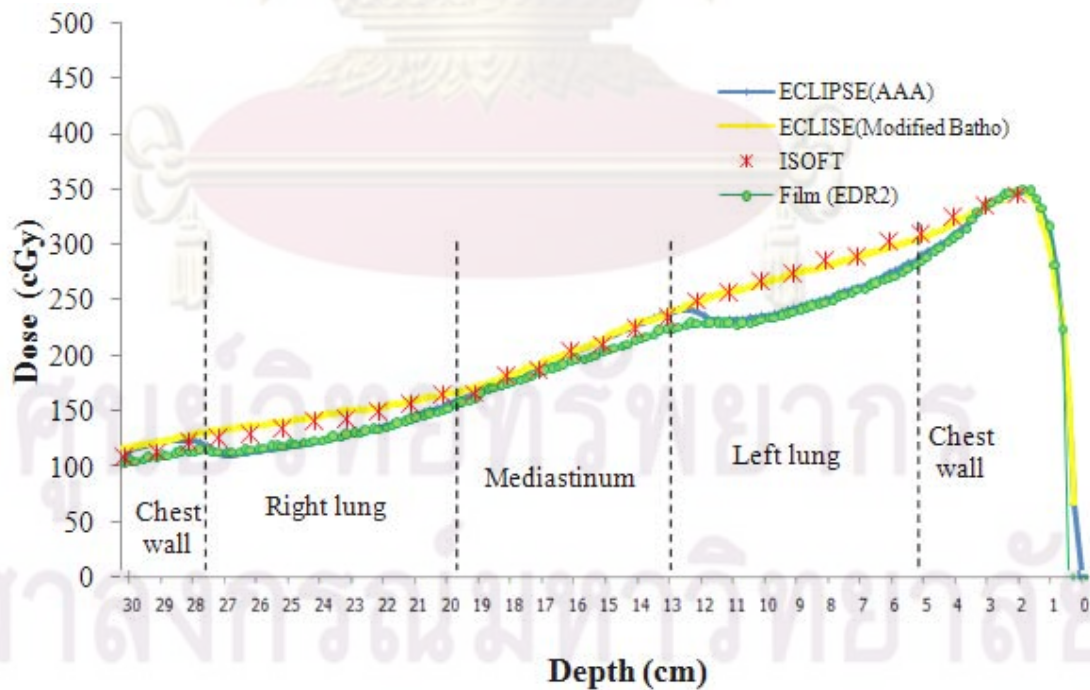


Figure 4.17 Central axis depth dose curve of 3D-CRT plan 2 with the beam irradiated from left to right side of CIRS thorax phantom.



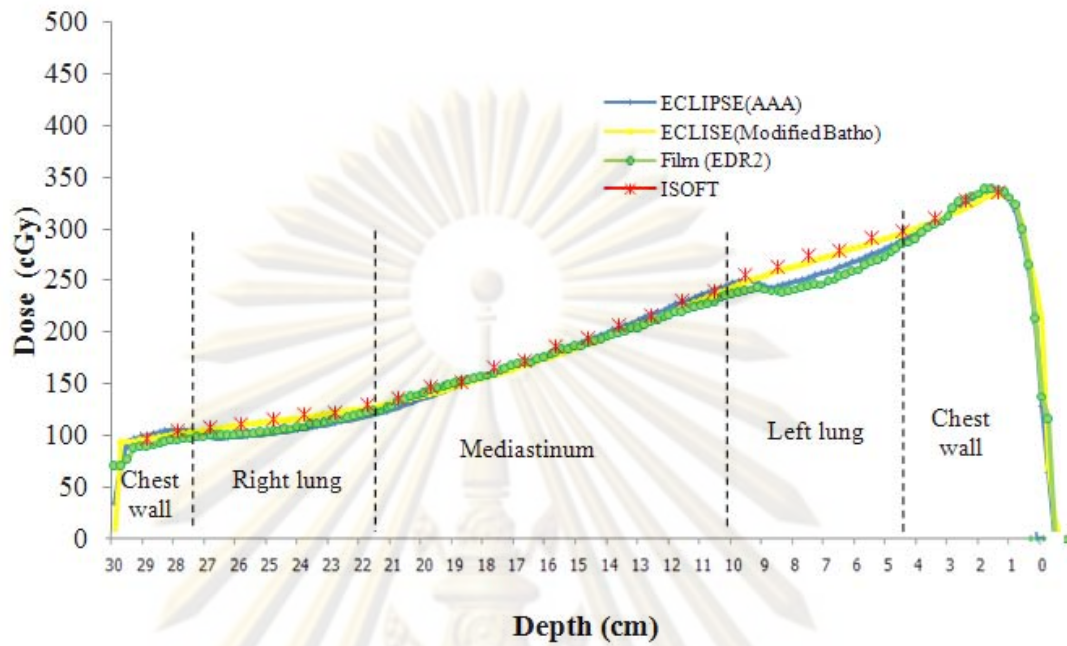


Figure 4.18 Central axis depth dose curve of IMRT plan 1 with the beam irradiated from left to right side of CIRS thorax phantom.

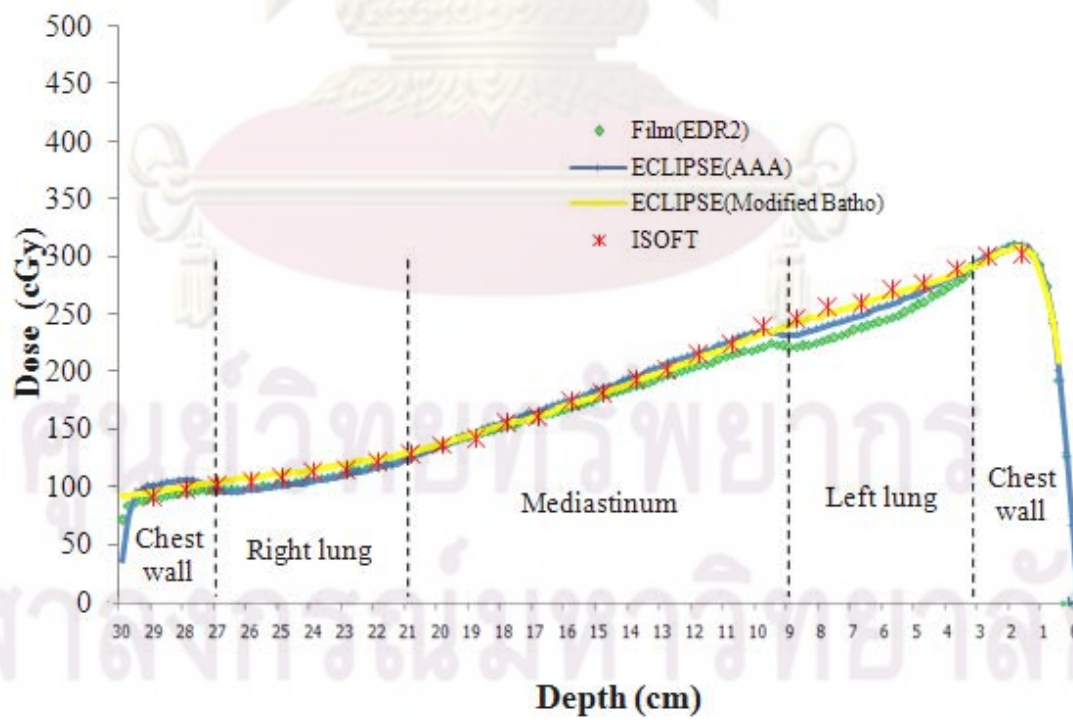


Figure 4.19 Central axis depth dose curve of IMRT plan 2 with the beam irradiated from left to right side of CIRS thorax phantom.

## CHAPTER V

### DISCUSSION AND CONCLUSION

Advanced techniques in radiotherapy, like intensity modulated radiotherapy (IMRT), increase the planning and delivery complexity. The dose distribution could be verified by measurement with ion chamber, film and detector array. These techniques are time consume, needed to be trained with more personnel. The independent dose calculation software is one of the alternative methods that is appropriate to verify dose distribution for the patient-specific QA of 3D-CRT and IMRT. The ISOFT software was developed to be a tool to calculate the point dose in term of absolute dose in both irregular shaped field and inhomogeneous medium for 3D-CRT and IMRT fields. The validation of the accuracy of this software, the Eclipse treatment planning system with dose measurement in homogeneous and thorax phantom are undertaken to prove that this ISOFT software can be used as a tool for patient specific QA.

#### 5.1 Dose verification of MLC fields in homogeneous phantom

The comparison between measurements by ion chamber and calculations by Eclipse system and ISOFT software in homogeneous water phantom for all field sizes and depth studied are in the criteria of acceptability according to IAEA TRS no. 430. For the square fields, the percent dose deviation is in good agreement within 1%. For rectangular fields, the dose agreement is within 1.5%. For shaped fields which included a series of corner block, circular field MLC, inverted Y field MLC and irregular field MLC, the overall agreement is within 2%. These results suggest the accurate point dose calculation of ISOFT. The ISOFT can calculate point dose at any points and depths of any types of irregular MLC fields in homogeneous phantom within few second and the deviation from the treatment plan is shown promptly.

#### 5.2 Dose verification of 3D-CRT and IMRT plans in inhomogeneous phantom

When the Clarkson method combined with 3D-BSM, the dose correction for both irregular shaped field and the effect of inhomogeneity is achieved. The program is

capable to import the CT base patient data with the correct CT number together with the treatment plan and the MLC file. The external contour could be constructed in this independent software and then the dose calculation is undertaken with the correction of the external contour.

The lung dose calculated by ISOFT for two plans of 3D-CRT field overestimates from the point dose measurement within 5.0%, but it is slightly better than the modified Batho from the treatment planning which showed 8.0% overestimated. The AAA shows lower lung dose than measured about 4.5%. However, for the 3-D inhomogeneity, the criterion of acceptability for the dose calculation is 5% [43]. When compared lung dose between ISOFT with modified Batho, they are overestimate from the measured in the same trend. ISOFT presents closer dose to the measured than modified Batho. The maximum difference between ISOFT and modified Batho is 3.0%. But the maximum difference between ISOFT and AAA algorithm is 9.2% because they are different from the measurement in the opposite direction.

The lung dose calculated by ISOFT for two plans of IMRT overestimates from the point dose measurement within 4.5%, but it is slightly better than the modified Batho from the treatment planning which showed 7.2% overestimate. The AAA shows both lower and higher lung dose than measured, the maximum deviation is about 2.8%. When compared lung dose between ISOFT with modified Batho, they overestimate from the measured in the same trend. ISOFT presents closer dose to the measured than modified Batho. The maximum difference between ISOFT and modifier Batho algorithm is 2.6%. But the maximum difference between ISOFT and AAA algorithm is 7.34%

The lung dose of both ISOFT and modified Batho overestimates due to the scattered doses are less in the low density medium. They are considered in the AAA but not taken properly in ISOFT and Modified Batho. The buildup due to the secondary electron at the interface is not considered in ISOFT and modified Batho. The presence of lungs with low density cause the electron disequilibrium. The severity increases with increasing energy and decreasing field size. Normally, the effects of inhomogeneity correction of IMRT were more complex than the conventional 3D-CRT due to the effect

of many small fields and steep fluence gradients. The errors of iterative inverse treatment planning of IMRT suggested inaccuracy dose calculation including systematic error and random error. The pencil beam algorithm were significant both of the systematic and random errors.

### 5.3 Limitation of ISOFT software

The ISOFT can calculate point doses in term of absolute doses in any section along the sagittal plane, but the isodose distribution could not be constructed. Only single field of  $10 \times 10 \text{ cm}^2$  could be applied at 90 degree gantry angle for both 3D-CRT and IMRT. The program could not support for composite plan, only one field can apply.

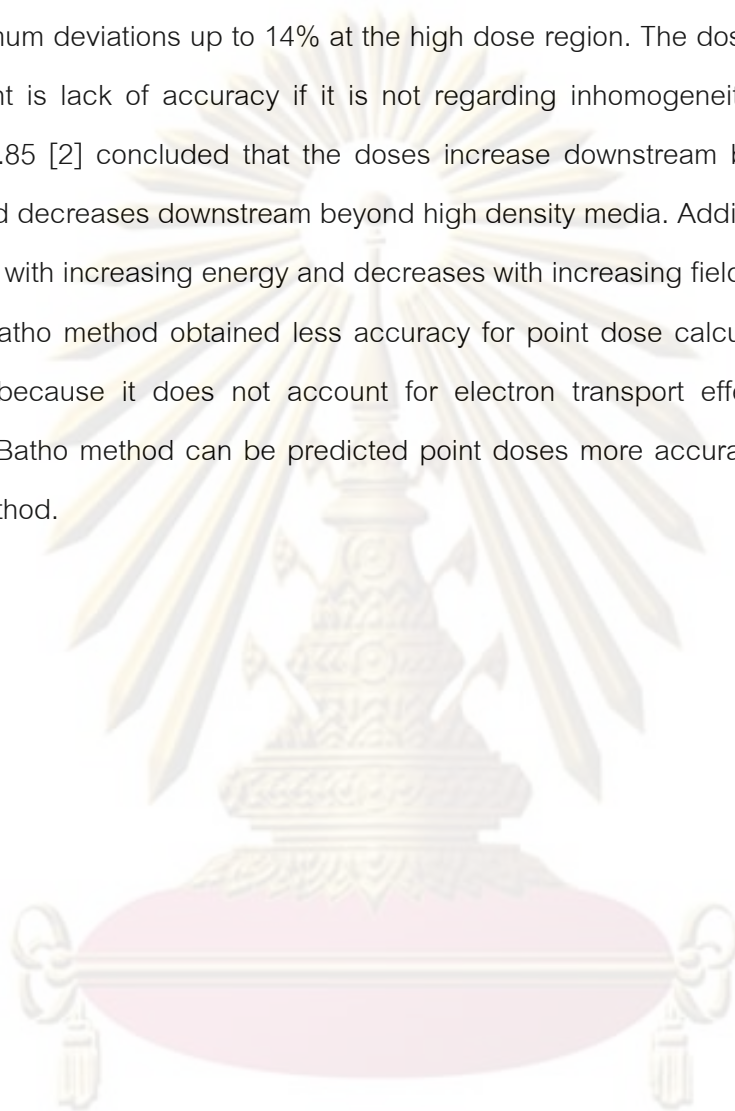
The off axis correction factor was not considered and the dose near the build up region both at the beam entrance and at the interface of two medium could not be calculated. The modified Batho that used for inhomogeneity correction are valid for high energy photons as soon as the electronic equilibrium is achieved, but IMRT uses small beamlets, so the electronic equilibrium is difficult to establish in the lung region. The scatter dose in lung also could not be determined correctly by modifier Batho, it is taken into account only the scatter from each individual plane not for 3 dimensions.

The calculation time is about 6 hours, but this is the first step, the further development of the algorithm used in the software would improve the more accurate point doses in lung and at the interface. The calculation time should be reduced. However, the calculation time is comparable to the time taken when using film. The advantage is no time consuming and labor intensive.

### 5.4 Comparison with the other studies

The other independent software mostly do not account for the inhomogeneity correction. Haslam et al [7] implemented independent monitor unit verification software that called RadCalc. The average calculation dose of IMRT fields by RadCalc was 1.4% higher than the treatment planning dose. However, heterogeneity corrections were not performed and the contour patient's skin was manually obtained by operators. Georg et al [5] proposed independent dose calculation software that applied a pencil beam

model based on a beam quality index. The dose of intensity modulated beam (IMB) showed the deviation of 1.1% compared between independent software and RTPS, with the maximum deviations up to 14% at the high dose region. The dose calculation within the patient is lack of accuracy if it is not regarding inhomogeneities correction. The AAPM no.85 [2] concluded that the doses increase downstream beyond low density media and decreases downstream beyond high density media. Additionally, the severity increases with increasing energy and decreases with increasing field size. Normally, the original Batho method obtained less accuracy for point dose calculation in high dose gradient because it does not account for electron transport effects. However, the modified Batho method can be predicted point doses more accurate than the original Batho method.



ศูนย์วิทยุทรัพยากร  
จุฬาลงกรณ์มหาวิทยาลัย

## REFERENCES

- [1] ICRU. Determination of Absorbed Dose in a Patient Irradiated by Beams of X or Gamma Rays in Radiotherapy Procedures. ICRU Report 24, International Committee of Radiation Units and Measurements, Washington DC, USA, 1976.
- [2] AAPM Report 85. Tissue inhomogeneity corrections for megavoltage photon beams: Report of the AAPM radiation therapy committee task group 65, Madison, WI, USA: Medical Physics Publishing, 2001.
- [3] John, P., G. Monitor unit calculations for external photon and electron beams. AAPM Annual meeting refresher course, Utah, USA, (2001): 1-10.
- [4] Lombardi, P., et al. Monitor unit calculation in 6 MV irregularly shaped beams-accuracy in clinical practice. British Journal of Radiology 70, 834 (1997): 638-644.
- [5] George, S., et al. Monitor unit calculations as part of beam commissioning for a radiation treatment planning system. Proceedings of the 22<sup>th</sup> Annual EMBS International conference, Chicago, USA, (2000): 1187-1190.
- [6] Chen, Y., et al. Implementation of A Clarkson Summation Algorithm for Dose Verification in MLC-based IMRT. Proceedings of the 22<sup>th</sup> Annual EMBS International Conference, Chicago, USA, (2000): 1534-1537.
- [7] Haslam, J. J., et al. Comparison of dose calculated by an intensity modulated radiotherapy treatment planning system and an independent monitor unit verification program. American College of Medical Physics 4, 3 (2003): 224-230.
- [8] Jingeng, Z., Fang-Fang, Y., Jae, H. K. Point dose verification for intensity modulated radiosurgery using Clarkson's method. Medical Physics 30, 8(2003): 2218-2221.
- [9] Kung, J. H., Chen, F. H., Kuchnir, F. K. A monitor unit verification in intensity modulated radiotherapy as a dosimetry quality assurance. Medical Physics 27 (2000): 2226-2230.
- [10] Xing, L., et al. Monitor unit calculation for intensity modulated photon field. Proceedings of the 22<sup>th</sup> Annual EMBS International conference, Chicago, USA, (2000): 173-176.

- [11] Kappas, K., and Rosenwald, J. C. A 3-D beam subtraction method for inhomogeneity correction in high energy X-ray radiotherapy. Radiotherapy and Oncology 5, (1986): 223-233.
- [12] Sotirios, S., et al. An inhomogeneity correction algorithm for irregular fields of high-energy photon beams based on Clarkson integration and the 3D beam subtraction method. American College of Medical Physics 7, 1 (2006): 1-13.
- [13] Jacob, V. D. The Modern Technology of Radiation Oncology: A Compendium for Medical Physicists and Radiation Oncologists. 2<sup>nd</sup> ed. USA: Medical Physics Pub, (2005).
- [14] Shahine, B. H., Al-Ghazi, M. S. A. L., and El-Khatib, E. Experimental Evaluation of interface doses in the presence of air cavities compared with treatment planning algorithms. Medical Physics 26, 3, (1999): 350-355.
- [15] Khan, F. M. The Physics of Radiation Therapy. 3<sup>rd</sup> ed. USA: Lippincott Williams & Wilkins, 2003.
- [16] Sotirios, S. Development of heterogeneity algorithms for high-energy photon beams in radiotherapy. Ph.D. Thesis, Medical Physics Department, University of Patras, (2005).
- [17] Sontag, M. R. Cunningham, J. R. Clinical application of a CT based treatment planning system. Computer Assisted Tomography 2, 2, (1978): 117-130.
- [18] Batho, M. F. Lung corrections in Co-60 beam therapy. Journal of the Canadian Association of Radiologists 15 (1964): 79-83.
- [19] Young, M. E., and Gaylord, J. D. Experimental tests of corrections for tissue inhomogeneities in radiotherapy. British Journal of Radiology 43, 509 (1970): 349-355.
- [20] Sontag, M. R., and Cunningham, J. R. Corrections to absorbed dose calculations for issue inhomogeneities. Medical Physics 4, 5 (1977): 431-436.
- [21] Sontag, M. R., Cunningham, J. R. The equivalent tissue-air ratio method for making absorbed dose calculations in a heterogeneous medium. Radiology, 129, 3 (1978): 787-794.

- [22] Webb, S., and Fox, R. A. Verification by Monte Carlo methods of a power law tissue-air ratio algorithm for inhomogeneity corrections in photon beam dose calculations. Physics in Medicine&Biology 25 (1980): 225–240.
- [23] Kappas, C., Rosenwald, J. C. Quality control of inhomogeneity correction algorithms used in treatment planning systems. International Journal of Radiation Oncology, Biology, Physics 32, 3 (1995): 847-858.
- [24] Kappas, K., and Rosenwald, J. C. Theoretical and experimental analysis of scatter from inhomogeneous slabs in a  $^{60}\text{Co}$  beam: the differential tissue-air ratio method (DTAR). Physics in Medicine&Biology 11 (1986): 1211 -1228.
- [25] O'Connor, J. E. The variation of scattered x-rays with density in an irradiated body. Physics in Medicine&Biology 1 (1957): 352–369.
- [26] Engelsman, M., et al. Impact of simple tissue inhomogeneity correction algorithms on conformal radiotherapy of lung tumors. Radiation Oncology 60 (2001): 299-309.
- [27] Sievinen, J., Ulmer, W., and Kaissl, W., AAA photon dose calculation in Eclipse, Varian documentation RAD #7170B (2005).
- [28] Esch, A. V., et al. Testing of the analytical anisotropic algorithm for photon dose calculation, Medical Physics 33, 11 (2006): 4130-4148.
- [29] Isabelle, M. G., and Sergei, Z. Evaluation of the analytical anisotropic algorithm in an extreme water-lung interface phantom using Monte Carlo dose calculations. American College of Medical Physics 8, 1 (2007): 33-46.
- [30] Arno, J. M., and John, C. R. Intensity modulated radiation therapy. London : BC Decker, 2005.
- [31] Hendee, R. W., Ibbott, S. G., and Hendee, G. E. Radiation Therapy Physics. 3<sup>rd</sup> ed. New Jersey: John Wiley & Sons, 2005.
- [32] International Atomic Energy Agency. TRS no.430: Commissioning and quality assurance of computerized planning system for radiation treatment of cancer. Vienna, 2004.
- [33] Dyk, J. V., et al. Commissioning and quality assurance of treatment planning computer. International Journal of Radiation Oncology, Biology, Physics 26 (1993): 172-173.



- [34] Mijnheer, B., et al. Quality assurance of treatment planning systems practical examples for non-IMRT photon beams. ESTRO, 2004.
- [35] Fraass, B., Doppke, K., Hunt, M., et al. American Association of Physicists in Medicine Radiation Therapy Committee Task Group 53: quality assurance for clinical radiotherapy treatment planning. Medical Physics 25 (1998): 1773-1829.
- [36] CIRS tissue simulation & Phantom technology. [cited 2006 Sep 10] Available from: URL:[http://www.cirsinc.com/002pra\\_rad.htm](http://www.cirsinc.com/002pra_rad.htm).
- [37] Plessis, F. C. P., et al. Comparison of the Batho, ETAR and Monte Carlo dose calculation methods in CT based patient models. Medical Physics 28, 4 (2001): 582-589.
- [38] Zhu, X. R. Evaluation of Kodak EDR2 film for dose verification of intensity modulated radiation therapy delivered by a static multileaf collimator. Medical Physics 29, 8 (2002): 1687-1692.
- [39] Nathan, L. C. et al. Dosimetric accuracy of Kodak EDR2 film for IMRT verifications. Medical Physics 32, 2 (2005): 539-548.
- [40] International Atomic Energy Agency. TRS 398 Absorbed dose determination in phantom and electron beams. USA: IAEA, 2004.
- [41] Chen, Z., et al. Independent monitor unit calculation for intensity modulated radiotherapy using the MIMic multileaf collimator. Medical Physics 29, 9 (2002): 2041-2051.
- [42] Basic Applications of Multileaf collimators: Report of the AAPM radiation therapy committee task group 50, Medical Physics, WI, USA: Madison, 2001.



APPENDICES

ศูนย์วิทยทรัพยากร  
จุฬาลงกรณ์มหาวิทยาลัย

## Appendix A The table of beam data requirement

Table 1 Tissue maximum ratio  $TMR_{(d,r)}$  in a water phantom with field size of  $1 \times 1 \text{ cm}^2$  to  $40 \times 40 \text{ cm}^2$  and depth of 1.5 cm to 40 cm.

Depth/FS	1x1	2x2	3x3	4x4	5x5	6x6	7x7	8x8	9x9	10x10	11x11	12x12	13x13	14x14	15x15	16x16	17x17	18x18	19x19	20x20
1.5	1.00	1.00	1.00	1.00	1.00	1.00	1.00	1.00	1.00	1.00	1.00	1.00	1.00	1.00	1.00	1.00	1.00	1.00	1.00	1.00
2.0	0.99	0.99	1.00	1.00	1.00	1.00	1.00	1.00	1.00	1.00	1.00	0.99	0.99	0.99	0.99	0.99	0.99	0.99	0.99	0.99
2.5	0.97	0.97	0.98	0.98	0.99	0.99	0.99	0.99	0.99	0.99	0.99	0.98	0.98	0.98	0.99	0.99	0.99	0.99	0.99	0.99
3.0	0.94	0.95	0.96	0.97	0.97	0.97	0.97	0.98	0.98	0.98	0.98	0.97	0.97	0.97	0.98	0.98	0.98	0.98	0.98	0.98
3.5	0.92	0.93	0.94	0.95	0.96	0.96	0.96	0.96	0.96	0.96	0.96	0.96	0.96	0.96	0.96	0.97	0.97	0.97	0.97	0.97
4.0	0.90	0.91	0.92	0.94	0.94	0.95	0.95	0.95	0.95	0.95	0.95	0.95	0.95	0.95	0.95	0.95	0.96	0.96	0.96	0.96
4.5	0.88	0.89	0.90	0.92	0.92	0.93	0.93	0.93	0.93	0.94	0.94	0.94	0.94	0.94	0.94	0.94	0.94	0.94	0.94	0.95
5.0	0.86	0.87	0.88	0.90	0.90	0.91	0.91	0.92	0.92	0.92	0.92	0.92	0.92	0.92	0.93	0.93	0.93	0.93	0.93	0.93
5.3	0.85	0.86	0.87	0.89	0.90	0.90	0.91	0.91	0.91	0.92	0.92	0.92	0.92	0.92	0.92	0.92	0.92	0.93	0.93	0.93
5.5	0.84	0.85	0.86	0.88	0.89	0.89	0.90	0.90	0.90	0.91	0.91	0.91	0.91	0.91	0.91	0.92	0.92	0.92	0.92	0.92
5.8	0.82	0.84	0.85	0.87	0.88	0.88	0.89	0.89	0.90	0.90	0.90	0.90	0.90	0.90	0.91	0.91	0.91	0.91	0.92	0.92
6.0	0.81	0.83	0.85	0.86	0.87	0.88	0.88	0.89	0.89	0.90	0.90	0.90	0.89	0.90	0.90	0.91	0.91	0.91	0.91	0.91
6.3	0.81	0.82	0.84	0.85	0.86	0.87	0.87	0.88	0.88	0.89	0.89	0.89	0.89	0.89	0.90	0.90	0.90	0.90	0.90	0.90
6.5	0.80	0.81	0.83	0.84	0.85	0.86	0.87	0.87	0.87	0.88	0.88	0.88	0.88	0.88	0.89	0.89	0.89	0.90	0.90	0.90
6.8	0.79	0.81	0.82	0.83	0.84	0.85	0.86	0.86	0.87	0.87	0.87	0.88	0.88	0.88	0.88	0.89	0.89	0.89	0.89	0.89
7.0	0.78	0.80	0.81	0.83	0.84	0.84	0.85	0.85	0.86	0.86	0.87	0.87	0.87	0.87	0.88	0.88	0.88	0.88	0.88	0.89
7.3	0.77	0.79	0.80	0.82	0.83	0.84	0.84	0.85	0.85	0.86	0.86	0.86	0.86	0.87	0.87	0.87	0.87	0.88	0.88	0.88
7.5	0.76	0.77	0.79	0.81	0.82	0.83	0.83	0.84	0.84	0.85	0.85	0.86	0.86	0.86	0.86	0.87	0.87	0.87	0.87	0.87
7.8	0.75	0.76	0.78	0.80	0.81	0.82	0.82	0.83	0.84	0.84	0.85	0.85	0.85	0.85	0.86	0.86	0.86	0.86	0.87	0.87
8.0	0.73	0.75	0.77	0.79	0.80	0.81	0.82	0.82	0.83	0.84	0.84	0.84	0.84	0.85	0.85	0.85	0.86	0.86	0.86	0.86
8.3	0.73	0.74	0.76	0.78	0.79	0.80	0.81	0.82	0.82	0.83	0.84	0.84	0.83	0.84	0.84	0.85	0.85	0.85	0.86	0.86

Depth/FS	1x1	2x2	3x3	4x4	5x5	6x6	7x7	8x8	9x9	10x10	11x11	12x12	13x13	14x14	15x15	16x16	17x17	18x18	19x19	20x20
8.5	0.72	0.74	0.75	0.77	0.78	0.79	0.80	0.81	0.81	0.82	0.83	0.83	0.83	0.83	0.84	0.84	0.84	0.85	0.85	0.85
8.8	0.72	0.73	0.75	0.76	0.78	0.79	0.80	0.80	0.81	0.81	0.82	0.82	0.82	0.83	0.83	0.83	0.84	0.84	0.84	0.85
9.0	0.71	0.72	0.74	0.75	0.77	0.78	0.79	0.79	0.80	0.81	0.81	0.81	0.81	0.82	0.82	0.83	0.83	0.84	0.84	0.84
9.3	0.70	0.72	0.73	0.75	0.76	0.77	0.78	0.79	0.79	0.80	0.81	0.81	0.81	0.81	0.82	0.82	0.83	0.83	0.83	0.83
9.5	0.69	0.71	0.72	0.74	0.75	0.76	0.77	0.78	0.79	0.79	0.80	0.80	0.80	0.81	0.81	0.81	0.82	0.82	0.82	0.83
9.8	0.68	0.70	0.71	0.73	0.74	0.75	0.76	0.77	0.78	0.78	0.79	0.79	0.80	0.80	0.80	0.81	0.81	0.81	0.82	0.82
10.0	0.67	0.69	0.71	0.72	0.73	0.75	0.76	0.76	0.77	0.78	0.79	0.79	0.79	0.79	0.80	0.80	0.80	0.81	0.81	0.81
10.3	0.66	0.68	0.70	0.71	0.73	0.74	0.75	0.76	0.76	0.77	0.78	0.78	0.78	0.79	0.79	0.79	0.80	0.80	0.81	0.81
10.5	0.66	0.67	0.69	0.71	0.72	0.73	0.74	0.75	0.76	0.76	0.77	0.77	0.77	0.78	0.78	0.79	0.79	0.80	0.80	0.80
10.8	0.65	0.67	0.68	0.70	0.71	0.72	0.73	0.74	0.75	0.76	0.76	0.77	0.77	0.77	0.78	0.78	0.79	0.79	0.79	0.80
11.0	0.64	0.66	0.67	0.69	0.70	0.72	0.73	0.74	0.74	0.75	0.75	0.76	0.76	0.76	0.77	0.78	0.78	0.78	0.79	0.79
11.3	0.63	0.65	0.67	0.68	0.70	0.71	0.72	0.73	0.74	0.74	0.75	0.75	0.75	0.76	0.76	0.77	0.77	0.78	0.78	0.78
11.5	0.63	0.64	0.66	0.68	0.69	0.70	0.71	0.72	0.73	0.73	0.74	0.74	0.75	0.75	0.76	0.76	0.77	0.77	0.77	0.78
11.8	0.62	0.63	0.65	0.67	0.68	0.69	0.70	0.71	0.72	0.73	0.73	0.74	0.74	0.74	0.75	0.76	0.76	0.76	0.77	0.77
12.0	0.61	0.63	0.64	0.66	0.67	0.68	0.69	0.70	0.71	0.72	0.73	0.73	0.73	0.74	0.74	0.75	0.75	0.76	0.76	0.76
12.3	0.60	0.62	0.64	0.65	0.67	0.68	0.69	0.70	0.71	0.71	0.72	0.73	0.73	0.73	0.74	0.74	0.75	0.75	0.75	0.76
12.5	0.60	0.61	0.63	0.64	0.66	0.67	0.68	0.69	0.70	0.71	0.71	0.72	0.72	0.72	0.73	0.74	0.74	0.74	0.75	0.75
12.8	0.59	0.61	0.62	0.64	0.65	0.66	0.67	0.68	0.69	0.70	0.71	0.71	0.71	0.72	0.72	0.73	0.74	0.74	0.74	0.74
13.0	0.58	0.60	0.61	0.63	0.64	0.65	0.67	0.67	0.68	0.69	0.70	0.71	0.71	0.71	0.72	0.72	0.73	0.73	0.74	0.74
13.3	0.58	0.59	0.61	0.62	0.64	0.65	0.66	0.67	0.68	0.69	0.70	0.70	0.70	0.70	0.71	0.72	0.72	0.73	0.73	0.73
13.5	0.57	0.59	0.60	0.62	0.63	0.64	0.65	0.66	0.67	0.68	0.69	0.69	0.69	0.70	0.70	0.71	0.72	0.72	0.72	0.73
13.8	0.57	0.58	0.60	0.61	0.62	0.64	0.65	0.66	0.66	0.67	0.68	0.69	0.69	0.69	0.70	0.70	0.71	0.72	0.72	0.72
14.0	0.56	0.58	0.59	0.60	0.62	0.63	0.64	0.65	0.66	0.66	0.67	0.68	0.68	0.68	0.69	0.70	0.71	0.71	0.71	0.72
14.3	0.56	0.57	0.58	0.60	0.61	0.62	0.64	0.64	0.65	0.66	0.67	0.67	0.68	0.68	0.69	0.69	0.70	0.70	0.71	0.71
14.5	0.55	0.56	0.58	0.59	0.60	0.62	0.63	0.64	0.64	0.65	0.66	0.67	0.67	0.67	0.68	0.69	0.69	0.70	0.70	0.70

Depth/FS	1x1	2x2	3x3	4x4	5x5	6x6	7x7	8x8	9x9	10x10	11x11	12x12	13x13	14x14	15x15	16x16	17x17	18x18	19x19	20x20
14.8	0.54	0.56	0.57	0.58	0.60	0.61	0.62	0.63	0.64	0.64	0.65	0.66	0.66	0.67	0.67	0.68	0.69	0.69	0.69	0.70
15.0	0.54	0.55	0.56	0.58	0.59	0.60	0.61	0.62	0.63	0.64	0.65	0.65	0.66	0.66	0.67	0.67	0.68	0.69	0.69	0.69
15.5	0.52	0.54	0.55	0.56	0.58	0.59	0.60	0.61	0.62	0.63	0.63	0.64	0.64	0.65	0.65	0.66	0.67	0.67	0.68	0.68
16.0	0.51	0.52	0.54	0.55	0.56	0.57	0.59	0.59	0.60	0.61	0.62	0.63	0.63	0.63	0.64	0.65	0.65	0.66	0.66	0.67
16.5	0.50	0.51	0.52	0.54	0.55	0.56	0.57	0.58	0.59	0.60	0.61	0.62	0.62	0.62	0.63	0.63	0.64	0.65	0.65	0.65
17.0	0.49	0.50	0.51	0.53	0.54	0.55	0.56	0.57	0.58	0.59	0.60	0.60	0.61	0.61	0.62	0.62	0.63	0.64	0.64	0.64
17.5	0.47	0.49	0.50	0.52	0.53	0.54	0.55	0.56	0.57	0.58	0.59	0.59	0.60	0.60	0.61	0.61	0.62	0.62	0.63	0.63
18.0	0.46	0.48	0.49	0.50	0.52	0.53	0.54	0.55	0.56	0.57	0.58	0.59	0.59	0.59	0.59	0.60	0.61	0.61	0.62	0.62
18.5	0.45	0.47	0.48	0.49	0.50	0.52	0.53	0.54	0.55	0.55	0.56	0.57	0.58	0.58	0.58	0.59	0.60	0.60	0.61	0.61
19.0	0.45	0.46	0.47	0.48	0.49	0.50	0.52	0.52	0.53	0.54	0.55	0.56	0.56	0.57	0.57	0.58	0.59	0.59	0.60	0.60
19.5	0.43	0.45	0.46	0.47	0.48	0.49	0.51	0.51	0.52	0.53	0.54	0.55	0.55	0.56	0.56	0.57	0.57	0.58	0.58	0.59
20.0	0.42	0.44	0.45	0.46	0.47	0.48	0.50	0.50	0.51	0.52	0.53	0.54	0.54	0.54	0.55	0.56	0.56	0.57	0.57	0.58
21.0	0.41	0.42	0.43	0.44	0.45	0.46	0.47	0.48	0.49	0.50	0.51	0.52	0.52	0.52	0.53	0.54	0.54	0.55	0.56	0.56
22.0	0.39	0.40	0.41	0.42	0.43	0.44	0.45	0.46	0.47	0.48	0.49	0.50	0.50	0.51	0.51	0.52	0.52	0.53	0.53	0.54
23.0	0.37	0.38	0.39	0.40	0.41	0.43	0.44	0.45	0.45	0.46	0.47	0.48	0.48	0.49	0.49	0.50	0.50	0.51	0.52	0.52
24.0	0.35	0.36	0.37	0.38	0.39	0.41	0.42	0.42	0.43	0.44	0.45	0.45	0.46	0.46	0.47	0.47	0.48	0.49	0.49	0.50
25.0	0.34	0.35	0.36	0.37	0.38	0.39	0.40	0.41	0.41	0.42	0.43	0.44	0.45	0.45	0.45	0.46	0.46	0.47	0.47	0.48
26.0	0.33	0.33	0.34	0.35	0.36	0.37	0.38	0.39	0.40	0.40	0.41	0.42	0.43	0.43	0.43	0.44	0.45	0.45	0.46	0.46
27.0	0.31	0.32	0.33	0.34	0.35	0.36	0.36	0.37	0.38	0.39	0.39	0.40	0.41	0.41	0.42	0.42	0.43	0.43	0.44	0.44
28.0	0.30	0.31	0.32	0.32	0.33	0.34	0.35	0.36	0.36	0.37	0.38	0.39	0.39	0.40	0.40	0.41	0.41	0.42	0.42	0.43
29.0	0.28	0.29	0.30	0.31	0.32	0.33	0.33	0.34	0.35	0.36	0.36	0.37	0.38	0.38	0.39	0.39	0.40	0.40	0.41	0.41
30.0	0.27	0.28	0.29	0.30	0.30	0.31	0.32	0.33	0.33	0.34	0.35	0.36	0.36	0.37	0.37	0.37	0.38	0.39	0.39	0.40
31.0	0.26	0.26	0.27	0.28	0.29	0.30	0.31	0.32	0.32	0.33	0.33	0.34	0.35	0.35	0.35	0.36	0.37	0.37	0.38	0.38
32.0	0.24	0.25	0.26	0.27	0.28	0.29	0.29	0.30	0.31	0.31	0.32	0.33	0.33	0.34	0.34	0.34	0.35	0.36	0.36	0.37
33.0	0.23	0.24	0.25	0.26	0.26	0.27	0.28	0.29	0.29	0.30	0.31	0.31	0.32	0.32	0.33	0.33	0.34	0.34	0.35	0.35

Depth\FS	1x1	2x2	3x3	4x4	5x5	6x6	7x7	8x8	9x9	10x10	11x11	12x12	13x13	14x14	15x15	16x16	17x17	18x18	19x19	20x20
34.0	0.22	0.23	0.24	0.24	0.25	0.26	0.27	0.28	0.28	0.29	0.29	0.30	0.31	0.31	0.31	0.32	0.32	0.33	0.33	0.34
35.0	0.21	0.22	0.23	0.23	0.24	0.25	0.26	0.26	0.27	0.28	0.28	0.29	0.29	0.30	0.30	0.30	0.31	0.31	0.32	0.33
36.0	0.20	0.21	0.21	0.22	0.23	0.24	0.25	0.25	0.26	0.26	0.27	0.28	0.28	0.29	0.29	0.29	0.30	0.30	0.31	0.31
37.0	0.19	0.20	0.20	0.21	0.22	0.23	0.23	0.24	0.25	0.25	0.26	0.26	0.27	0.28	0.28	0.28	0.28	0.29	0.30	0.30
38.0	0.18	0.19	0.19	0.20	0.21	0.22	0.22	0.23	0.24	0.24	0.25	0.25	0.26	0.26	0.27	0.27	0.27	0.28	0.28	0.29
39.0	0.17	0.18	0.19	0.19	0.20	0.21	0.21	0.22	0.23	0.23	0.24	0.24	0.25	0.25	0.26	0.26	0.26	0.27	0.27	0.28
40.0	0.16	0.17	0.18	0.18	0.19	0.20	0.20	0.21	0.22	0.22	0.23	0.23	0.24	0.24	0.25	0.25	0.25	0.26	0.26	0.27

ศูนย์วิทยทรัพยากร  
จุฬาลงกรณ์มหาวิทยาลัย

Table 1 Tissue maximum ratio  $TMR_{(d,r)}$  in a water phantom with field size of  $1 \times 1 \text{ cm}^2$  to  $40 \times 40 \text{ cm}^2$  and depth of 1.5 cm to 40 cm. (Continue)

Depth/FS	21x21	22x22	23x23	24x24	25x25	26x26	27x27	28x28	29x29	30x30	31x31	32x32	33x33	34x34	35x35	36x36	37x37	38x38	39x39	40x40
1.5	1	1	1	1	1	1	1	1	1	1	1	1	1	1	1	1	1	1	1	1
2.0	0.99	1.00	1.00	1.00	1.00	1.00	1.00	1.00	1.00	1.00	1.00	1.00	1.00	1.00	1.00	1.00	1.00	1.00	1.00	1.00
2.5	0.99	0.99	0.99	0.99	0.99	0.99	0.99	0.99	0.99	0.99	0.99	0.99	0.99	0.99	0.99	0.99	0.99	0.99	0.99	0.99
3.0	0.98	0.98	0.98	0.98	0.98	0.98	0.98	0.98	0.98	0.98	0.98	0.98	0.98	0.98	0.98	0.98	0.98	0.98	0.98	0.98
3.5	0.97	0.97	0.97	0.97	0.97	0.97	0.97	0.97	0.97	0.97	0.97	0.97	0.97	0.97	0.97	0.97	0.97	0.97	0.97	0.97
4.0	0.96	0.96	0.96	0.96	0.96	0.96	0.96	0.96	0.96	0.96	0.96	0.96	0.96	0.96	0.96	0.96	0.96	0.96	0.96	0.96
4.5	0.95	0.95	0.95	0.95	0.95	0.95	0.95	0.95	0.95	0.95	0.95	0.95	0.95	0.95	0.95	0.95	0.95	0.95	0.95	0.95
5.0	0.94	0.94	0.94	0.94	0.94	0.94	0.94	0.94	0.94	0.94	0.94	0.94	0.94	0.94	0.94	0.95	0.95	0.95	0.95	0.95
5.3	0.93	0.93	0.93	0.93	0.93	0.93	0.93	0.93	0.93	0.93	0.94	0.94	0.94	0.94	0.94	0.94	0.94	0.94	0.94	0.94
5.5	0.92	0.92	0.93	0.93	0.93	0.93	0.93	0.93	0.93	0.93	0.93	0.93	0.93	0.93	0.93	0.93	0.93	0.93	0.93	0.93
5.8	0.92	0.92	0.92	0.92	0.92	0.92	0.92	0.92	0.92	0.92	0.92	0.92	0.93	0.93	0.93	0.93	0.93	0.93	0.93	0.93
6.0	0.91	0.91	0.91	0.92	0.92	0.92	0.92	0.92	0.92	0.92	0.92	0.92	0.92	0.92	0.92	0.92	0.92	0.92	0.92	0.92
6.3	0.91	0.91	0.91	0.91	0.91	0.91	0.91	0.91	0.91	0.91	0.91	0.91	0.91	0.92	0.92	0.92	0.92	0.92	0.92	0.92
6.5	0.90	0.90	0.90	0.90	0.91	0.91	0.91	0.91	0.91	0.91	0.91	0.91	0.91	0.91	0.91	0.91	0.91	0.91	0.91	0.91
6.8	0.89	0.89	0.90	0.90	0.90	0.90	0.90	0.90	0.90	0.90	0.90	0.90	0.90	0.91	0.91	0.91	0.91	0.91	0.91	0.91
7.0	0.89	0.89	0.89	0.89	0.89	0.90	0.90	0.90	0.90	0.90	0.90	0.90	0.90	0.90	0.90	0.90	0.90	0.90	0.90	0.90
7.3	0.88	0.88	0.88	0.89	0.89	0.89	0.89	0.89	0.89	0.89	0.89	0.89	0.89	0.90	0.90	0.90	0.90	0.90	0.90	0.90
7.5	0.88	0.88	0.88	0.88	0.88	0.88	0.89	0.89	0.89	0.89	0.89	0.89	0.89	0.89	0.89	0.89	0.89	0.89	0.89	0.89
7.8	0.87	0.87	0.87	0.87	0.88	0.88	0.88	0.88	0.88	0.88	0.88	0.88	0.88	0.89	0.89	0.89	0.89	0.89	0.89	0.89
8.0	0.87	0.87	0.87	0.87	0.87	0.87	0.87	0.87	0.87	0.88	0.88	0.88	0.88	0.88	0.88	0.88	0.88	0.88	0.88	0.88
8.3	0.86	0.86	0.86	0.86	0.86	0.87	0.87	0.87	0.87	0.87	0.87	0.87	0.87	0.87	0.88	0.88	0.88	0.88	0.88	0.88
8.5	0.85	0.86	0.86	0.86	0.86	0.86	0.86	0.86	0.86	0.86	0.86	0.87	0.87	0.87	0.87	0.87	0.87	0.87	0.87	0.87
8.8	0.85	0.85	0.85	0.85	0.85	0.85	0.86	0.86	0.86	0.86	0.86	0.86	0.86	0.86	0.87	0.87	0.87	0.87	0.87	0.87
9.0	0.84	0.84	0.84	0.85	0.85	0.85	0.85	0.85	0.85	0.85	0.85	0.85	0.85	0.86	0.86	0.86	0.86	0.86	0.86	0.86

Depth/FS	1x1	2x2	3x3	4x4	5x5	6x6	7x7	8x8	9x9	10x10	11x11	12x12	13x13	14x14	15x15	16x16	17x17	18x18	19x19	20x20
9.3	0.84	0.84	0.84	0.84	0.84	0.84	0.84	0.84	0.85	0.85	0.85	0.85	0.85	0.85	0.85	0.86	0.86	0.86	0.86	0.86
9.5	0.83	0.83	0.83	0.83	0.83	0.84	0.84	0.84	0.84	0.84	0.84	0.84	0.84	0.85	0.85	0.85	0.85	0.85	0.85	0.85
9.8	0.82	0.83	0.83	0.83	0.83	0.83	0.83	0.83	0.83	0.83	0.84	0.84	0.84	0.84	0.84	0.84	0.84	0.84	0.85	0.85
10.0	0.82	0.82	0.82	0.82	0.82	0.82	0.82	0.83	0.83	0.83	0.83	0.83	0.83	0.83	0.84	0.84	0.84	0.84	0.84	0.84
10.3	0.81	0.81	0.81	0.81	0.82	0.82	0.82	0.82	0.82	0.82	0.82	0.83	0.83	0.83	0.83	0.83	0.83	0.83	0.83	0.83
10.5	0.80	0.81	0.81	0.81	0.81	0.81	0.81	0.82	0.82	0.82	0.82	0.82	0.82	0.82	0.83	0.83	0.83	0.83	0.83	0.83
10.8	0.80	0.80	0.80	0.80	0.80	0.81	0.81	0.81	0.81	0.81	0.82	0.82	0.82	0.82	0.82	0.82	0.82	0.82	0.82	0.82
11.0	0.79	0.79	0.79	0.80	0.80	0.80	0.80	0.81	0.81	0.81	0.81	0.81	0.81	0.82	0.82	0.82	0.82	0.82	0.82	0.82
11.3	0.78	0.79	0.79	0.79	0.79	0.79	0.80	0.80	0.80	0.80	0.80	0.81	0.81	0.81	0.81	0.81	0.81	0.81	0.81	0.81
11.5	0.78	0.78	0.78	0.78	0.78	0.79	0.79	0.79	0.79	0.80	0.80	0.80	0.80	0.80	0.81	0.81	0.81	0.81	0.81	0.81
11.8	0.77	0.77	0.77	0.78	0.78	0.78	0.78	0.78	0.79	0.79	0.79	0.79	0.80	0.80	0.80	0.80	0.80	0.80	0.80	0.80
12.0	0.76	0.77	0.77	0.77	0.77	0.77	0.78	0.78	0.78	0.78	0.78	0.79	0.79	0.79	0.79	0.79	0.80	0.80	0.80	0.80
12.3	0.76	0.76	0.76	0.76	0.77	0.77	0.77	0.77	0.77	0.78	0.78	0.78	0.78	0.79	0.79	0.79	0.79	0.79	0.79	0.79
12.5	0.75	0.75	0.76	0.76	0.76	0.76	0.77	0.77	0.77	0.77	0.77	0.78	0.78	0.78	0.78	0.78	0.79	0.79	0.79	0.79
12.8	0.75	0.75	0.75	0.75	0.75	0.76	0.76	0.76	0.77	0.77	0.77	0.77	0.77	0.78	0.78	0.78	0.78	0.78	0.78	0.78
13.0	0.74	0.74	0.75	0.75	0.75	0.75	0.76	0.76	0.76	0.76	0.76	0.77	0.77	0.77	0.77	0.77	0.78	0.78	0.78	0.78
13.3	0.74	0.74	0.74	0.74	0.74	0.75	0.75	0.75	0.75	0.76	0.76	0.76	0.76	0.76	0.77	0.77	0.77	0.77	0.77	0.77
13.5	0.73	0.73	0.73	0.74	0.74	0.74	0.74	0.75	0.75	0.75	0.75	0.75	0.76	0.76	0.76	0.76	0.76	0.76	0.76	0.77
13.8	0.72	0.73	0.73	0.73	0.73	0.73	0.74	0.74	0.74	0.74	0.75	0.75	0.75	0.75	0.75	0.76	0.76	0.76	0.76	0.76
14.0	0.72	0.72	0.72	0.72	0.73	0.73	0.73	0.73	0.74	0.74	0.74	0.74	0.74	0.75	0.75	0.75	0.75	0.75	0.75	0.75
14.3	0.71	0.71	0.72	0.72	0.72	0.72	0.73	0.73	0.73	0.73	0.73	0.74	0.74	0.74	0.74	0.75	0.75	0.75	0.75	0.75
14.5	0.71	0.71	0.71	0.71	0.71	0.72	0.72	0.72	0.73	0.73	0.73	0.73	0.73	0.74	0.74	0.74	0.74	0.74	0.74	0.74
14.8	0.70	0.70	0.70	0.71	0.71	0.71	0.71	0.72	0.72	0.72	0.73	0.73	0.73	0.73	0.73	0.74	0.74	0.74	0.74	0.74
15.0	0.69	0.70	0.70	0.70	0.70	0.71	0.71	0.71	0.72	0.72	0.72	0.72	0.73	0.73	0.73	0.73	0.73	0.73	0.73	0.73
15.5	0.68	0.68	0.69	0.69	0.69	0.69	0.70	0.70	0.70	0.71	0.71	0.71	0.71	0.72	0.72	0.72	0.72	0.72	0.72	0.72



Depth/FS	1x1	2x2	3x3	4x4	5x5	6x6	7x7	8x8	9x9	10x10	11x11	12x12	13x13	14x14	15x15	16x16	17x17	18x18	19x19	20x20
16.0	0.67	0.67	0.67	0.68	0.68	0.68	0.68	0.69	0.69	0.69	0.70	0.70	0.70	0.70	0.71	0.71	0.71	0.71	0.71	0.71
16.5	0.66	0.66	0.66	0.67	0.67	0.67	0.67	0.68	0.68	0.68	0.69	0.69	0.69	0.69	0.70	0.70	0.70	0.70	0.70	0.70
17.0	0.65	0.65	0.65	0.66	0.66	0.66	0.66	0.67	0.67	0.67	0.68	0.68	0.68	0.68	0.69	0.69	0.69	0.69	0.69	0.69
17.5	0.64	0.64	0.64	0.64	0.65	0.65	0.65	0.66	0.66	0.66	0.67	0.67	0.67	0.67	0.68	0.68	0.68	0.68	0.68	0.68
18.0	0.62	0.63	0.63	0.63	0.64	0.64	0.64	0.65	0.65	0.65	0.65	0.66	0.66	0.66	0.66	0.67	0.67	0.67	0.67	0.67
18.5	0.61	0.62	0.62	0.62	0.63	0.63	0.63	0.64	0.64	0.64	0.64	0.65	0.65	0.65	0.65	0.66	0.66	0.66	0.66	0.66
19.0	0.60	0.61	0.61	0.61	0.62	0.62	0.62	0.63	0.63	0.63	0.63	0.64	0.64	0.64	0.64	0.65	0.65	0.65	0.65	0.65
19.5	0.59	0.59	0.60	0.60	0.60	0.61	0.61	0.61	0.62	0.62	0.63	0.63	0.63	0.63	0.63	0.64	0.64	0.64	0.64	0.64
20.0	0.58	0.58	0.59	0.59	0.59	0.60	0.60	0.60	0.61	0.61	0.62	0.62	0.62	0.62	0.63	0.63	0.63	0.63	0.63	0.63
21.0	0.56	0.56	0.57	0.57	0.57	0.57	0.58	0.58	0.59	0.59	0.59	0.60	0.60	0.60	0.60	0.60	0.61	0.61	0.61	0.61
22.0	0.54	0.54	0.55	0.55	0.55	0.56	0.56	0.56	0.57	0.57	0.58	0.58	0.58	0.58	0.58	0.59	0.59	0.59	0.59	0.59
23.0	0.52	0.53	0.53	0.53	0.53	0.54	0.54	0.54	0.55	0.55	0.55	0.56	0.56	0.56	0.57	0.57	0.57	0.57	0.57	0.57
24.0	0.50	0.50	0.51	0.51	0.51	0.52	0.52	0.53	0.53	0.53	0.54	0.54	0.54	0.55	0.55	0.55	0.55	0.55	0.55	0.55
25.0	0.48	0.49	0.49	0.49	0.49	0.50	0.50	0.50	0.51	0.51	0.52	0.52	0.52	0.52	0.52	0.53	0.53	0.53	0.53	0.53
26.0	0.46	0.47	0.47	0.47	0.48	0.48	0.48	0.49	0.49	0.49	0.50	0.50	0.50	0.51	0.51	0.51	0.52	0.52	0.52	0.52
27.0	0.45	0.45	0.45	0.46	0.46	0.46	0.47	0.47	0.47	0.48	0.48	0.49	0.49	0.49	0.49	0.49	0.50	0.50	0.50	0.50
28.0	0.43	0.43	0.44	0.44	0.44	0.45	0.45	0.45	0.46	0.46	0.46	0.47	0.47	0.47	0.48	0.48	0.48	0.48	0.48	0.49
29.0	0.42	0.42	0.42	0.42	0.43	0.43	0.43	0.43	0.44	0.44	0.44	0.45	0.45	0.45	0.46	0.46	0.46	0.46	0.46	0.47
30.0	0.40	0.40	0.41	0.41	0.41	0.41	0.42	0.42	0.42	0.42	0.43	0.43	0.43	0.44	0.44	0.44	0.45	0.45	0.45	0.45
31.0	0.38	0.39	0.39	0.39	0.40	0.40	0.40	0.40	0.41	0.41	0.41	0.42	0.42	0.42	0.43	0.43	0.43	0.43	0.43	0.44
32.0	0.37	0.37	0.38	0.38	0.38	0.38	0.39	0.39	0.39	0.40	0.40	0.40	0.41	0.41	0.41	0.41	0.42	0.42	0.42	0.42
33.0	0.36	0.36	0.36	0.36	0.37	0.37	0.37	0.38	0.38	0.38	0.38	0.39	0.39	0.39	0.40	0.40	0.40	0.40	0.40	0.41
34.0	0.34	0.35	0.35	0.35	0.35	0.36	0.36	0.36	0.37	0.37	0.37	0.37	0.38	0.38	0.38	0.39	0.39	0.39	0.39	0.39
35.0	0.33	0.33	0.34	0.34	0.34	0.34	0.35	0.35	0.35	0.35	0.36	0.36	0.36	0.37	0.37	0.37	0.37	0.38	0.38	0.38
36.0	0.32	0.32	0.32	0.33	0.33	0.33	0.33	0.34	0.34	0.34	0.35	0.35	0.35	0.36	0.36	0.36	0.36	0.36	0.36	0.37

Depth\FS	1x1	2x2	3x3	4x4	5x5	6x6	7x7	8x8	9x9	10x10	11x11	12x12	13x13	14x14	15x15	16x16	17x17	18x18	19x19	20x20
37.0	0.30	0.31	0.31	0.31	0.32	0.32	0.32	0.32	0.33	0.33	0.33	0.34	0.34	0.34	0.34	0.35	0.35	0.35	0.35	0.35
38.0	0.29	0.30	0.30	0.30	0.30	0.31	0.31	0.31	0.31	0.32	0.32	0.32	0.33	0.33	0.33	0.33	0.34	0.34	0.34	0.34
39.0	0.28	0.28	0.29	0.29	0.29	0.30	0.30	0.30	0.30	0.31	0.31	0.31	0.32	0.32	0.32	0.32	0.32	0.33	0.33	0.33
40.0	0.27	0.27	0.28	0.28	0.28	0.28	0.29	0.29	0.29	0.29	0.30	0.30	0.30	0.31	0.31	0.31	0.31	0.31	0.32	0.32



ศูนย์วิทยทรัพยากร  
จุฬาลงกรณ์มหาวิทยาลัย

Table 2 Tissue maximum ratio  $TMR_{(d,0)}$  in a water phantom with field size of  $0 \times 0 \text{ cm}^2$  and depth of 1.5 cm to 40 cm.

Radius(cm) Depth	0x0	Radius(cm) Depth	0x0	Radius(cm) Depth	0x0	Radius(cm) Depth	0x0
1.5	1.00	9	0.69	14.75	0.52	32	0.23
2	0.99	9.25	0.68	15	0.52	33	0.22
2.5	0.97	9.5	0.67	15.5	0.50	34	0.21
3	0.94	9.75	0.66	16	0.49	35	0.20
3.5	0.92	10	0.65	16.5	0.48	36	0.19
4	0.90	10.25	0.65	17	0.47	37	0.18
4.5	0.87	10.5	0.64	17.5	0.45	38	0.17
5	0.85	10.75	0.63	18	0.44	39	0.16
5.25	0.84	11	0.62	18.5	0.43	40	0.15
5.5	0.83	11.25	0.61	19	0.43		
5.75	0.82	11.5	0.60	19.5	0.42		
6	0.80	11.75	0.60	20	0.40		
6.25	0.80	12	0.59	21	0.39		
6.5	0.79	12.25	0.58	22	0.37		
6.75	0.78	12.5	0.58	23	0.35		
7	0.77	12.75	0.57	24	0.34		
7.25	0.76	13	0.56	25	0.32		
7.5	0.74	13.25	0.56	26	0.31		
7.75	0.73	13.5	0.55	27	0.30		
8	0.72	13.75	0.55	28	0.29		
8.25	0.71	14	0.54	29	0.27		
8.5	0.70	14.25	0.54	30	0.26		
8.75	0.70	14.5	0.53	31	0.25		

Table 3 Scatter maximum ratio  $SMR_{(d,r)}$  in a water phantom with radius of 0.56 to 40x40 cm<sup>2</sup> and depth of 0.56 cm to 16.93 cm.

Radius Depth	0.56	1.13	1.69	2.26	2.82	3.39	3.95	4.51	5.08	5.64	6.21	6.77	7.33	7.90	8.46	9.03	9.59	10.16	10.72	11.28
1.5	1.00	1.00	1.00	1.00	1.00	1.00	1.00	1.00	1.00	1.00	1.00	1.00	1.00	1.00	1.00	1.00	1.00	1.00	1.00	1.00
2.0	0.99	0.99	1.00	1.00	1.00	1.00	1.00	1.00	1.00	1.00	1.00	0.99	0.99	0.99	0.99	0.99	0.99	0.99	0.99	0.99
2.5	0.97	0.97	0.98	0.98	0.99	0.99	0.99	0.99	0.99	0.99	0.99	0.98	0.98	0.98	0.99	0.99	0.99	0.99	0.99	0.99
3.0	0.94	0.95	0.96	0.97	0.97	0.97	0.97	0.98	0.98	0.98	0.98	0.97	0.97	0.97	0.98	0.98	0.98	0.98	0.98	0.98
3.5	0.92	0.93	0.94	0.95	0.96	0.96	0.96	0.96	0.96	0.96	0.96	0.96	0.96	0.96	0.96	0.97	0.97	0.97	0.97	0.97
4.0	0.90	0.91	0.92	0.94	0.94	0.95	0.95	0.95	0.95	0.95	0.95	0.95	0.95	0.95	0.95	0.95	0.96	0.96	0.96	0.96
4.5	0.88	0.89	0.90	0.92	0.92	0.93	0.93	0.93	0.93	0.94	0.94	0.94	0.94	0.94	0.94	0.94	0.94	0.94	0.94	0.95
5.0	0.86	0.87	0.88	0.90	0.90	0.91	0.91	0.92	0.92	0.92	0.92	0.92	0.92	0.92	0.92	0.93	0.93	0.93	0.93	0.93
5.3	0.85	0.86	0.87	0.89	0.90	0.90	0.91	0.91	0.91	0.92	0.92	0.92	0.92	0.92	0.92	0.92	0.92	0.92	0.93	0.93
5.5	0.84	0.85	0.86	0.88	0.89	0.89	0.90	0.90	0.90	0.91	0.91	0.91	0.91	0.91	0.91	0.92	0.92	0.92	0.92	0.92
5.8	0.82	0.84	0.85	0.87	0.88	0.88	0.89	0.89	0.90	0.90	0.90	0.90	0.90	0.90	0.91	0.91	0.91	0.91	0.92	0.92
6.0	0.81	0.83	0.85	0.86	0.87	0.88	0.88	0.89	0.89	0.90	0.90	0.90	0.89	0.90	0.90	0.91	0.91	0.91	0.91	0.91
6.3	0.81	0.82	0.84	0.85	0.86	0.87	0.87	0.88	0.88	0.89	0.89	0.89	0.89	0.89	0.90	0.90	0.90	0.90	0.90	0.90
6.5	0.80	0.81	0.83	0.84	0.85	0.86	0.87	0.87	0.87	0.88	0.88	0.88	0.88	0.88	0.89	0.89	0.89	0.90	0.90	0.90
6.8	0.79	0.81	0.82	0.83	0.84	0.85	0.86	0.86	0.87	0.87	0.87	0.88	0.88	0.88	0.88	0.89	0.89	0.89	0.89	0.89
7.0	0.78	0.80	0.81	0.83	0.84	0.84	0.85	0.85	0.86	0.86	0.87	0.87	0.87	0.87	0.88	0.88	0.88	0.88	0.88	0.89
7.3	0.77	0.79	0.80	0.82	0.83	0.84	0.84	0.85	0.85	0.86	0.86	0.86	0.86	0.87	0.87	0.87	0.87	0.88	0.88	0.88
7.5	0.76	0.77	0.79	0.81	0.82	0.83	0.83	0.84	0.84	0.85	0.85	0.86	0.86	0.86	0.86	0.87	0.87	0.87	0.87	0.87
7.8	0.75	0.76	0.78	0.80	0.81	0.82	0.82	0.83	0.84	0.84	0.85	0.85	0.85	0.85	0.86	0.86	0.86	0.86	0.87	0.87
8.0	0.73	0.75	0.77	0.79	0.80	0.81	0.82	0.82	0.83	0.84	0.84	0.84	0.84	0.85	0.85	0.85	0.86	0.86	0.86	0.86
8.3	0.73	0.74	0.76	0.78	0.79	0.80	0.81	0.82	0.82	0.83	0.84	0.84	0.83	0.84	0.84	0.85	0.85	0.85	0.86	0.86
8.5	0.72	0.74	0.75	0.77	0.78	0.79	0.80	0.81	0.81	0.82	0.83	0.83	0.83	0.83	0.84	0.84	0.84	0.85	0.85	0.85
8.8	0.72	0.73	0.75	0.76	0.78	0.79	0.80	0.80	0.81	0.81	0.82	0.82	0.82	0.83	0.83	0.83	0.84	0.84	0.84	0.85

Radius Depth	0.56	1.13	1.69	2.26	2.82	3.39	3.95	4.51	5.08	5.64	6.21	6.77	7.33	7.90	8.46	9.03	9.59	10.16	10.72	11.28
9.0	0.71	0.72	0.74	0.75	0.77	0.78	0.79	0.79	0.80	0.81	0.81	0.81	0.81	0.82	0.82	0.83	0.83	0.84	0.84	0.84
9.3	0.70	0.72	0.73	0.75	0.76	0.77	0.78	0.79	0.79	0.80	0.81	0.81	0.81	0.81	0.82	0.82	0.83	0.83	0.83	0.83
9.5	0.69	0.71	0.72	0.74	0.75	0.76	0.77	0.78	0.79	0.79	0.80	0.80	0.80	0.81	0.81	0.81	0.82	0.82	0.82	0.83
9.8	0.68	0.70	0.71	0.73	0.74	0.75	0.76	0.77	0.78	0.78	0.79	0.79	0.80	0.80	0.80	0.81	0.81	0.81	0.82	0.82
10.0	0.67	0.69	0.71	0.72	0.73	0.75	0.76	0.76	0.77	0.78	0.79	0.79	0.79	0.79	0.80	0.80	0.80	0.81	0.81	0.81
10.3	0.66	0.68	0.70	0.71	0.73	0.74	0.75	0.76	0.76	0.77	0.78	0.78	0.78	0.79	0.79	0.79	0.80	0.80	0.81	0.81
10.5	0.66	0.67	0.69	0.71	0.72	0.73	0.74	0.75	0.76	0.76	0.77	0.77	0.77	0.78	0.78	0.79	0.79	0.80	0.80	0.80
10.8	0.65	0.67	0.68	0.70	0.71	0.72	0.73	0.74	0.75	0.76	0.76	0.77	0.77	0.77	0.78	0.78	0.79	0.79	0.79	0.80
11.0	0.64	0.66	0.67	0.69	0.70	0.72	0.73	0.74	0.74	0.75	0.75	0.76	0.76	0.76	0.77	0.78	0.78	0.78	0.79	0.79
11.3	0.63	0.65	0.67	0.68	0.70	0.71	0.72	0.73	0.74	0.74	0.75	0.75	0.75	0.76	0.76	0.77	0.77	0.78	0.78	0.78
11.5	0.63	0.64	0.66	0.68	0.69	0.70	0.71	0.72	0.73	0.73	0.74	0.74	0.75	0.75	0.76	0.76	0.77	0.77	0.77	0.78
11.8	0.62	0.63	0.65	0.67	0.68	0.69	0.70	0.71	0.72	0.73	0.73	0.74	0.74	0.74	0.75	0.76	0.76	0.76	0.77	0.77
12.0	0.61	0.63	0.64	0.66	0.67	0.68	0.69	0.70	0.71	0.72	0.73	0.73	0.73	0.74	0.74	0.75	0.75	0.76	0.76	0.76
12.3	0.60	0.62	0.64	0.65	0.67	0.68	0.69	0.70	0.71	0.71	0.72	0.73	0.73	0.73	0.74	0.74	0.75	0.75	0.75	0.76
12.5	0.60	0.61	0.63	0.64	0.66	0.67	0.68	0.69	0.70	0.71	0.71	0.72	0.72	0.72	0.73	0.74	0.74	0.74	0.75	0.75
12.8	0.59	0.61	0.62	0.64	0.65	0.66	0.67	0.68	0.69	0.70	0.71	0.71	0.71	0.72	0.72	0.73	0.74	0.74	0.74	0.74
13.0	0.58	0.60	0.61	0.63	0.64	0.65	0.67	0.67	0.68	0.69	0.70	0.71	0.71	0.71	0.72	0.72	0.73	0.73	0.74	0.74
13.3	0.58	0.59	0.61	0.62	0.64	0.65	0.66	0.67	0.68	0.69	0.70	0.70	0.70	0.70	0.71	0.72	0.72	0.73	0.73	0.73
13.5	0.57	0.59	0.60	0.62	0.63	0.64	0.65	0.66	0.67	0.68	0.69	0.69	0.69	0.70	0.70	0.71	0.72	0.72	0.72	0.73
13.8	0.57	0.58	0.60	0.61	0.62	0.64	0.65	0.66	0.66	0.67	0.68	0.69	0.69	0.69	0.70	0.70	0.71	0.72	0.72	0.72
14.0	0.56	0.58	0.59	0.60	0.62	0.63	0.64	0.65	0.66	0.66	0.67	0.68	0.68	0.68	0.69	0.70	0.71	0.71	0.71	0.72
14.3	0.56	0.57	0.58	0.60	0.61	0.62	0.64	0.64	0.65	0.66	0.67	0.67	0.68	0.68	0.69	0.69	0.70	0.70	0.71	0.71
14.5	0.55	0.56	0.58	0.59	0.60	0.62	0.63	0.64	0.64	0.65	0.66	0.67	0.67	0.67	0.68	0.69	0.69	0.70	0.70	0.70
14.8	0.54	0.56	0.57	0.58	0.60	0.61	0.62	0.63	0.64	0.64	0.65	0.66	0.66	0.67	0.67	0.68	0.69	0.69	0.69	0.70

Radius Depth	0.56	1.13	1.69	2.26	2.82	3.39	3.95	4.51	5.08	5.64	6.21	6.77	7.33	7.90	8.46	9.03	9.59	10.16	10.72	11.28
15.0	0.54	0.55	0.56	0.58	0.59	0.60	0.61	0.62	0.63	0.64	0.65	0.65	0.66	0.66	0.67	0.67	0.68	0.69	0.69	0.69
15.5	0.52	0.54	0.55	0.56	0.58	0.59	0.60	0.61	0.62	0.63	0.63	0.64	0.64	0.65	0.65	0.66	0.67	0.67	0.68	0.68
16.0	0.51	0.52	0.54	0.55	0.56	0.57	0.59	0.59	0.60	0.61	0.62	0.63	0.63	0.63	0.64	0.65	0.65	0.66	0.66	0.67
16.5	0.50	0.51	0.52	0.54	0.55	0.56	0.57	0.58	0.59	0.60	0.61	0.62	0.62	0.62	0.63	0.63	0.64	0.65	0.65	0.65
17.0	0.49	0.50	0.51	0.53	0.54	0.55	0.56	0.57	0.58	0.59	0.60	0.60	0.61	0.61	0.62	0.62	0.63	0.64	0.64	0.64
17.5	0.47	0.49	0.50	0.52	0.53	0.54	0.55	0.56	0.57	0.58	0.59	0.59	0.60	0.60	0.61	0.61	0.62	0.62	0.63	0.63
18.0	0.46	0.48	0.49	0.50	0.52	0.53	0.54	0.55	0.56	0.57	0.58	0.59	0.59	0.59	0.59	0.60	0.61	0.61	0.62	0.62
18.5	0.45	0.47	0.48	0.49	0.50	0.52	0.53	0.54	0.55	0.55	0.56	0.57	0.58	0.58	0.58	0.59	0.60	0.60	0.61	0.61
19.0	0.45	0.46	0.47	0.48	0.49	0.50	0.52	0.52	0.53	0.54	0.55	0.56	0.56	0.57	0.57	0.58	0.59	0.59	0.60	0.60
19.5	0.43	0.45	0.46	0.47	0.48	0.49	0.51	0.51	0.52	0.53	0.54	0.55	0.55	0.56	0.56	0.57	0.57	0.58	0.58	0.59
20.0	0.42	0.44	0.45	0.46	0.47	0.48	0.50	0.50	0.51	0.52	0.53	0.54	0.54	0.54	0.55	0.56	0.56	0.57	0.57	0.58
21.0	0.41	0.42	0.43	0.44	0.45	0.46	0.47	0.48	0.49	0.50	0.51	0.52	0.52	0.52	0.53	0.54	0.54	0.55	0.56	0.56
22.0	0.39	0.40	0.41	0.42	0.43	0.44	0.45	0.46	0.47	0.48	0.49	0.50	0.50	0.51	0.51	0.52	0.52	0.53	0.53	0.54
23.0	0.37	0.38	0.39	0.40	0.41	0.43	0.44	0.45	0.45	0.46	0.47	0.48	0.48	0.49	0.49	0.50	0.50	0.51	0.52	0.52
24.0	0.35	0.36	0.37	0.38	0.39	0.41	0.42	0.42	0.43	0.44	0.45	0.45	0.46	0.46	0.47	0.47	0.48	0.49	0.49	0.50
25.0	0.34	0.35	0.36	0.37	0.38	0.39	0.40	0.41	0.41	0.42	0.43	0.44	0.45	0.45	0.45	0.46	0.46	0.47	0.47	0.48
26.0	0.33	0.33	0.34	0.35	0.36	0.37	0.38	0.39	0.40	0.40	0.41	0.42	0.43	0.43	0.43	0.44	0.45	0.45	0.46	0.46
27.0	0.31	0.32	0.33	0.34	0.35	0.36	0.36	0.37	0.38	0.39	0.39	0.40	0.41	0.41	0.42	0.42	0.43	0.43	0.44	0.44
28.0	0.30	0.31	0.32	0.32	0.33	0.34	0.35	0.36	0.36	0.37	0.38	0.39	0.39	0.40	0.40	0.41	0.41	0.42	0.42	0.43
29.0	0.28	0.29	0.30	0.31	0.32	0.33	0.33	0.34	0.35	0.36	0.36	0.37	0.38	0.38	0.39	0.39	0.40	0.40	0.41	0.41
30.0	0.27	0.28	0.29	0.30	0.30	0.31	0.32	0.33	0.33	0.34	0.35	0.36	0.36	0.37	0.37	0.37	0.38	0.39	0.39	0.40
31.0	0.26	0.26	0.27	0.28	0.29	0.30	0.31	0.32	0.32	0.33	0.33	0.34	0.35	0.35	0.35	0.36	0.37	0.37	0.38	0.38
32.0	0.24	0.25	0.26	0.27	0.28	0.29	0.29	0.30	0.31	0.31	0.32	0.33	0.33	0.34	0.34	0.34	0.35	0.36	0.36	0.37
33.0	0.23	0.24	0.25	0.26	0.26	0.27	0.28	0.29	0.29	0.30	0.31	0.31	0.32	0.32	0.33	0.33	0.34	0.34	0.35	0.35

<b>Radius</b> <b>Depth</b>	<b>0.56</b>	<b>1.13</b>	<b>1.69</b>	<b>2.26</b>	<b>2.82</b>	<b>3.39</b>	<b>3.95</b>	<b>4.51</b>	<b>5.08</b>	<b>5.64</b>	<b>6.21</b>	<b>6.77</b>	<b>7.33</b>	<b>7.90</b>	<b>8.46</b>	<b>9.03</b>	<b>9.59</b>	<b>10.16</b>	<b>10.72</b>	<b>11.28</b>
34.0	0.22	0.23	0.24	0.24	0.25	0.26	0.27	0.28	0.28	0.29	0.29	0.30	0.31	0.31	0.31	0.32	0.32	0.33	0.33	0.34
35.0	0.21	0.22	0.23	0.23	0.24	0.25	0.26	0.26	0.27	0.28	0.28	0.29	0.29	0.30	0.30	0.30	0.31	0.31	0.32	0.33
36.0	0.20	0.21	0.21	0.22	0.23	0.24	0.25	0.25	0.26	0.26	0.27	0.28	0.28	0.29	0.29	0.29	0.30	0.30	0.31	0.31
37.0	0.19	0.20	0.20	0.21	0.22	0.23	0.23	0.24	0.25	0.25	0.26	0.26	0.27	0.28	0.28	0.28	0.28	0.29	0.30	0.30
38.0	0.18	0.19	0.19	0.20	0.21	0.22	0.22	0.23	0.24	0.24	0.25	0.25	0.26	0.26	0.27	0.27	0.27	0.28	0.28	0.29
39.0	0.17	0.18	0.19	0.19	0.20	0.21	0.21	0.22	0.23	0.23	0.24	0.24	0.25	0.25	0.26	0.26	0.26	0.27	0.27	0.28
40.0	0.16	0.17	0.18	0.18	0.19	0.20	0.20	0.21	0.22	0.22	0.23	0.23	0.24	0.24	0.25	0.25	0.25	0.26	0.26	0.27

ศูนย์วิทยทรัพยากร  
จุฬาลงกรณ์มหาวิทยาลัย

Table 3 Scatter maximum ratio  $SMR_{(d,r)}$  in a water phantom with radius of 0.56 to 40x40 cm<sup>2</sup> and depth of 0.56 cm to 16.93 cm. (Continue)

<b>Radius</b> <b>Depth</b>	<b>11.85</b>	<b>12.41</b>	<b>12.98</b>	<b>13.54</b>	<b>14.10</b>	<b>14.67</b>	<b>15.23</b>	<b>15.80</b>	<b>16.36</b>	<b>16.93</b>
1.5	0.069	0.072	0.074	0.076	0.078	0.079	0.079	0.080	0.080	0.081
2.0	0.088	0.090	0.091	0.093	0.095	0.096	0.096	0.097	0.098	0.099
2.5	0.106	0.108	0.109	0.110	0.111	0.112	0.113	0.114	0.115	0.116
3.0	0.116	0.117	0.118	0.120	0.121	0.122	0.123	0.124	0.125	0.127
3.5	0.125	0.127	0.128	0.130	0.131	0.132	0.133	0.134	0.136	0.137
4.0	0.136	0.139	0.140	0.142	0.144	0.145	0.146	0.147	0.148	0.150
4.5	0.147	0.150	0.151	0.154	0.156	0.158	0.159	0.160	0.161	0.162
5.0	0.153	0.156	0.157	0.160	0.162	0.164	0.165	0.166	0.167	0.169
5.3	0.158	0.161	0.163	0.166	0.169	0.171	0.172	0.173	0.174	0.175
5.5	0.164	0.167	0.170	0.172	0.175	0.178	0.179	0.179	0.180	0.181
5.8	0.170	0.173	0.175	0.179	0.182	0.184	0.186	0.186	0.187	0.188
6.0	0.171	0.174	0.177	0.180	0.183	0.186	0.188	0.188	0.188	0.189
6.3	0.171	0.175	0.178	0.181	0.185	0.188	0.190	0.190	0.190	0.191
6.5	0.172	0.176	0.179	0.182	0.186	0.189	0.192	0.192	0.192	0.193
6.8	0.173	0.176	0.180	0.184	0.188	0.191	0.194	0.194	0.194	0.194
7.0	0.181	0.185	0.188	0.191	0.195	0.198	0.201	0.201	0.201	0.202
7.3	0.190	0.193	0.196	0.199	0.202	0.205	0.208	0.208	0.209	0.210
7.5	0.198	0.201	0.204	0.207	0.210	0.212	0.215	0.216	0.217	0.218
7.8	0.206	0.210	0.212	0.214	0.217	0.219	0.222	0.223	0.224	0.226
8.0	0.207	0.210	0.212	0.214	0.217	0.219	0.222	0.223	0.225	0.226
8.3	0.206	0.210	0.212	0.214	0.217	0.219	0.222	0.223	0.225	0.226
8.5	0.206	0.210	0.212	0.214	0.217	0.219	0.222	0.223	0.225	0.227
8.8	0.206	0.210	0.212	0.214	0.217	0.219	0.221	0.223	0.225	0.227



Radius Depth	11.85	12.41	12.98	13.54	14.10	14.67	15.23	15.80	16.36	16.93
9.0	0.209	0.213	0.215	0.217	0.220	0.222	0.224	0.226	0.228	0.230
9.3	0.212	0.216	0.218	0.220	0.222	0.224	0.226	0.228	0.230	0.232
9.5	0.215	0.219	0.221	0.223	0.225	0.227	0.229	0.231	0.233	0.235
9.8	0.218	0.222	0.224	0.226	0.228	0.230	0.231	0.234	0.236	0.238
10.0	0.219	0.224	0.225	0.228	0.230	0.232	0.235	0.237	0.239	0.241
10.3	0.221	0.225	0.227	0.230	0.232	0.235	0.238	0.240	0.242	0.245
10.5	0.222	0.226	0.228	0.232	0.235	0.238	0.241	0.244	0.246	0.248
10.8	0.224	0.227	0.230	0.233	0.237	0.240	0.244	0.247	0.249	0.251
11.0	0.224	0.228	0.231	0.234	0.237	0.241	0.244	0.247	0.250	0.252
11.3	0.225	0.229	0.231	0.235	0.238	0.241	0.244	0.248	0.250	0.253
11.5	0.226	0.229	0.232	0.235	0.238	0.241	0.245	0.248	0.251	0.254
11.8	0.227	0.230	0.233	0.236	0.239	0.242	0.245	0.248	0.251	0.255
12.0	0.227	0.230	0.233	0.236	0.239	0.242	0.246	0.249	0.252	0.255
12.3	0.227	0.231	0.233	0.237	0.240	0.243	0.246	0.250	0.253	0.256
12.5	0.227	0.231	0.234	0.237	0.241	0.244	0.247	0.251	0.254	0.257
12.8	0.227	0.231	0.234	0.238	0.241	0.245	0.248	0.252	0.255	0.258
13.0	0.226	0.230	0.233	0.236	0.240	0.243	0.246	0.250	0.253	0.256
13.3	0.225	0.229	0.232	0.235	0.238	0.241	0.245	0.248	0.251	0.254
13.5	0.223	0.227	0.230	0.233	0.237	0.240	0.243	0.246	0.250	0.252
13.8	0.222	0.226	0.229	0.232	0.235	0.238	0.241	0.244	0.248	0.250
14.0	0.222	0.226	0.229	0.232	0.236	0.239	0.242	0.246	0.249	0.252
14.3	0.223	0.227	0.230	0.233	0.237	0.240	0.244	0.248	0.251	0.254
14.5	0.223	0.227	0.230	0.233	0.237	0.241	0.245	0.249	0.253	0.256
14.8	0.224	0.227	0.230	0.234	0.238	0.242	0.246	0.250	0.255	0.258

<b>Radius</b>										
<b>Depth</b>	<b>11.85</b>	<b>12.41</b>	<b>12.98</b>	<b>13.54</b>	<b>14.10</b>	<b>14.67</b>	<b>15.23</b>	<b>15.80</b>	<b>16.36</b>	<b>16.93</b>
15.0	0.225	0.229	0.233	0.236	0.240	0.244	0.248	0.252	0.257	0.260
15.5	0.227	0.231	0.235	0.239	0.242	0.246	0.250	0.254	0.259	0.262
16.0	0.51	0.52	0.54	0.55	0.56	0.57	0.59	0.59	0.60	0.61
16.5	0.50	0.51	0.52	0.54	0.55	0.56	0.57	0.58	0.59	0.60
17.0	0.49	0.50	0.51	0.53	0.54	0.55	0.56	0.57	0.58	0.59
17.5	0.47	0.49	0.50	0.52	0.53	0.54	0.55	0.56	0.57	0.58
18.0	0.46	0.48	0.49	0.50	0.52	0.53	0.54	0.55	0.56	0.57
18.5	0.45	0.47	0.48	0.49	0.50	0.52	0.53	0.54	0.55	0.55
19.0	0.45	0.46	0.47	0.48	0.49	0.50	0.52	0.52	0.53	0.54
19.5	0.43	0.45	0.46	0.47	0.48	0.49	0.51	0.51	0.52	0.53
20.0	0.42	0.44	0.45	0.46	0.47	0.48	0.50	0.50	0.51	0.52
21.0	0.41	0.42	0.43	0.44	0.45	0.46	0.47	0.48	0.49	0.50
22.0	0.39	0.40	0.41	0.42	0.43	0.44	0.45	0.46	0.47	0.48
23.0	0.37	0.38	0.39	0.40	0.41	0.43	0.44	0.45	0.45	0.46
24.0	0.35	0.36	0.37	0.38	0.39	0.41	0.42	0.42	0.43	0.44
25.0	0.34	0.35	0.36	0.37	0.38	0.39	0.40	0.41	0.41	0.42
26.0	0.33	0.33	0.34	0.35	0.36	0.37	0.38	0.39	0.40	0.40
27.0	0.31	0.32	0.33	0.34	0.35	0.36	0.36	0.37	0.38	0.39
28.0	0.30	0.31	0.32	0.32	0.33	0.34	0.35	0.36	0.36	0.37
29.0	0.28	0.29	0.30	0.31	0.32	0.33	0.33	0.34	0.35	0.36
30.0	0.27	0.28	0.29	0.30	0.30	0.31	0.32	0.33	0.33	0.34
31.0	0.26	0.26	0.27	0.28	0.29	0.30	0.31	0.32	0.32	0.33
32.0	0.24	0.25	0.26	0.27	0.28	0.29	0.29	0.30	0.31	0.31
33.0	0.23	0.24	0.25	0.26	0.26	0.27	0.28	0.29	0.29	0.30

<b>Radius</b>										
<b>Depth</b>	<b>11.85</b>	<b>12.41</b>	<b>12.98</b>	<b>13.54</b>	<b>14.10</b>	<b>14.67</b>	<b>15.23</b>	<b>15.80</b>	<b>16.36</b>	<b>16.93</b>
34.0	0.22	0.23	0.24	0.24	0.25	0.26	0.27	0.28	0.28	0.29
35.0	0.21	0.22	0.23	0.23	0.24	0.25	0.26	0.26	0.27	0.28
36.0	0.20	0.21	0.21	0.22	0.23	0.24	0.25	0.25	0.26	0.26
37.0	0.19	0.20	0.20	0.21	0.22	0.23	0.23	0.24	0.25	0.25
38.0	0.18	0.19	0.19	0.20	0.21	0.22	0.22	0.23	0.24	0.24
39.0	0.17	0.18	0.19	0.19	0.20	0.21	0.21	0.22	0.23	0.23
40.0	0.16	0.17	0.18	0.18	0.19	0.20	0.20	0.21	0.22	0.22

ศูนย์วิทยทรัพยากร  
จุฬาลงกรณ์มหาวิทยาลัย

Table 4 Phantom scatter factor  $S_p(r)$  in a water phantom with radius of 0 cm to 17.39 cm and depth of 1.5 cm to 17.39 cm.

<b>Radius(cm)</b>	<b><math>S_p(r)</math></b>	<b>Radius(cm)</b>	<b><math>S_p(r)</math></b>	<b>Radius(cm)</b>	<b><math>S_p(r)</math></b>	<b>Radius(cm)</b>	<b><math>S_p(r)</math></b>	<b>Radius(cm)</b>	<b><math>S_p(r)</math></b>
0.00	0.9600	6.43	1.0042	8.92	1.0148	11.28	1.0228	14.10	1.0310
2.26	0.9790	6.56	1.0049	9.03	1.0150	11.42	1.0230	14.38	1.0314
2.52	0.9810	6.68	1.0056	9.10	1.0154	11.56	1.0234	14.67	1.0316
2.82	0.9820	6.77	1.0060	9.18	1.0156	11.70	1.0240	14.93	1.0318
3.09	0.9830	6.91	1.0066	9.27	1.0160	11.85	1.0244	15.23	1.0320
3.39	0.9860	7.02	1.0070	9.36	1.0165	11.97	1.0248	15.45	1.0322
3.57	0.9870	7.14	1.0076	9.44	1.0170	12.10	1.0252	15.71	1.0325
3.78	0.9880	7.25	1.0080	9.52	1.0172	12.23	1.0256	15.80	1.0328
3.95	0.9895	7.33	1.0085	9.59	1.0174	12.36	1.0260	15.96	1.0330
4.18	0.9910	7.46	1.0088	9.69	1.0176	12.41	1.0265	16.21	1.0333
4.37	0.9920	7.57	1.0096	9.77	1.0178	12.49	1.0268	16.36	1.0338
4.51	0.9935	7.78	1.0100	9.85	1.0182	12.62	1.0270	16.45	1.0341
4.72	0.9942	7.90	1.0110	9.93	1.0184	12.74	1.0272	16.69	1.0346
4.89	0.9955	7.98	1.0112	10.01	1.0186	12.87	1.0276	16.93	1.0350
5.08	0.9965	8.08	1.0116	10.09	1.0190	12.98	1.0278	17.39	1.0355
5.20	0.9972	8.18	1.0120	10.16	1.0192	13.11	1.0280		
5.35	0.9980	8.27	1.0124	10.25	1.0196	13.23	1.0284		
5.64	1.0000	8.37	1.0128	10.40	1.0198	13.35	1.0290		
5.78	1.0010	8.46	1.0130	10.56	1.0204	13.47	1.0294		
5.92	1.0015	8.56	1.0134	10.72	1.0210	13.54	1.0295		
6.05	1.0020	8.65	1.0137	10.85	1.0212	13.59	1.0296		
6.21	1.0030	8.74	1.0140	11.00	1.0218	13.70	1.0298		
6.31	1.0035	8.83	1.0144	11.14	1.0222	13.82	1.0298		

## Appendix B An example of .mlc file of square MLC fields for dose verification

Field = MLC 10 x 10.0			
Index = 0.00			
Carriage Group = 1			
Operator = Physicist			
Collimator = 0.00			
Leaf 1A = 0.00	Leaf 22A = 5.00	Leaf 1B = 0.00	Leaf 21B = 5.00
Leaf 2A = 0.00	Leaf 23A = 5.00	Leaf 2B = 0.00	Leaf 22B = 5.00
Leaf 3A = 0.00	Leaf 24A = 5.00	Leaf 3B = 0.00	Leaf 23B = 5.00
Leaf 4A = 0.00	Leaf 25A = 5.00	Leaf 4B = 0.00	Leaf 24B = 5.00
Leaf 5A = 0.00	Leaf 26A = 0.00	Leaf 5B = 0.00	Leaf 25B = 5.00
Leaf 6A = 0.00	Leaf 27A = 0.00	Leaf 6B = 0.00	Leaf 26B = 0.00
Leaf 7A = 0.00	Leaf 28A = 0.00	Leaf 7B = 0.00	Leaf 27B = 0.00
Leaf 8A = 0.00	Leaf 29A = 0.00	Leaf 8B = 0.00	Leaf 28B = 0.00
Leaf 9A = 0.00	Leaf 30A = 0.00	Leaf 9B = 0.00	Leaf 29B = 0.00
Leaf 10A = 0.00	Leaf 31A = 0.00	Leaf 10B = 0.00	Leaf 30B = 0.00
Leaf 11A = 0.00	Leaf 32A = 0.00	Leaf 11B = 0.00	Leaf 31B = 0.00
Leaf 12A = 0.00	Leaf 33A = 0.00	Leaf 12B = 0.00	Leaf 32B = 0.00
Leaf 13A = 0.00	Leaf 34A = 0.00	Leaf 13B = 0.00	Leaf 33B = 0.00
Leaf 14A = 0.00	Leaf 35A = 0.00	Leaf 14B = 0.00	Leaf 34B = 0.00
Leaf 15A = 0.00	Leaf 36A = 0.00	Leaf 15B = 0.00	Leaf 35B = 0.00
Leaf 16A = 5.00	Leaf 37A = 0.00	Leaf 16B = 5.00	Leaf 36B = 0.00
Leaf 17A = 5.00	Leaf 38A = 0.00	Leaf 17B = 5.00	Leaf 37B = 0.00
Leaf 18A = 5.00	Leaf 39A = 0.00	Leaf 18B = 5.00	Leaf 38B = 0.00
Leaf 19A = 5.00	Leaf 40A = 0.00	Leaf 19B = 5.00	Leaf 39B = 0.00
Leaf 20A = 5.00		Leaf 20B = 5.00	Leaf 40B = 0.00
Leaf 21A = 5.00			Note = 0
			Shape = 0
			Magnification = 1.00
			CRC = D835

## Appendix C An example of .mlc file of static 3D-CRT field

Field = Lt. Lat 3D-CRT			
Index = 90.00			
Carriage Group = 1			
Operator = Physicist			
Collimator = 0.00			
Leaf 1A = 0.00		Leaf 1B = 0.05	Leaf 21B = 3.95
Leaf 2A = 0.00	Leaf 21A = 3.44	Leaf 2B = 0.05	Leaf 22B = 4.19
Leaf 3A = 0.00	Leaf 22A = 3.37	Leaf 3B = 0.05	Leaf 23B = 4.29
Leaf 4A = 0.00	Leaf 23A = 3.14	Leaf 4B = 0.05	Leaf 24B = 4.20
Leaf 5A = 0.00	Leaf 24A = 3.43	Leaf 5B = 0.05	Leaf 25B = 3.64
Leaf 6A = 0.00	Leaf 25A = 3.13	Leaf 6B = 0.05	Leaf 26B = 0.05
Leaf 7A = 0.00	Leaf 26A = 0.00	Leaf 7B = 0.05	Leaf 27B = 0.05
Leaf 8A = 0.00	Leaf 27A = 0.00	Leaf 8B = 0.05	Leaf 28B = 0.05
Leaf 9A = 0.00	Leaf 28A = 0.00	Leaf 9B = 0.05	Leaf 29B = 0.05
Leaf 10A = 0.00	Leaf 29A = 0.00	Leaf 10B = 0.05	Leaf 30B = 0.05
Leaf 11A = 0.00	Leaf 30A = 0.00	Leaf 11B = 0.05	Leaf 31B = 0.05
Leaf 12A = 0.00	Leaf 31A = 0.00	Leaf 12B = 0.05	Leaf 32B = 0.05
Leaf 13A = 0.00	Leaf 32A = 0.00	Leaf 13B = 0.05	Leaf 33B = 0.05
Leaf 14A = 0.00	Leaf 33A = 0.00	Leaf 14B = 0.05	Leaf 34B = 0.05
Leaf 15A = 0.00	Leaf 34A = 0.00	Leaf 15B = 0.05	Leaf 35B = 0.05
Leaf 16A = 3.04	Leaf 35A = 0.00	Leaf 16B = 3.05	Leaf 36B = 0.05
Leaf 17A = 3.37	Leaf 36A = 0.00	Leaf 17B = 3.66	Leaf 37B = 0.05
Leaf 18A = 3.17	Leaf 37A = 0.00	Leaf 18B = 3.44	Leaf 38B = 0.05
Leaf 19A = 3.44	Leaf 38A = 0.00	Leaf 19B = 3.80	Leaf 39B = 0.05
Leaf 20A = 3.60	Leaf 39A = 0.00	Leaf 20B = 3.53	Leaf 40B = 0.05
	Leaf 40A = 0.00		Note = 0
			Shape = 0
			Magnification = 1.00
			CRC = E52E

## Appendix D The user manual of ISOFT software

### 1. Introduction

This manual provides information on the background knowledge necessary for using the application that this manual is meant for, and the notation used throughout this manual. This guide is written mainly for medical staffs who wish to use ISOFT software. In this manual we will try to help the user to use the ISOFT software. Step-by-step instructions are provided in this manual.

### 2. Requirements

The requirements of the systems will be divided in two categories: Hardware and Software requirements

#### 2.1. Software requirements

The first that has to be mentioned is that the program should run under the same operating system of the Microsoft Window operating system since the problems with different versions of compiler. The ISOFT software runs under Microsoft Windows 32 bit operating systems (Windows95/98/NT/2000/XP). In our lab, Microsoft Window XP Version 2002 is used as the operating system. The ISOFT software packages allow installation to any personal computer. The manual provides a short overview of the use and the workflow followed in the workspaces. The procedures included in the workflow are then described in more detail, providing some step-by-step instructions to get started with the procedures.

#### 2.2. Hardware requirements

A minimum requirement of PC equipped is at least 64 MB of RAM and a processor of at least 120 MHz clock frequency is recommended for the use of the program. The program files require approximately 10 MB of free disk space; additionally, the user should have at least 60 MB free disk space for the measurement data will be generate. The present version also requires a sufficiently large display matrix size: the ISOFT form needs a desktop area of at least 1,024 x 768 to be fully visible. For best graphics quality, it require the display mode of your PC to use at least 16 bit colour depth (65,536 colours); in the 8-bit display mode the graphics in the program will be of poor quality due to the small number of available colors. The VGA cards should be compatible with the Microsoft Window OS.

### 3. Using the program

To start ISOFT, double-click its icon on the desktop, or choose ISOFT from the programs folder after pressing the “Start”-button on the task bar. The main window of program will be pop up.

The ISOFT software is designed for 2D image viewing, electron density conversion, patient contouring and image reconstruction. This topic describes the use of the image viewing, patient data transfer and contouring of the ISOFT software to prepare image data for use in dose calculation.

#### 3.1. Homogeneous phantom and MLC window

To start homogeneous phantom and MLC window, double-click **PhotonBeam** icon, the window will be displayed as shown in figure 1.

To calculate dose from photon beam window

1. From the photon beam window, click **Load MLC sagittal** bottom. The MLC explorer window appears as shown in figure 2.

2. Select the appropriate import filter.

3. Select the data to be imported from the appropriate directory.

4. Select the MLC position file

5. Click **OK** to start the import image of MLC as shown in figure 3. In the 2D view, the MLCs are displayed at the field end closer to the treatment unit. The intersection of the field and the plane show the MLC shape as an outline.

6. Do all of the following:

- Entering the value of tumor depth in *Tumour Depth* in cm.
- Entering the value of source to surface distance in *SSD* in cm.
- Entering the value of monitor unit in *Input MU* in MU.

7. You can select the calculation point by clicking in the field size of image: the cursor point then becomes the calculation point.

8. Click **None corr. Inhomogeneity 3D-CRT** bottom to start the calculation of dose in homogeneous water phantom.



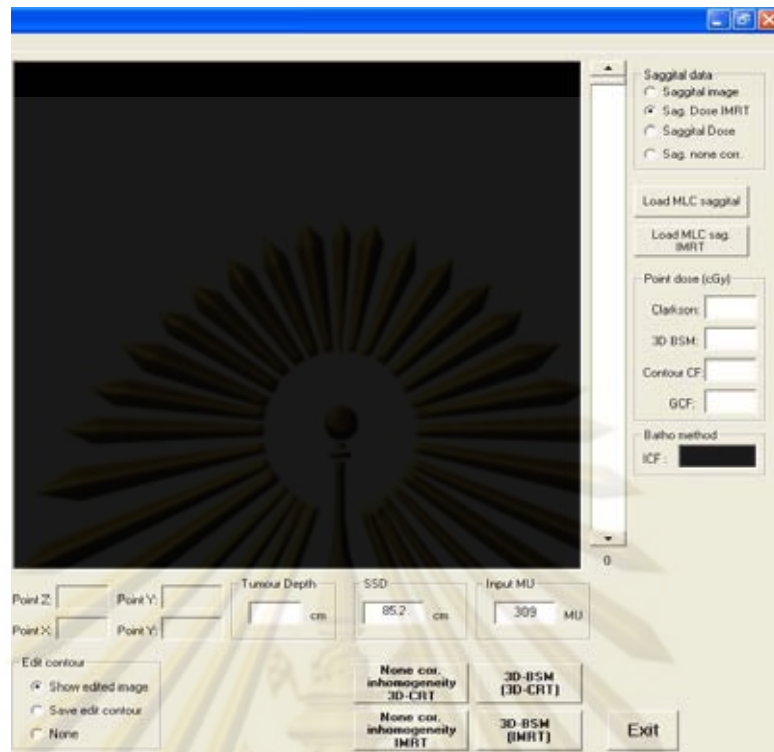


Figure 1 The homogeneous phantom and MLC window of ISOFT.

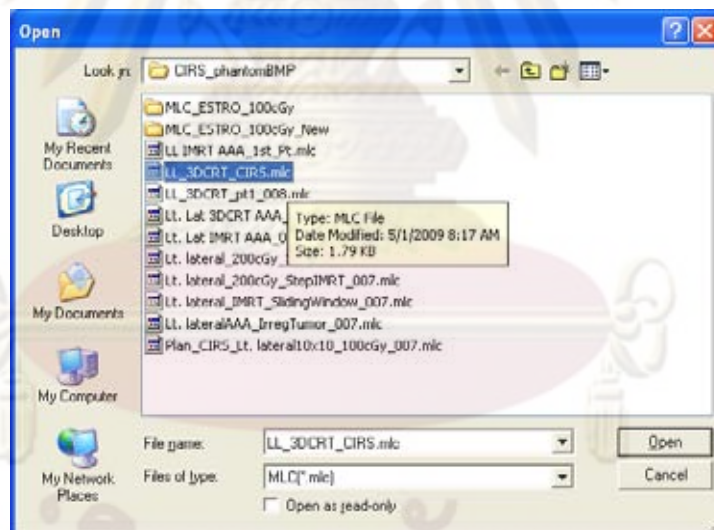


Figure 2 MLC explorer window.

ศูนย์วิทยุทางการแพทย์  
จุฬาลงกรณ์มหาวิทยาลัย

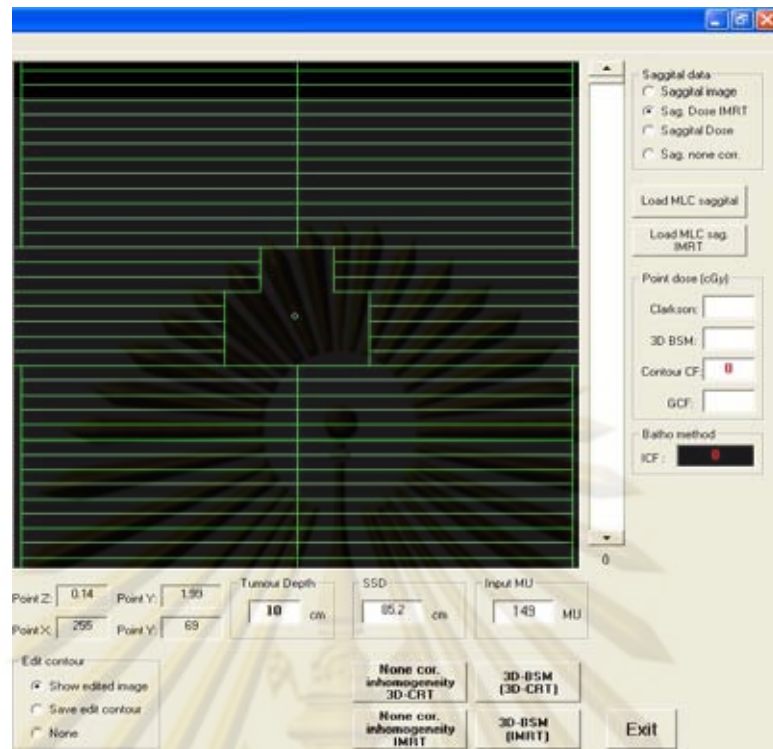


Figure 3 The homogeneous phantom and MLC window showed the MLC position.

### 3.2. Inhomogeneous phantom window

To start Inhomogeneous phantom window, double-click **Inhomophan** icon, the window will be pop up as shown in figure 4.

The procedure of import images from menu bar

1. From the **File** menu, select **Open...CT images**. The empty patient explorer window appears as shown in figure 5.
2. Select the appropriate import filter.
3. Select the data to be imported from the appropriate directory.
4. Select an image file using the mouse.
5. Click **OK** to start the import images as shown in figure 6.

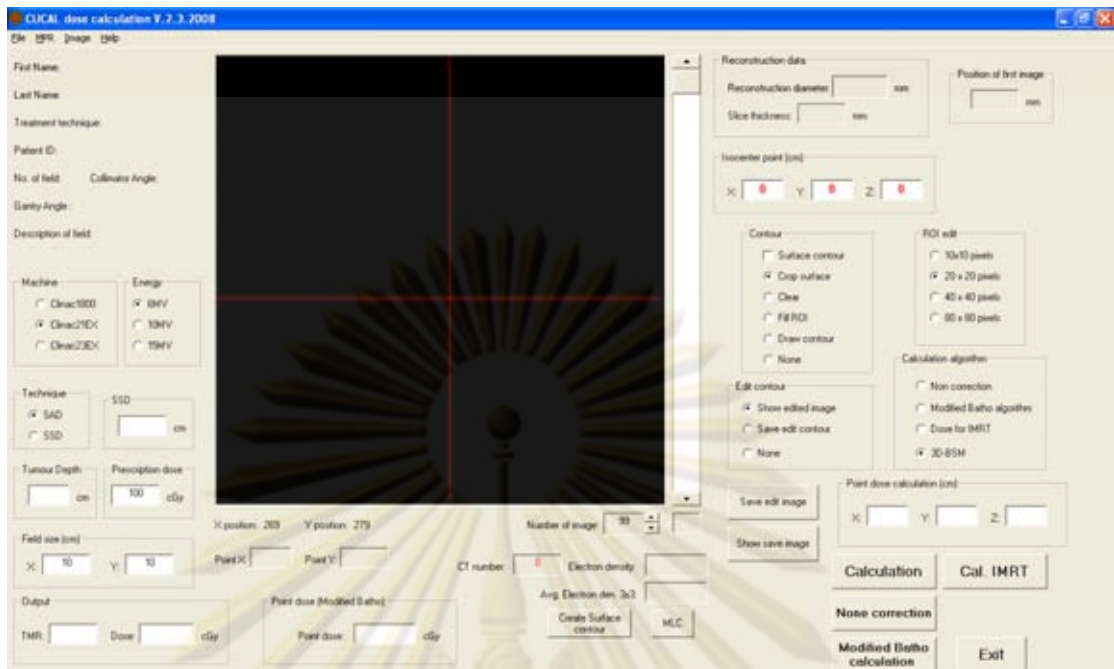


Figure 4 The Inhomogeneous phantom window of ISOFT.

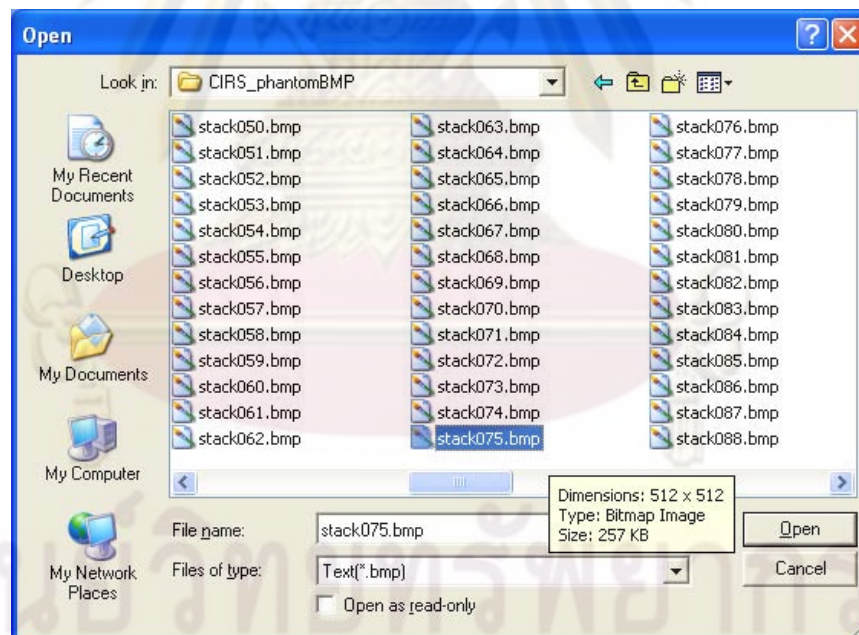


Figure 5 Patient explorer window.

จุฬาลงกรณ์มหาวิทยาลัย

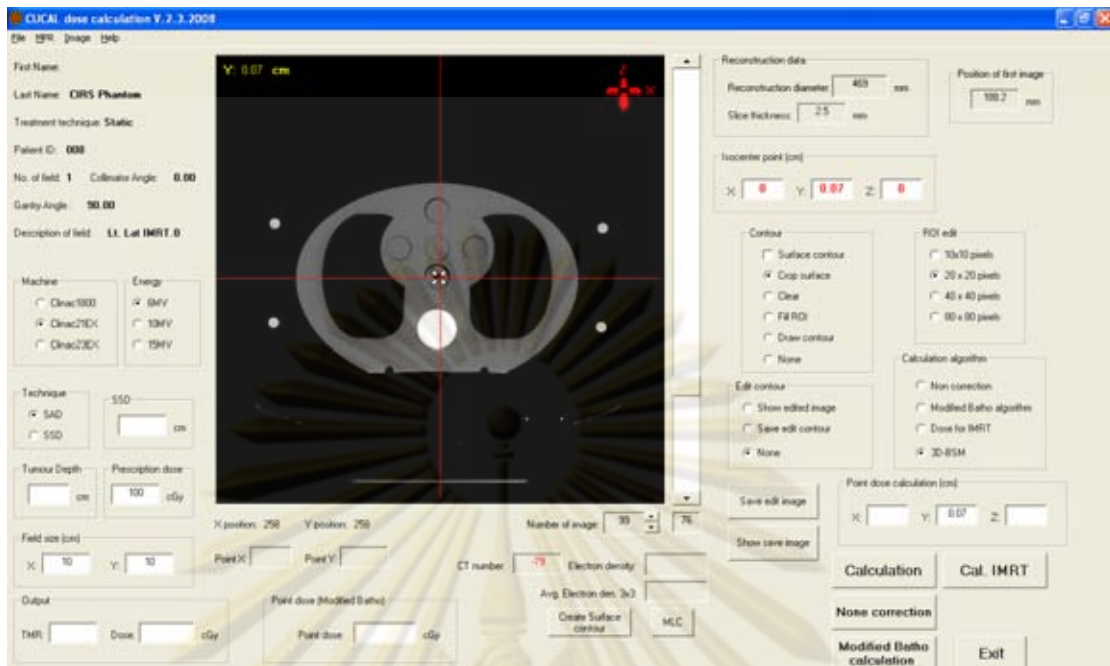


Figure 6 The Inhomogeneous phantom window of ISOFT. The phantom image is represented.

From figures, the patient information (at the left of the form) shows the first name, last name, treatment technique, patient ID, number of field, collimator angle, gantry angle and description of field. If no file has been specified there is no text. The radio button of machine, energy and technique are for specifying patient data. The SSD (Source to surface distance) technique of each patient is obtained either by entering their proper values (in cm) or the value 0.0 in the fields of these data. *X position* and *Y position* are the coordinates of an arbitrary point inside the CT image. The *Point X* and *Point Y*, *Tumour Depth* and *Prescription dose* will show the points, tumour depth in cm and prescription dose in cGy for point dose calculation after clicking on the CT image as shown in figure 7. The CT number and electron density value are shown with the coordinates of an arbitrary point inside the image.

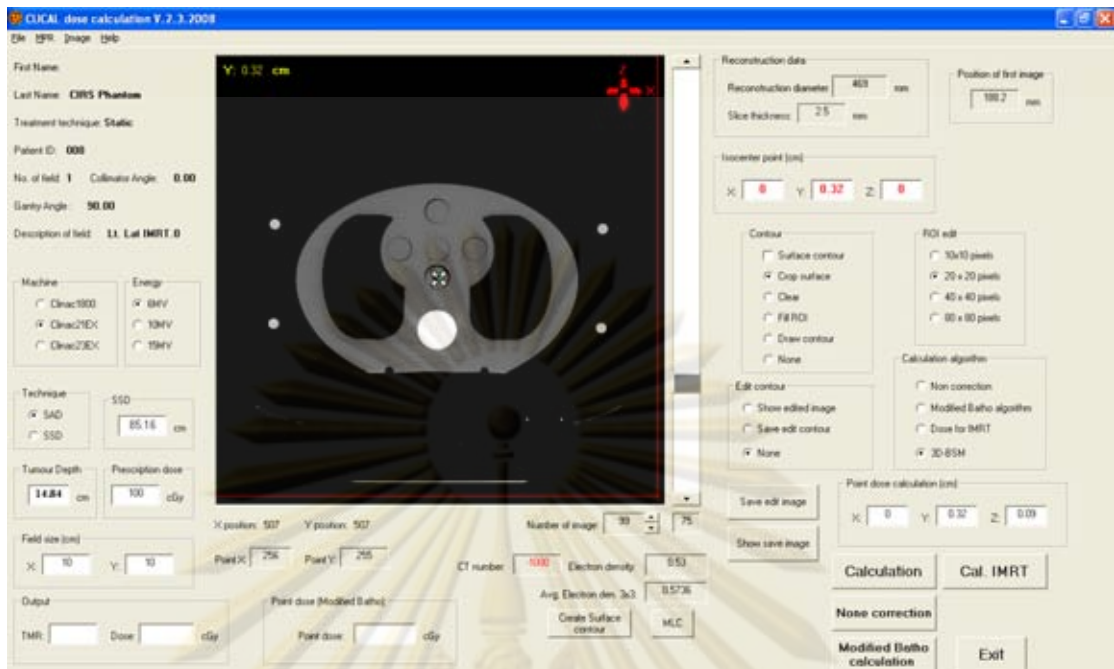


Figure 7 Show output data at the calculation point.

In the inhomogeneous phantom window, user can view 2D contouring of patient images using an automatic contouring and segmenting methods. The Contouring provides tools for defining accurate data for each patient to achieve precise patient dosimetry. This data includes the body structure from CT images. The radio button of *Contour* is created for patient skin contour by drag mouse cover the patient outline on axial image as shown in figure 8. The user can save the contour file by clicking the *Save edit contour* radio buttons. When ready, the user can show the patient skin contour in inhomogeneity phantom window by clicking the vertical score bar. The image of patient skin contour is shown in figure 9.

ศูนย์วิทยุทรัพยากร  
จุฬาลงกรณ์มหาวิทยาลัย

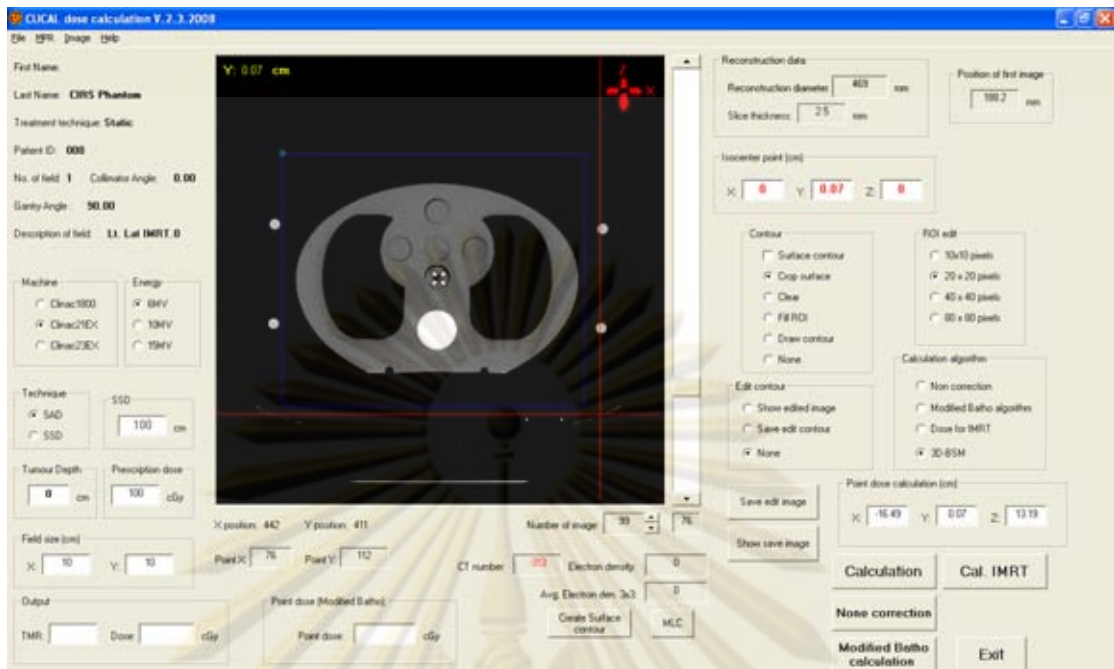


Figure 8 The inhomogeneous phantom window of ISOFT with the external contour which was created by ISOFT software.

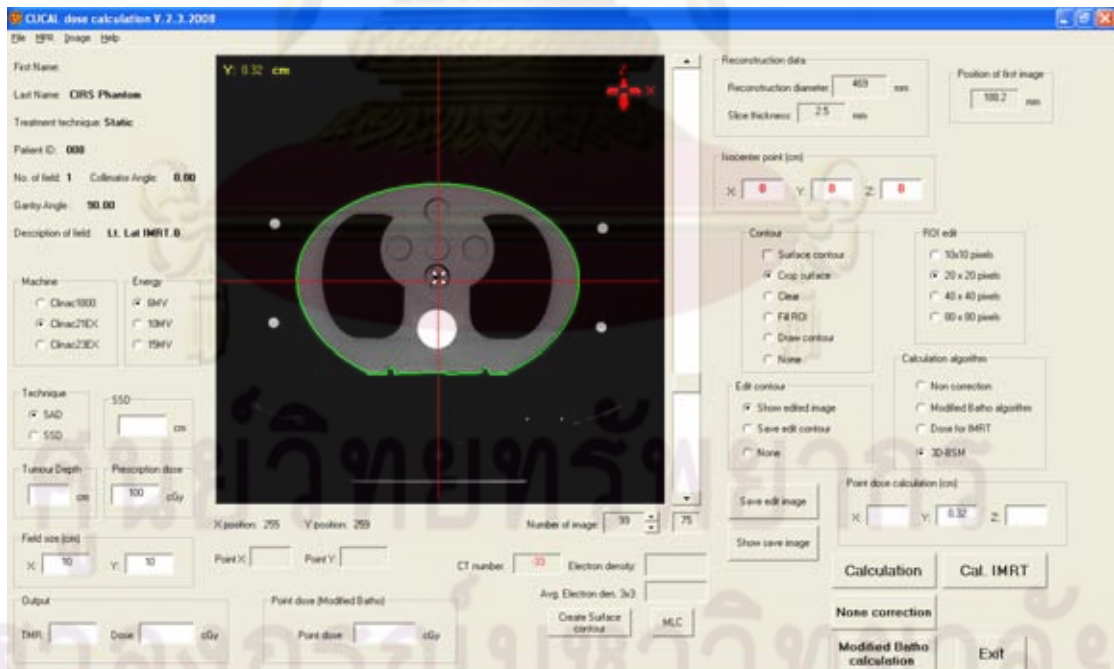


Figure 9 The inhomogeneous phantom window of ISOFT with the external contour which was created by ISOFT software.

The procedure of calculate an inhomogeneity correction:

1. From the inhomogeneous phantom window, click **Calculation** button.
2. Give a new name for the inhomogeneity correction files.
3. Save the changes.

### 3.3. MLC window

To start MLC window, double-click **3D-BSM** icon, the window will be pop up as shown in figure 10.

The procedure of import images from menu bar

1. From the **File** menu, select **Open...CT images**. The empty patient explorer window appears.
2. Select the appropriate import filter.
3. Select the data to be imported from the appropriate directory.
4. Select an image file using the mouse.
5. Click **OK** to start the import images.
6. The user can select the point to generate MPR image for sagittal view by clicking in the axial image.
7. Do all of the following:
  - Entering the value of source to surface distance in *SSD* in cm.
  - Entering the value of monitor unit in *Input MU* in MU.
8. Click **Load MLC sagittal** bottom. The MLC explorer window appears.
9. Select the appropriate import filter.
10. Select the data to be imported from the appropriate directory.
11. Select an MLC position file using the mouse.
12. Click **OK** to start the import image of MLC. In the 2D view, the MLCs are displayed at the field end closer to the treatment unit. The intersection of the field and the plane show the MLC shape as an outline as shown in figure 11.
13. The user can select the calculation point by clicking in the field size of image: the cursor point then becomes the calculation point.
14. Do one of the following:

- Click 3D-BSM (3D-CRT) bottom to start the calculation of dose inhomogeneous correction by 3D-CRT technique.

- Click 3D-BSM (IMRT) bottom to start the calculation of dose inhomogeneous correction by IMRT technique.



ศูนย์วิทยทรัพยากร  
จุฬาลงกรณ์มหาวิทยาลัย





Figure 10 The MLC window of ISOFT with the surface contour which was created by ISOFT software.

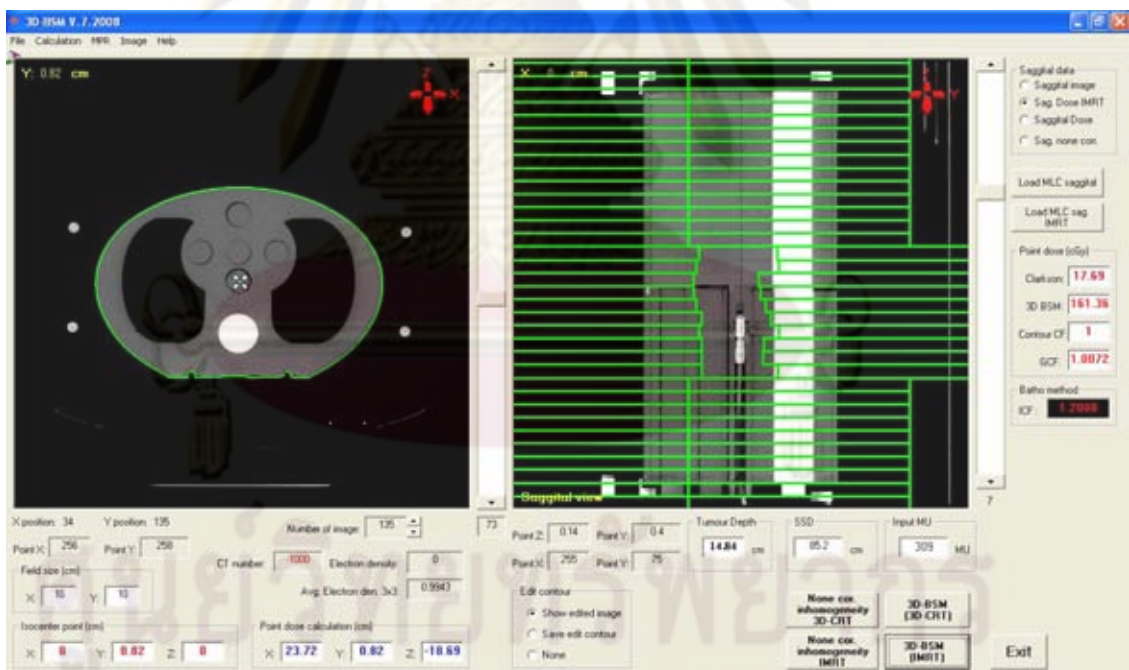


Figure 11 The MLC window of ISOFT that contained CT images, patient information and MLC position of treatment field.

## VITAE

NAME	Mr Nuntawat Oudee
SEX	Male
NATIONALITY	Thai
DATE OF BIRTH	February 16 1981
PLACE OF BIRTH	Nakhon Sawan, Thailand
INSTITUTIONS ATTENDED	Naresuan University, 2003: Bachelor of Science (Radiological Technology) Mahidol University, 2005: Master of Science (Medical Physics)
HOME ADDRESS	197/5 Sangradsadontri Road, Chumsang, Nakhon Sawan Thailand 60120 Tel. 056-282113 Nun_oudee@hotmail.com

ศูนย์วิทยทรัพยากร  
จุฬาลงกรณ์มหาวิทยาลัย